UC Berkeley
UC Berkeley Electronic Theses and Dissertations

Title
Spin orbit torque driven magnetic switching for low power computing and memory

Permalink
https://escholarship.org/uc/item/304131vh

Author
Bhowmik, Debanjan

Publication Date
2015

Peer reviewed|Thesis/dissertation

eScholarship.org Powered by the California Digital Library
University of California

Spin orbit torque driven magnetic switching for low power computing and memory

by

Debanjan Bhowmik

A dissertation submitted in partial satisfaction of the

requirements for the degree of

Doctor of Philosophy

in

Engineering–Electrical Engineering and Computer Sciences

in the

Graduate Division

of the

University of California, Berkeley

Committee in charge:

Professor Sayeef Salahuddin, Chair
Professor Jeffrey Bokor
Professor Irfan Siddiqi

Fall 2015

Spin orbit torque driven magnetic switching for low power computing and memory

Copyright 2015
by
Debanjan Bhowmik

Abstract

Spin orbit torque driven magnetic switching
for low power computing and memory

by

Debanjan Bhowmik

Doctor of Philosophy in Engineering–Electrical Engineering and Computer Sciences

University of California, Berkeley

Professor Sayeef Salahuddin, Chair

Spintronics has rapidly emerged as a highly pursued research area in solid-state physics and devices owing to its potential application in low power memory and logic as well as the rich physics associated with it. Traditionally in spintronics, spin transfer torque in magnetic tunnel junctions and spin valves has been used to manipulate ferromagnets. Spin orbit torque has recently emerged as an alternative mechanism for manipulating such ferromagnets, which offers advantages of lower energy consumption, simpler device structure, etc. For a ferromagnet- heavy metal bilayer, electrons flowing through the heavy metal separate based on the direction of their spin. This results in the accumulation of spin polarized electrons at the interface, which in turn applies a torque, known as spin orbit torque, on the ferromagnet. A typical such heavy metal is tantalum (Ta) and typical such ferromagnet is CoFeB. The research presented in this dissertation shows how in a perpendicularly polarized Ta/CoFeB/MgO heterostructure, spin orbit torque at the interface of the Ta and CoFeB layers can be used to manipulate the magnetic moments of the CoFeB layer for low power memory and logic applications.

The main results presented in this dissertation are fourfold. First, we report experiments showing spin orbit torque driven magnetic switching in a perpendicularly polarized Ta/CoFeB/MgO heterostructure and explain the microscopic mechanism of the switching. Using that microscopic mechanism, we show a new kind of ferromagnetic domain wall motion. Traditionally a ferromagnetic domain wall is known to flow parallel or antiparallel to the direction of the current, but here we show that spin orbit torque, owing to its unique symmetry, can be used to move the domain wall orthogonal to the current direction. Second, we experimentally demonstrate the application of this spin orbit torque driven switching in nanomagnetic logic, which is a low power alternative to CMOS based computing. Previous demonstrations of nanomagnetic logic needed an external magnetic field, the generation of which needed a large amount of current rendering such logic scheme uncompetitive compared to its CMOS counterpart. Here we show that spin orbit torque eliminates the need of an

external magnetic field for nanomagnetic logic and hence spin orbit torque driven nanomagnetic logic consumes 100 times lower current than magnetic field driven nanomagnetic logic at room temperature.

Though we can demonstrate magnetic logic with spin orbit torque in the absence of the magnetic field, spin orbit torque driven deterministic switching of a perpendicular magnet from up to down and down to up still needs the application of an external magnetic field unless the symmetry of the system is broken. This renders such switching scheme not very useful for real memory devices. In the third part of the thesis, we show through micromagnetic simulations that if the magnet has a wedge shape, the symmetry of the system is broken and the magnet can be deterministically switched from up to down and down to up even in the absence of an external magnetic field. Our simulations are supported by recent experiments, performed in our group. In the last part, we show how a bilayer of two heavy metals (Ta and Pt) can be used to increase the spin orbit torque efficiency. Interfaces of ferromagnet with Ta and that of ferromagnet with Pt exhibit spin orbit torques in opposite directions, so it is expected that their effects will cancel. Instead, in our experiments we find that the spin orbit torque efficiency at the Ta/CoFeB interface increases if a Pt layer exists under the Ta layer. Modeling of the system based on conventional spin transport physics cannot explain this result.

To
Stephen Hawking

Contents

Contents ii

List of Figures iv

1 Introduction 1

2 Background Theory and Experiments 7
- 2.1 Theory of spin orbit torque 8
- 2.2 Experiments on spin orbit torque driven magnetization switching 12
- 2.3 Experiments on spin orbit torque driven domain wall motion 20

3 Microscopic mechanism of spin orbit torque driven magnetic switching and domain wall motion 24
- 3.1 Spin orbit torque driven magnetic switching in the presence of out of plane magnetic field 24
- 3.2 Spin orbit torque driven magnetic switching in the presence of in plane magnetic field 27
- 3.3 Macrospin modeling of spin orbit torque driven magnetic switching 28
- 3.4 Micromagnetic analysis of spin orbit torque driven magnetic switching 30
- 3.5 Deterministic Domain Wall Motion Orthogonal To Current Flow Due To Spin Orbit Torque 34
- 3.6 Microscopic mechanism of spin orbit torque driven magnetic switching: A revision 49
- 3.7 Measurement of Joule heating due to current 52

4 Spin orbit torque driven clocking in a nanomagnetic logic circuit 54
- 4.1 Underlying physics of the clocking mechanism 54
- 4.2 Driving a single nanomagnet to a meta-stable state 57
- 4.3 Dipole coupling between adjacent dots 59
- 4.4 Propagation of signal from an input magnet along a chain of nanomagnets . 64

5 Deterministic spin orbit torque switching of a perpendicularly polarized magnet for low power memory 71

5.1 Physical mechanism of the switching: Tilting of the anisotropy axis 73
5.2 Tilting of the anisotropy axis due to wedge shape of the ferromagnetic layer 74
5.3 Spin orbit torque from a current pulse drives the magnetic moments in-plane 76
5.4 Deterministic evolution of the magnet to up or down state after the current pulse 78
5.5 Comparison with experiment 79

6 Enhancement of spin orbit torque in bilayers of two metals with opposite polarities of spin orbit torque 82
6.1 Device Structure and Experimental Results 82
6.2 Spin diffusion based modeling 85

7 Conclusion and Future Work 90

Bibliography 93

List of Figures

1.1 (a) Evolution of operating voltage of CMOS over time shows that it cannot be reduced below a certain limit. (b) Evolution of clock frequency over the last couple of decade shows that the clock frequency has reached a saturation. (b) Evolution of power consumption density over the last couple of decades shows a gradual increase. (Adapted from Danowitz *et al.* [2]) 2

1.2 (a) Physical distribution and hierarchy of memory in a computer. The lower panel shows speed (as order of magnitude), number of processor (CPU) cycles needed to access the memory, and size of the different memories. (used from Wong, P. S. *et al.*[7] with permission) (b) Schematic of the basic unit of STTMRAM. Arrows inside the magnetic layers show direction of the moments. Moment of the pinned layer is always pointing right, but the moment of the free layer can be switched from left to right and right to left with spin transfer torque from the current flowing vertically through the tunnel junction. Data is stored as direction of moment of the free layer. 4

2.1 (a) Rashba effect- Conduction electrons in the ferromagnet moving with a velocity proportional to $\vec{k}$ (in +x direction here) experience an electric field along the z-axis due to structural inversion asymmetry at the interface, which transforms to an effective magnetic field $\vec{H_R}$ in the rest frame of the electron. (b) Spin Hall effect- Conduction electrons in the heavy metal moving with a velocity proportional to $\vec{k}$ (in +x direction here) drift either in +z or -z direction based on their direction of spin polarization. This results in creation of a spin current perpendicular to the charge current in the heavy metal. 11

2.2 (a) When current flows through the 500 nm wide nanowires made from the Pt/Co/AlOx stack the conduction electrons experience a Rashba magnetic field $\vec{H_R}$ due to the electric field at the interface. Due to s-d exchange coupling between the conduction electrons and the local moments of the ferromagnet, the ferromagnet experiences an effective magnetic field $\vec{H_s}d$. (b) When a current pulse is applied on the nanowires at zero magnetic field, the $\vec{H_s}d$ experienced by the magnet nucleates reverse polarized domains in them (black patches in the images obtained by differential Kerr microscopy). The nucleation of reverse domains can be enhanced or suppressed by applying an external magnetic field $\vec{H_e}xt$ parallel or anti-parallel to $\vec{H_s}d$. (Reproduced from Miron *et al. Nature Mater.* 9, 230-234 (2010) [9].) 14

2.3 Current pulses are applied on a 500 nm by 500 nm dot made from the Pt/Co/AlOx in the presence of an externally applied magnetic field along the direction of the current. When the current pulse Ip is negative and the field is positive, the final magnetization is in the upward direction (M_z=1). When the current pulse Ip is positive, the final magnetization is in the downward direction (M_z=-1). When the current pulse Ip is negative and the field is negative, the final magnetization is in the downward direction (M_z=-1). When the current pulse I_p is positive, the final magnetization is in the upward direction (M_z=1). (Reproduced from Miron, I. M. *et al. Nature* 476, 189-194 (2011) [24].) 15

2.4 Hall bars are fabricated from the Pt/Co/AlOx stack, exhibiting perpendicular anisotropy. The ratio of the Hall voltage measured to the current applied gives the anomalous Hall resistance R_H, which is 4.5 Ω when the magnetization of the Co layer is up (M_z = 1) and -4.5 Ω when the magnetization of the Co layer is down (M_z = -1) (c,d). Plot of RH versus current flowing through the Hall bar (I_{dc}), in the presence of external magnetic field, shows a hysteresis behaviour. For a positive field of 10mT in +y direction, positive current supports negative (in z) magnetization and negative current supports positive magnetization. For a field of 10mT in -y direction, positive current supports positive (in z) magnetization and negative current supports negative magnetization (a,b). This result is consistent with the result obtained by Miron *et al.* (Figure 3). Current flowing through Pt creates an accumulation of spin-polarized electrons at the Pt/Co interface. The final direction of the magnetization is the cross-product of the externally applied magnetic field ($\vec{B_{ext}}$) and the spin polarization of the electrons at the interface ($\vec{\tau_{ext}}$). (Reproduced from Liu *et al. Phys. Rev. Lett.* 109, 096602 (2012) [25].) . 17

2.5 (a) Hall bars are fabricated from the Ta/CoFeB/MgO stack, exhibiting perpendicular anisotropy. The ratio of the Hall voltage measured to the current applied gives the anomalous Hall resistance R_H, which is 1 Ω when the magnetization of the CoFeB layer is up ($M_z = 1$) and -1 Ω when the magnetization of the CoFeB layer is down ($M_z =$ -1). (b) Plot of R_H versus current flowing through the Hall bar (I_dc), in the presence of external magnetic field, shows a hysteresis similar to the Co/Pt/AlOx stack, but the sense of the hysteresis is reversed because the direction of spin polarization of the electrons at the Ta/CoFeB interface is opposite to that of Pt/Co interface for the same polarity of current. Thus even in this case, the final direction of the magnetization= externally applied magnetic field × direction of spin polarization at the interface. (Reproduced from Liu *et al. Science* 336, 555-558 (2012) [10].) 18

2.6 (a) Calculations performed by Haney *et al.* show that for different thicknesses (t_{NM}) of the normal metal (also called heavy metal in literature) in the normal metal/ferromagnetic metal system, the damping like torque (τ_D) is high while the field like torque (τ_F) when the spin Hall effect of the normal metal is only considered. When the Rashba effect at the interface is considered only and spin Hall effect is neglected, the damping like torque (τ_D) is negligible while the field like torque (τ_F) is high. (b) Calculations for different thicknesses (tFM) of the ferromagnetic metal also show similar results. (Reproduced from Haney, P. M. *et al. Phys. Rev. B.* 87, 174411 (2013).[29]) 19

2.7 (a) Configuration of the magnetic moments inside a ferromagnetic domain wall of the Bloch type is shown. As one moves across the domain wall (in +x direction) the moment transitions from out of plane (+z) to into the plane (-z) by rotating in the yz plane. (b) For the Neel wall, the moment transitions from +z to -z by rotating in the xz plane. The chirality of the domain wall is determined by the direction of the vector ($\vec{D_{ij}}$) where i and j refer to two adjacent sites for magnetic moments. This is because Dzyaloshinskii Moriya interaction dictates ($\vec{M}_i \times \vec{M}_j$ to be parallel to $\vec{D_{ij}}$). 21

2.8 (a)A domain wall is injected at the end of 500 nm wide nanowires made from Pt/CoFe/MgO and Ta/CoFe/MgO stack exhibiting perpendicular magnetic anisotropy. The out of plane magnetic field needed to propagate the domain wall along the wire (H_{prop}) is measured as a function of the electron current (j_e) along the wire. For Pt/CoFe/MgO nanowire a higher field is needed to propagate the wall when j_e is positive (electrons flow along the direction of propagation of the wall) and lower field is needed to propagate the wall when j_e is negative. Thus the domain wall is hindered in the electron flow direction for a Pt/CoFe/MgO nanowire. On the other hand for a Ta/CoFe/MgO nanowire, the propagation field is lower for positive j_e , which means domain wall motion is assisted in the direction of electron flow. (b) For a Pt/CoFe/MgO nanowire, the domain wall is of Neel type and the moment rotates inside the domain wall following a left handed chirality. Electron current j_e in +x direction causes accumulation of electrons with spin polarization ($\vec{\sigma}$) in +y direction. For the up/down domain wall, the average magnetization of the wall ($\vec{M_{avg}}$) is in -x direction. So the wall experiences an effective out of plane field ($\vec{H_{eff}}$), given by $\vec{M_{avg}} \times \vec{\sigma}$ in -z direction which moves the domain wall in -x direction. Similarly for the down/up domain wall, $\vec{M_{avg}}$ is in +x direction and $\vec{H_{eff}}$ is in +z direction, which makes the wall move in the -x direction. (Reproduced from Emori *et al. Nature Mater.* 12, 611-616 (2013) [28].) 22

3.1 Schematic shows the origin of spin orbit torque due to flow of current in perpendicularly polarized ferromagnet (CoFeB) / heavy metal (Ta) heterostructures. It also shows the device geometry for anomalous Hall effect (AHE) measurements on these thin film stacks. 25

3.2 (a) Anamolous Hall Resistance is normalized to correspond to the out of plane magnetization component of CoFeB and plotted against the magnetic field applied in perpendicular direction. At very low current density, the AHE response shows that the magnet has its easy axis out of plane with coercivity of 60 Oe. As more current flows through Ta, coercivity of CoFeB is reduced. (b) Reversing the direction of current reverses the direction of spin torque, but does not break any symmetry in out of plane direction. So coercivity change should be similar for positive and negative currents as observed in our experiments. (c) For an average of three devices, coercivity of 1 nm layer of CoFeB decreases linearly with increase in current density following a slope of -17×10^{-6} Oe/(A/cm^2) or -17 gauss per 10^6 A/cm^2 through Ta. 26

3.3 In-plane magnetic field breaks the symmetry with respect to spin torque and its direction determines whether up or down magnetization would be stabilized for given polarity of spin torque. So we observe experimentally through AHE measurements a hysteric magnetic switching for applied in-plane current and the curve is either left handed (a) or right handed (b) based on direction of magnetic field. 27

3.4 (a)The magnetization being initially upward (+z), in the absence of spin torque, application of downward magnetic field equal to half the coercive field ($H_{coercive,0}$) is unable to switch the magnet to down(-z) as expected. (b) However in the presence of in-plane spin torque with strength half that of $H_{coercive,0}$ the same value of applied magnetic field can switch the magnet from +z to -z direction. . 28

3.5 (a) With magnetization initially in +z state (M_z=1), torque generated by -y directed spin accumulation (σ) and torque generated by +x directed magnetic field add up to cause rotation from +z (M_z=+1) to -z (M_z=-1) while torque generated by +y directed spin accumulation and torque generated by +x directed magnetic field counteract to keep the magnet in +z state (M_z=+1). (b) When magnetic field is -x direction, +y directed spin accumulation switches the magnet from +z to -z while -y directed spin accumulation keeps the magnet in +z state 29

3.6 (a)Vibrating Sample Magnetometry (VSM) measurement on thin films of Si (substrate)/ SiO_2 (100 nm)/ Ta (10 nm)/ CoFeB (1 nm)/ MgO (1 nm)/ Ta (2 nm) shows that the stack exhibits perpendicular magnetic anisotropy. As a result, a large field (∼2000 gauss here) is needed to saturate the magnet in the in-plane direction (red plot). However the out of plane hysteresis loop shows that a very small field can switch the magnet in the out of plane direction (black plot). This behavior is observed for any Co/Pt/AlOx stack or Ta/CoFeB/MgO stack that exhibits perpendicular magnetic anisotropy. (b) Energy landscape of a single domain magnet shows that an anisotropy field of ∼2000 gauss is needed to switch the magnet by 180^0 in the out of plane direction. (c) The ferromagnetic domain wall moves by a distance $\delta\theta$ through the rotation of each moment in the domain wall by an angle $\delta\theta$. (d) Switching of a magnet with perpendicular anisotropy from up/ out of the plane (blue color) to down/ into the plane (red color) is shown schematically. Starting from a saturated state (all blue), reversed domain (red circle) nucleates with a small magnetic field into the plane. However, the domain wall is pinned at defects and hence cannot move. When the field is high enough to depin the domain wall, it moves and the reverse domain (red circle) expands to switch the magnet to into the plane (red square). (e) Minimum magnetic field needed to switch the magnet is plotted as a function of the angle between the direction of the applied magnetic field and normal to the surface of the film. . . 32

3.7 A domain wall, under the influence of a magnetic field (H) in x direction and spin accumulation ($\vec{\sigma}$) in -y direction, moves to the left (-x) such that the entire magnet switches from +z to -z 33

3.8 (a) Current flows across a transverse domain wall. Green arrows represent the magnetic moments. (b) Current flows along a longitudinal domain wall. (c) When current flows through the Ta in x direction (electrons in -x direction) electrons with spin polarization in -y direction accumulate at the interface of the Ta and CoFeB. This results in the transfer of spin orbit torque to the domain wall in CoFeB. The green parallelogram represents the plane of the sample and the three arrows show the directions of x, y and z-axes. The z-axis points in the direction of the vector product of x and y axes following the right hand rule, which is into the plane (⊗). (d) The MOKE image of the 20 microns wide magnetic bar shows the formation of a longitudinal wall along it when current flows in the +x direction. The longitudinal domain wall at y=0 separates an "out of the plane" (⊙) polarized domain for y < 0 and an "into the plane" (⊗) polarized domain for y > 0. Anomalous Hall voltage is measured across the orthogonal bar. 35

3.9 Current flows in the +x direction, i.e. electrons move in the -x direction to apply the bulk spin torque on the transverse domain wall. Blue dots with red background represent moments pointing out of the plane (-z) while red dots with blue background represent moments pointing into the plane (+z). We see that the transverse domain wall moves along the flow of electrons with time as expected. 38

3.10 Current flows in +x direction, i.e. electrons move in -x direction, but it cannot apply a bulk spin torque on the longitudinal domain wall. No magnetic field is applied. We see that the longitudinal domain wall does not move with time. . . 39

3.11 Current flows in +x direction, i.e. electrons move in -x direction. An in-plane magnetic field of 10 G is applied in +x direction. We see that the longitudinal domain wall does not move with time. 40

3.12 (a) Anomalous Hall resistance (R_{AHE}) measurement shows that the magnet can be switched between a saturated "into the plane" (⊗) polarized state ($m_z = 1$ or $R_{AHE} = 1.2\Omega$) and a saturated "out of the plane" (⊙) polarized state ($_{=} - 1$ or $R_{AHE} = -1.2\Omega$) with a switching field of ∼30 gauss. Starting from the $m_z = 1$ state, a current pulse of magnitude 7.5×10^6 A/cm^2 is applied along the bar in +x direction at a zero magnetic field. At the end of the pulse R_{AHE} is measured to be 0 Ω. This corresponds to the "mixed state" of the bar. MOKE image of the "mixed state" shows a longitudinal domain wall with a $m_z = -1$ polarized domain for $y < 0$ and a $m_z = 1$ polarized domain for $y > 0$. When out of plane magnetic field is applied in z direction on the "mixed" state, R_{AHE} does not change till ∼15 G. Beyond that, R_{AHE} increases till the magnet reaches the saturated "into the plane" state ($m_z = 1$, $R_{AHE} = 1.2\Omega$) - red plot. Applying another current pulse of magnitude 7.5×10^6 A/cm^2 on the saturated state creates the "mixed state" with a longitudinal domain wall again. Now applying a magnetic field in -z direction causes reduction in R_{AHE} till the magnet gets saturated in the "out of plane" direction ($m_z = -1$, $R_{AHE} = -1.2\Omega$) - blue plot. 42

3.12 (b) MOKE images of the magnetic bar under the application of "into the plane" (+z) field shows the movement of the longitudinal domain wall in -y direction so that the average magnetization is aligned with the field. When "out of the plane" (-z) field is applied, the longitudinal domain wall moves in +y direction. (c) Mixed state, formed by a positive current pulse (current I along +x) has "out of the plane" ($\odot$) polarized domains for $y < 0$ and "into the plane" ($\otimes$) polarized domains for $y > 0$ whereas mixed state, formed by a negative current pulse (I along -x) has "into the plane" ($\otimes$) polarized domains for y¡0 and "out of the plane" ($\odot$) polarized domains for $y > 0$. (d) Minimum field needed to move the longitudinal domain wall from the centre of the bar is plotted against the angle of application of the field. 43

3.13 (a) Current in +x direction creates a domain wall at the upper edge of the bar ($y < 0$) because of its Oersted field. Micromagnetic simulation shows that starting from the upper edge of the bar the domain wall moves to the center of the bar at a zero magnetic field to lower its magnetostatic energy.(b) Current in -x direction creates a domain wall at the lower edge of the bar ($y > 0$) because of its Oersted field. Micromagnetic simulation shows that starting from the lower edge of the bar the domain wall moves to the center of the bar at a zero magnetic field to lower its magnetostatic energy. 44

3.14 (a) MOKE images of the magnetic bar after a positive current pulse of different magnitude is applied on a longitudinal domain wall ("mixed" state of Fig. 3.12a) in the presence of an in-plane field (H_{in}) in -x and +x direction. (b) Contour plots of final R_{AHE} after application of a current pulse versus the magnitude of the current and magnitude of the applied in-plane field for different combinations of positive and negative currents and fields. (c) Plots of R_{AHE} versus magnitude of current pulse for different values of magnetic field, applied in -x direction. . . 46

3.15 (a) (b) Micromagnetic simulation of a 600 nm long and 200 nm wide magnet shows the motion of a longitudinal domain wall under the application of a spin polarization in -y direction (current I in +x direction) and an in-plane magnetic field (H_{in}) in -x/+x direction. The direction of the net magnetic moment in the domain wall, shown by a black arrow, is initialized along the direction of applied field. (c) Micromagnetic simulation of the same magnet with spin polarization in +y direction (current I in -x direction) and magnetic field in -x direction. 49

3.16 (a) The domain wall formed around the reverse domain (red circle), nucleated in the ferromagnet, is of Neel type if the DMI is strong. In the absence of an external magnetic field, the configuration of the moments (green arrows) inside the domain wall is such that the effective out of plane magnetic field H_{eff} experienced by different parts of the domain wall cancels each other (H_{eff}= average magnetization inside the domain wall $\times\sigma$, where σ is the direction of spin accumulation at the interface). So the reverse domain does not expand and the magnet does not switch. When an external magnetic H_{ext} field is applied and it is strong enough to overcome the DMI, the moments inside the domain wall orient in that direction. So H_{eff} experienced by all parts of the wall is "into the plane" and the reverse domain expands to switch the magnet into the plane. (b) In the absence of DMI, the moments of the domain wall around the reverse domain can be easily switched by an external magnetic field H_{ext} in its direction. When H_{ext} is towards the right, the domain wall experiences an effective field in "out of plane" direction, which favors out of plane directed moments. So the reverse domain shrinks and the magnet remains in "out of plane" direction (blue). When H_{ext} is towards the left, the domain wall experiences an effective field in "into the plane" direction, which favors "into the plane" moments. So the reverse domain expands and the magnet switches to "into the plane" direction (red). It is to be noted that both for (a) and (b), the final direction of the magnetization= $\vec{H_{ext}} \times \vec{\sigma}$ 51

3.17 (a) Double Hall bar fabricated for four probe measurement of resistance (b) Change in resistance from resistance at room temperature plotted as a function of increase in temperature. (c) Change in resistance is plotted as a function of increase in dc current density. 53

4.1 (a) In plane current flowing through Ta along the x direction (electrons along -x direction) causes spin separation across the thickness of Ta (z direction). It results in the accumulation of electrons with y directed spins at the Ta-CoFeB interface, which offers spin orbit torque to the magnetization (green arrow) of CoFeB. This spin torque drives the magnetization of CoFeB from its easy axis in the out of plane direction to a meta stable in-plane state. (b) When current passes through the Ta bar below the magnetic dots, magnetizations of all the dots other than the large input dot are driven in-plane to a metastable state by the spin orbit torque. Current flows in -x direction here, so electrons with -y directed spins accumulate at the Ta-CoFeB interface resulting in the magnetizations of the dots being driven to -y direction. When the current pulse is removed, the magnets go to the dipole coupled least energy configuration. 56

4.2 (a,b) SEM images show a Hall bar structure with a square dot of side length 200 nm at its center . The dot retains Ta (10 nm)/CoFeB(1 nm)/MgO (1 nm)/Ta($\sim$ 10 nm), while regions outside the dot are etched till the bottom Ta layer of the stack. (c) Anomalous Hall resistance(R_{AHE}), proportional to the out of plane magnetization of the dot, is measured using the Hall bar structure, with a varying magnetic field applied out of the plane. We obtain a square hysteresis loop, which shows that the easy axis of the magnet is out of the plane. (d) Starting from the magnet initially in the up direction, 30 successive current pulses of magnitude 1.5×10^7 A/cm^2 are applied at 0 G. R_{AHE} is measured after every current pulse and plotted against the current pulse number. (e) The histogram, obtained from the results of the same experiment, shows that the magnet is either up (+z, or $R_{AHE} = 0.1\Omega$) or down (-z or $R_{AHE} = -0.1\Omega$) after a current pulse with almost 50 percent probability. Thus spin orbit torque from the current pulse drives the magnet to a meta-stable in-plane state after which thermal noise directs it to either up or down state. 58

4.3 (a) SEM image shows three circular magnetic dots of diameter 200nm at a separation of 30 nm. (b) Hysteresis loop (R_{AHE} vs out of plane magnetic field) shows three discrete jumps, each jump corresponding to one magnet switching between up (↑) and down (↓). Green arrow indicates direction of magnetization of each dot. The dot farthest from the cross-center (rightmost arrow) has the lowest contribution to R_{AHE}, while the one, which is closest (leftmost arrow), has the highest contribution to R_{AHE}. (c) Starting with all three magnets initially down, current pulse of magnitude 3×10^7 A/cm^2 is applied 20 times at 0 G field. R_{AHE} of final state after current pulse is plotted against current pulse number. Bold lines are drawn through the expected final states- “2 up 1 down” (↑↓↑) and “2 down 1 up” (↓↑↓), which we obtain 13 out of the 20 times. Other 7 times we obtain states where adjacent magnets are parallel to each other. These are the error bits, represented by crosses. (d) The histogram, obtained from the results of the same experiment, show the dominance of mutually anti-parallel aligned states; (↑↓↑) - 8 times and (↓↑↓) - 5 times. This is because dipole coupling between the adjacent dots makes these two states the least energy configuration. (e) When the same experiment is repeated with all magnets initially up, (↑↓↑) state is formed 10 times and (↓↑↓) state is formed 5 times. (f) When same current pulse is instead applied in the presence of 20 G field, the magnets initially being in all up state, they always go to (↑↓↑) state. Similarly at -20 G the current pulse drive them to (↓↑↓) state. Thus the bias magnetic field controls the final state of the magnets here. Either of these states, (↑↓↑) and (↓↑↓) is stable unless another large current pulse or a magnetic field, higher than the coercivity of the dots ($\sim$ 300G), is applied. 60

4.4 (a) SEM image of 3 dots of diameter 200nm each at a separation of 30nm, which are fabricated at the center of the Hall bars. (b) Anomalous Hall Resistance (R_{AHE}) vs magnetic field (out of plane) plot shows equal jumps in R_{AHE}, corresponding to switching of each magnet. 61

4.5 Anomalous Hall resistance (R_{AHE}) is measured while sweeping the magnetic field in the negative direction till all the three magnets become saturated in the downward magnetized state. The state of the three magnets after application of current pulse at 0 gauss is found out from the number and size of jumps in R_{AHE} on their way to saturation and is shown with respect to each R_{AHE} curve. Same notation is followed as that in text and Fig. 4.3 to represent the state of the magnets - (nearest magnet, middle magnet, farthest magnet) 62

4.6 Histogram, obtained from multiple trials of the experiment in Figure 4.3f (clocking the three magnetic dots of Figure 4.3a at a bias magnetic field), shows that (↑↓↑) state is always formed when current pulse is applied at +20 gauss and (↓↑↓) state is always formed when current pulse is applied at -20 gauss. 63

4.7 (a) SEM image shows three square magnetic dots of side length 500 nm at a separation of 30 nm, next to a larger dot with each side of a few microns length. This large magnet acts as the fixed input bit. (b) R_{AHE} measurement of the device shows two different types of jumps-larger change in R_{AHE} (0.4 Ω) corresponding to bigger input dot and three smaller jumps (0.08 Ω each) corresponding to the three smaller dots. (c) Current pulse of magnitude 2×10^7 A/cm^2 is applied at 20 G on the device with all magnets initially up. Input magnet, the magnetization direction of which is indicated by the big green arrow, remains up while other magnets (small green arrows) go to “2 down 1 up” state, thus following the input magnet. When current pulse is applied at -20 G with all magnets initially down, input magnet remains down while the other magnets go to “2 up 1 down” state. (d)(e) Histogram, obtained from multiple trials of the same experiment (c), shows that we always get “2 down 1 up” state when input magnet is up and “2 up 1 down” state when input magnet is down. Thus the magnetization state of the input magnet controls the final state of other magnets here. 65

4.8 (a) Blue plot shows the hysteresis loop of a square dot of side length 2 μm obtained by R_{AHE} measurement. Current pulse with magnitude of 1.5×10^7 A/cm^2 and duration 1s applied at 0 gauss drives the magnet from a saturated up state to a mixed state of up and down polarized domains ($R_{AHE} = 0$). After that, as magnetic field is swept upward the magnet gradually goes back to saturated up state between 20 and 30 gauss, represented by a gradual rise in R_{AHE} (red plot). Similarly if magnetic field is swept downward, the magnet goes to saturated down state gradually between -20 and -30 gauss (green plot). (b) Starting with the magnet in saturated up magnetization state, application of current pulse with same magnitude and duration as before (1.5×10^7 A/cm^2, 1 s) at 20 gauss does not change the state of the magnet since no change in R_{AHE} is observed. When magnetic field is swept in the positive direction R_{AHE} does not change (red plot). When magnetic field is swept in the negative direction after current pulse at 20 gauss, R_{AHE} changes sharply at -180 gauss, corresponding to a switch from saturated up to saturated down state (green plot). This shows that when current pulse is applied at 20 gauss on a large magnet of similar dimensions (2 μm by 5 μm) saturated in one direction, the final state of the magnet is same as the initial state. So it can be used as fixed input magnet. 67

4.8 (c) All magnets, including the large input magnet, are saturated upward. Current pulse of magnitude 2×10^7 A/cm^2 is applied on them at 0 gauss. Next magnetic field is applied in the positive direction and the magnets are driven back to saturation (upward), with simultaneous measurement of R_{AHE} (red plot). Gradual transition for the large magnet is observed at ∼20 gauss and sharper transition for the smaller magnets is observed at higher magnetic field (∼ 300 gauss). Next, current pulse is again applied on the upward saturated magnets at 0 gauss. This time, magnetic field is next swept in the negative direction till all magnets become saturated down (green plot). Similar results are observed. (d) Same experiment as in Figure S6c is performed on the same system of magnets, only difference being both for the orange and violet plots, the state of the magnets is all down before the application of current pulse. The large magnet again shows smooth transition to saturation, while the three smaller magnets show sharp switching. . 68

4.9 (a) All magnets, including the input magnet, are saturated upward. Current pulse of magnitude 2×10^7 A/cm^2 and duration 1s is applied on them at 20 gauss. Next magnetic field is applied in the positive direction and the magnets are driven back to saturation (upward), with simultaneous measurement of R (red plot). Two small jumps and no big jump in R_{AHE} show the formation of “2 down 1 up” (↓↑↓) state after application of the current pulse, along with input magnet remaining up. Again current pulse is applied on the upward saturated magnets at 20 gauss. This time, magnetic field is next swept in the negative direction till all magnets become saturated down (green plot). One small jump further establishes the formation of (↓↑↓) state after the current pulse. The big jump corresponds to the input magnet switching from up to down when we sweep the magnetic field in negative direction. (b) Same experiment as in (a) is performed on three dots with input magnet, only difference being both for the orange and violet plots, the state of the magnets is all down before application of current pulse and the current pulse is applied at -20 gauss. This time, saturation to all saturated up polarized state takes place through one small jump, corresponding to one small magnet switching from down to up, and one big jump, corresponding to the input magnet switching from down to up (violet plot). This shows that “2 up 1 down” (↑↓↑) state is formed after application of the current pulse at -20 gauss. It also shows that the input magnet did not change its state after the current pulse. Applying the current pulse again on downward saturated magnets at -20 gauss and sweeping the magnetic field in negative field further confirms the formation of (↑↓↑) state after the current pulse (two small jumps - orange plot). 69

5.1 (a) For a ferromagnetic (CoFeB) layer with the wedge is on the left side of the magnet looking in +y direction, the anisotropy axis tilts from the +z direction as shown. Current in -y direction results in accumulation of electrons with spins in +x direction at the interface of Ta and CoFeB. This drives the magnetization of the CoFeB layer into the +x direction. (b) Current in +y direction results in accumulation of electrons with spins in -x direction at the interface of Ta and CoFeB. This drives the magnetization of the CoFeB layer into the -x direction. (c) For a ferromagnet with wedge on the right side looking in +y direction, the anisotropy axis tilts in the opposite direction compared to the magnet with wedge on its left side. 72

5.2 (a) For a ferromagnetic layer with the wedge on the left side of the magnet looking in the +y direction, starting from all the moments in the ferromagnetic layer pointing in the +z direction, if the system is allowed to relax, the moments at the wedge tilt towards +x direction aligning along the sloped surface of the wedge, shown by the dotted white line. The image shows the direction of the moments after the system is allowed to relax after 20 ns. (b) Starting from all the moments pointing in the -z direction, when the system is allowed to relax (for 20 ns), the moments at the wedge tilt towards -x direction again aligning along the sloped surface of the wedge. (c) For a ferromagnetic layer with the wedge on the right side of the magnet looking in the +y direction, starting from all the moments in the ferromagnetic layer pointing in the +z direction, if the system is allowed to relax, the moments at the wedge tilt towards -x direction aligning along the sloped surface of the wedge, shown by the dotted white line. The image shows the direction of the moments after the system is allowed to relax after 20 ns. (d) Starting from all the moments pointing in the -z direction, when the system is allowed to relax (for 20 ns), the moments at the wedge tilt towards +x direction again aligning along the sloped surface of the wedge. (The plots are not drawn to scale in the z dimension. The direction of the moments is suggested by the head of the arrows. Also, red color means moments are in +z direction, blue color means moments are in -z direction and white means moments are in-plane.) 75
5.3 (a) Spin accumulation in +x direction (σ) at the interface of the ferromagnetic layer (CoFeB) and heavy metal (Ta) drives the magnetic moments of the ferromagnetic layer in-plane pointing in the +x direction. This image shows the direction of the magnetic moments after they are allowed to evolve in the presence of spin torque due to the spin accumulation for 1 ns. (b) Spin accumulation in -x direction at the interface drives the magnetic moments in -x direction (Image taken after 1 ns). (The plots are not drawn to scale in the z dimension. The direction of the moments is suggested by the head of the arrows. Also, red color means moments are in +z direction, blue color means moments are in -z direction and white means moments are in-plane.). 77

5.4 (a) For a ferromagnetic layer with a wedge on the left side of the magnet (looking in the +y direction) starting from the magnetic moments in the +x direction, driven by +x directed spins at the interface (Fig. 4.3a) if the system is allowed to evolve in the absence of spin torque (current pulse removed) the moments evolve such that in the majority of the magnet they point in the +z direction with the moments in the wedge aligned along the slope of the wedge in +x,+z direction as shown. This image shows the directions of the moments after the system was allowed to evolve for 1 ns after the removal of the spin torque (current pulse). (b) If the moments are allowed to evolve starting from -x direction, driven by -x polarized spins at the interface, (Fig. 4.3b) they finally point in the -z direction with moments in the wedge aligned along the surface of the wedge in -x,-z direction. (c) For a ferromagnetic layer with a wedge on the right side of the magnet (looking in the +y direction) starting from the magnetic moments in the +x direction, driven by +x directed spins at the interface, if the system is allowed to evolve in the absence of spin torque (current pulse removed) the moments evolve such that in the majority of the magnet they point in the -z direction with the moments in the wedge aligned along the slope of the wedge in +x,-z direction as shown. This image shows the directions of the moments after the system was allowed to evolve for 1 ns after the removal of the spin torque (current pulse). (d) If the moments are allowed to evolve starting from -x direction, driven by -x polarized spins at the interface, they finally point in the +z direction with moments in the wedge aligned along the surface of the wedge in -x,+z direction. (The plots are not drawn to scale in the z dimension. The direction of the moments is suggested by the head of the arrows. Also, red color means moments are in +z direction, blue color means moments are in -z direction and white means moments are in-plane.) 80

6.1 (a) The schematic describes the different stacks we used. Thickness of Ta layer below the ferromagnetic layer (CoFeB) is W_1 nm and thickness of Pt layer below it is W_1 nm, such that $W_1 + W_2 = 10$. (b) R_{AHE} versus out of plane magnetic field plot for Hall bars made from Si(substrate)/ SiO_2/ Ta(2 nm)/Pt (7 nm)/ Ta (3 nm)/ CoFeB(1 nm)/MgO(2 nm)/Ta(2 nm)) shows evidence of out of plane magnetic anisotropy. (c) Starting from an initial -z directed state (R_{AHE} = -0.045 Ω) a current pulse of a certain magnitude is applied in the presence of 100 G magnetic field in +x direction. The final R_{AHE} is measured. Then $\Delta R_{AHE} = R_{AHE,final} - R_{AHE,initial}$ and current density through Ta for the given current pulse flowing through the cross-section of the entire Hall bar are calculated.The magnet is reinitialized to -z state, another current pulse of different magnitude is applied and the same process is repeated. Finally, ΔR_{AHE} for the different current pulses is plotted against the current density through Ta for the current pulses. (d) We repeated the current pulsing experiment for different samples that had different widths of Ta and Pt layers, keeping the sum of the two constant ($W_1 + W_2 = 10$ nm). We observe that if the thickness of the Ta layer goes down or thickness of the Pt layer goes up, lower current density is needed to switch the magnet. 84
6.2 Current flowing in +x direction causes electrons with +y directed spins to go towards +z and -y directed spins to go towards -z. The opposite happens for Pt. Current flowing in +x direction drives electrons with -y directed spins to +z and +y directed spins to -z. 85
6.3 (a) Spin diffusion theory is used to simulate spin transport in a single layer of heavy metal (Ta here) of thickness W_1 in the presence of spin Hall effect. The figure shows the Ta layer which ranges from $z = 0$ to $z = W_1$. At the lower boundary ($z = 0$) spin current is 0 and at the upper boundary ($z = 0$ all the spins are absorbed by the ferromagnet above, and so the spin potential (difference between potential of +y and -y directed spins) is 0. (b) Spin current calculated at the upper boundary ($z = 0$) plotted against the thickness of the Ta layer ($W1$) shows saturation for a thickness which is much larger than the spin diffusion length (1.5 nm). 87

6.4 (a)A bilayer of Ta and Pt is shown for which the spin transport has been modeled. Ta ranges from $z = 0$ to $z = W_1$ while Pt ranges from $z = 0$ to $z = -W_1$. Thus thickness of Ta layer is W_1 and thickness of the Pt layer is W_2. (b) Current density through the Ta layer ($J_{x,1} = 10^6$ A/cm^2 is set equal to 1×10^6 A/cm^2 by keeping the electric field (E_x) that drives the current constant at 1.9×10^4 V/m ($J_{x,1} = C_1 E_x$). We see that as the thickness of the Ta layer goes down spin current also lowers and finally it reverses sign. This is because oppositely directed spins from Pt diffuse into Ta. (c) For three different combinations of Ta and Pt layers (7 nm Ta, 3 nm Pt; 5 nm Ta, 5 nm Pt; 3 nm Ta, 7 nm Pt) the current density is varied from 0 to 2×10^6 A/cm^2 by sweeping the electric field. As expected from the intuitive picture, when the thickness of Ta goes down and Pt goes up, larger current density through Ta needs to flow to generate the same amount of spin current density which will eventually switch the magnet. For example, in order to generate a spin current density of 10^5 A/cm^2 at the top surface of a bilayer of Ta and Pt, the current density that needs to flow through Ta is 8.2×10^5 A/cm^2 for a 7 nm thick Ta, 3 nm thick Pt bilayer (red plot) but it is equal to 1×10^6 A/cm^2 for a 3 nm thick Ta, 7 nm thick Pt bilayer (blue plot). Thus according to intuition and these calculations switching current density should go up for lower thickness of Ta but instead it goes down in the experiment (Fig. 6.1d) 89

Acknowledgments

I would like to thank my research adviser, Professor Sayeef Salahuddin, for his mentorship and guidance. It was a pleasure working with him. He was aware of every single detail of the projects I worked on and gave me advice whenever I needed. Yet he also gave me a lot of freedom to not only explore various areas of spintronics during my PhD but to spend time on courses of my liking so that I can develop a deeper understanding of science. His constant words of support and encouragement made my graduate school experience a lot more joyful. I am deeply grateful to him for whatever I have accomplished in my academic career so far.

I am also thankful to Professor Jeffrey Bokor, with whose group I collaborated for some of my projects. I have received constant support and words of encouragement from him as well. I would also like to thank Professor Irfan Siddiqi for being in my Qualifying Examinations committee and my Dissertation Committee, and Professor Vivek Subramanian for being in my Qualifying Examinations committee. I am also grateful to Dr. Dmitiri Nikonov of Intel Corporation who served as my Intel PhD Fellowship mentor.

Amongst my colleagues at UC Berkeley, I would like to particularly acknowledge the enormous support I have received from my collaborator, Dr. Long You, a postdoctoral researcher in Prof. Salahuddin's group. Long provided me with a lot of nanoscale magnetic devices that he fabricated in the Marvell nanolab of UC Berkeley. My projects would not have been successful without Long's nanofabrication skills. I would also like to express my gratitude to Mark Nowakowski who performed some magneto-optic Kerr effect experiments for my project. I am also indebted to Asif Islam Khan, Haron Abdel-Raziq, David Keating, OukJae Lee, Khalid Ashraf, John Heron, James Clarkson, Dominic Labanowski, Samuel Smith, Niklas Roschewsky, Weier Wan, Mihika Prabhu, Brian Lambson and Zheng Gu for collaboration and support.

I would like to thank the funding agencies: NSF Grants 1111733, 0939514, 1017575, NSF E3S Center, Berkeley STARNET FAME, DARPA NV Logic Program and Intel Ph.D. fellowship (2014-2015).

I would also like to thank my friends in Berkeley who made these last five years really pleasant. The times I spent with Aamod Shanker, Sebastian Schweigert, Haron Abdel-Raziq, Arka Aloke Bhattacharya, Justin Clune, Shrikant Kshirsagar, Ajay Yadav, Deepan Raj Prabhakar, Perri Al-Rahim, Alex Gonzalez Recuenco, Guillaume Wilemme, Hikaru Wakabayashi, Megumi Arita, Varun Mishra, Avinash Nayak, Robert Martin-Short, Akshay Pattabi and Waqas Khalid in this magnificent college town truly resulted in the expansion of my consciousness. Angik Sarkar, who currently works at Intel, deserves special credit for introducing me to the field of spintronics during my undergrad days and always finding time to discuss physics with me during the course of my Ph.D. Last but not the least, I would like to thank my parents, Mr. Prabir Bhowmik and Mrs. Dipa Bhowmik, and my grandparents, Mr. N.G. Bhowmik and Mrs. Anima Bhowmik, for their constant support and encouragement. Last five years, I have really missed them and also missed my house in Calcutta, India, where they still live together.

Chapter 1

Introduction

The present era is considered an era of information owing to the rapid advancement of computers, widespread use of the internet, the massive popularity of “smart” phones and the rise of the social networks. Computation has become more and more ubiquitous with computational units spreading from servers and desktop computers to laptops, tablets, mobile phones and even wireless sensors which are integrated with the environment. Complementary metal oxide semiconductor (CMOS) transistor is at the heart of a modern computational unit and the relentless downscaling of CMOS over past four decades has driven this information revolution.

The major challenge of CMOS scaling is power dissipation. Total power dissipation depends upon the density of transistors, the operation frequency and the square of the voltage of operation of the transistor. In the early days of CMOS scaling, with the reduction in the dimension of the transistor for every new technology generation, the density of transistors used to go up. The clock frequency also used to go up as a smaller channel length led to a higher on current of the transistor. The operating voltage also used to get scaled down with every generation to keep the power dissipation constant [1,2]. Thus we had higher performance computing with every new technology generation without increasing the power consumption. However, it is hard to reduce the operating voltage of the transistor below a certain value, owing to the fundamental physics of transistor operation. The sub-threshold swing, which is the slope of gate voltage versus drain current curve during on to off transition of a MOSFET, cannot go below 60 mV/decade, which is called the Boltzmann limit [3]. As a result, in order to have the off current of the transistor sufficiently low and the on current sufficiently high, the transistor needs to be operated at a relatively high voltage. Since operating voltage of the transistor could not be lowered, the operation frequency or the clock frequency was not increased beyond 3 GHz after 2005 [1,2,4]. Companies still shrink the transistor but with the operating voltage still stuck at about 1 V, increasing the operating frequency as in the past will cause unsupportable increase in power dissipation and heat generation [4]. As the transistor approaches its physical limits, researchers have identified the need to bring about fundamental changes in the operating physics of the transistor [3,4]

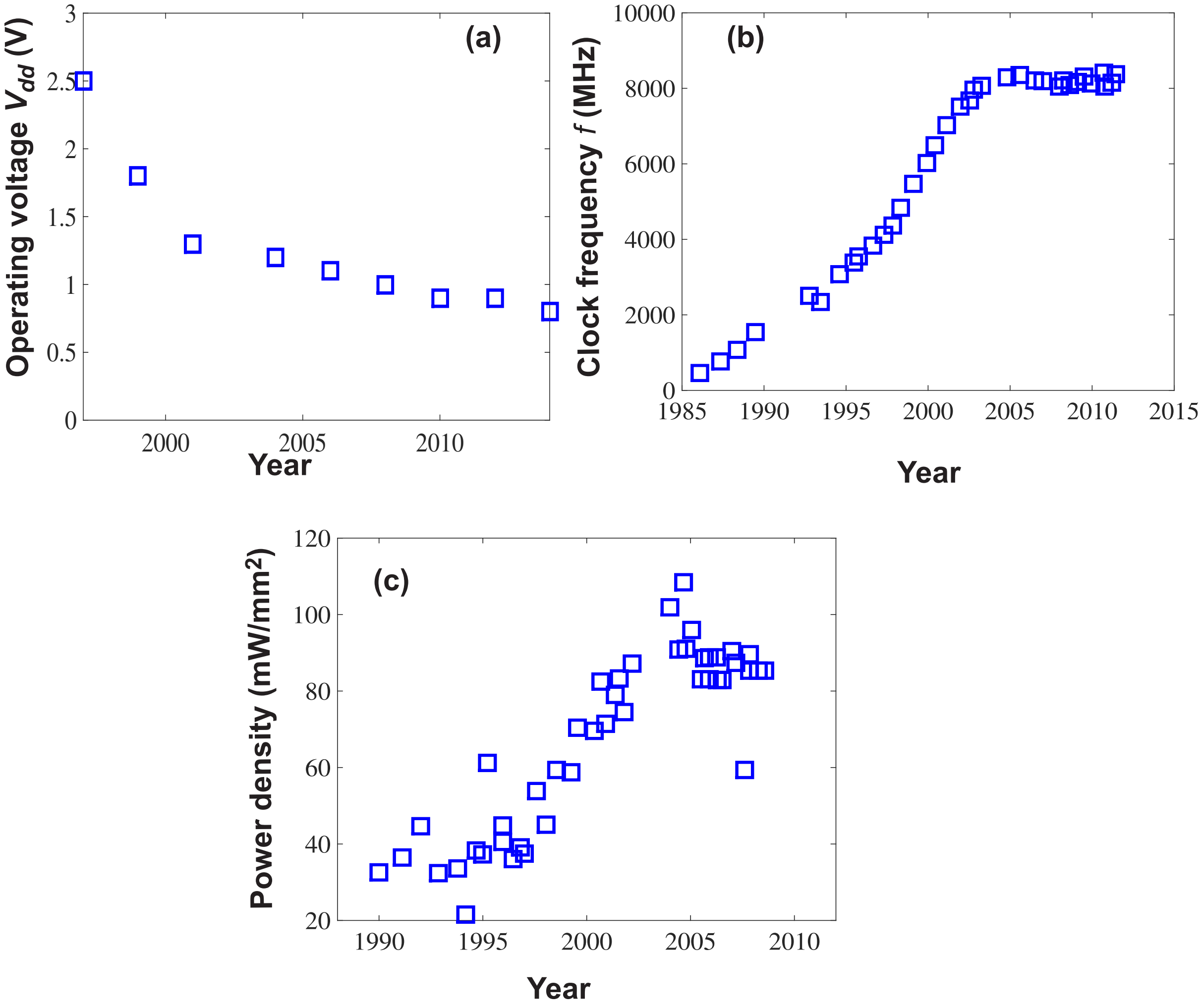

Figure 1.1: (a) Evolution of operating voltage of CMOS over time shows that it cannot be reduced below a certain limit. (b) Evolution of clock frequency over the last couple of decade shows that the clock frequency has reached a saturation. (b) Evolution of power consumption density over the last couple of decades shows a gradual increase. (Adapted from Danowitz *et al.* [2])

or replace the transistor with some different device altogether. Various types of devices have been explored in that regard and they are together referred to as “beyond CMOS” devices [5]. These devices promise to be less power consuming than a transistor. The demand for low power computing is also very high in the fields of mobile computing, medical device technology embedded to monitor the health of patients and wireless sensor networks.

In this thesis we choose one area in the field of "beyond CMOS" devices, which is spintronics, and try to solve some basic challenges in that area. Spintronics uses the dipole moment of a magnet to store information [5]. Computation takes place in a spintronic circuit by manipulating the magnetic moment, which typically involves a large magnetic field. It takes a large amount of current to generate such high magnetic field, thereby causing a lot of power dissipation. Spin transfer torque has emerged as a lower power alternative to magnetic field driven switching. However, the critical current needed to switch a magnet with spin transfer torque is still pretty high [6]. In this work, we have explored an alternative physical mechanism, known as spin orbit torque, to switch the dipole moment of the magnet. Apart from reducing the current consumption for switching in nanomagnetic logic, which is an example of "beyond CMOS" computing, spin orbit torque also promises to lower the power consumption in Magnetic Random Access Memory (MRAM) which is considered as an alternative to the charge based memories commercially available today- SRAM and DRAM.

Computing systems of today use a hierarchy of volatile and non-volatile memory. The part of the memory which is closest to the processor core, accessed frequently and hence has high speed is called cache memory [7]. Since the clock frequency of the processor has not increased significantly over the last decade, the trend has been to increase the number of cores and the cache capacity to enhance the processor performance. Cache memory is usually made of SRAM (Static Random Access Memory) which is a volatile memory and energy is consumed to retain the information in it. There have been two major issues with cache memory, the first being that SRAM based cache has a large leakage power loss and the second being SRAM occupies a large memory area especially for the last level cache (LLC), L3 cache for example [8]. Recently eDRAM is used as LLC, but it is difficult to be reduce its dimensions much and it also consumes a lot of power as it has a low retentions times and needs a frequent refresh operation. Spin Transfer Torque Magnetic Random Access Memory (STTMRAM), owing to its non volatile nature, has been considered an alternative to SRAM and eDRAM. Information is stored as the direction of magnetic moment of the "free" magnetic layer, data is written by switching the magnetization with a large current pulse through the tunnel junction that applies spin transfer torque on the magnetization and data is read by passing a small current through the same tunnel junction and measuring the tunneling magnetoresistance (TMR) signal. The power consumption of MRAM can be reduced by reducing the write current. Recent results show that STTMRAM can be superior to SRAM and eDRAM based cache memory both in terms of one bit area and write energy [8]. Spin orbit torque based magnetic switching, which we discuss in details in this thesis, has the promise of lowering the write current even further compared to conventional STTMRAM. Thus apart from potential application in computing, spin orbit torque has a potential application in memory and hence is an interesting phenomenon to study.

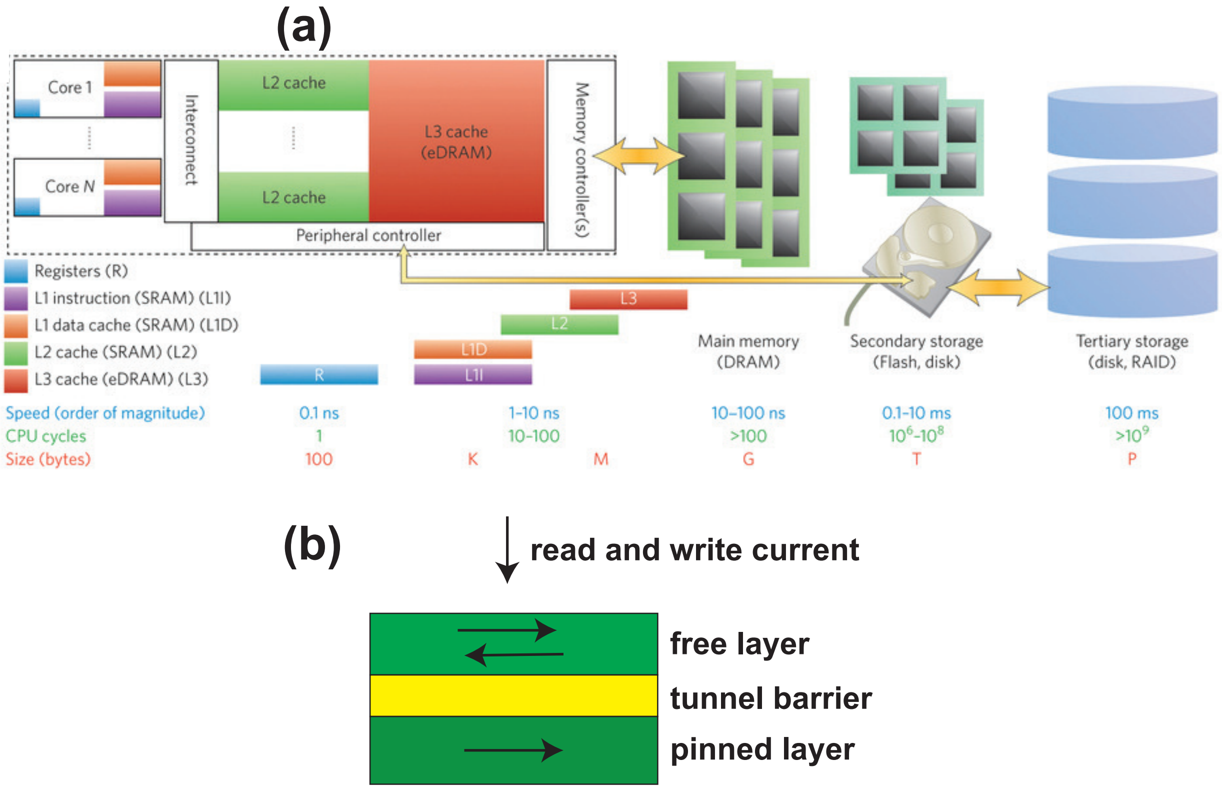
(a)
Core 1
Core N
Interconnect
L2 cache
L2 cache
L3 cache (eDRAM)
Memory controller(s)
Peripheral controller
Registers (R)
L1 instruction (SRAM) (L1I)
L1 data cache (SRAM) (L1D)
L2 cache (SRAM) (L2)
L3 cache (eDRAM) (L3)
R
L1D
L1I
L2
L3
Main memory (DRAM)
Secondary storage (Flash, disk)
Tertiary storage (disk, RAID)
Speed (order of magnitude)
CPU cycles
Size (bytes)
0.1 ns
1
100
K
1-10 ns
10-100
M
10-100 ns
>100
G
0.1-10 ms
10^6-10^8
T
100 ms
$>10^9$
P
(b)
read and write current
free layer
tunnel barrier
pinned layer

Figure 1.2: (a) Physical distribution and hierarchy of memory in a computer. The lower panel shows speed (as order of magnitude), number of processor (CPU) cycles needed to access the memory, and size of the different memories. (used from Wong, P. S. *et al.*[7] with permission) (b) Schematic of the basic unit of STTMRAM. Arrows inside the magnetic layers show direction of the moments. Moment of the pinned layer is always pointing right, but the moment of the free layer can be switched from left to right and right to left with spin transfer torque from the current flowing vertically through the tunnel junction. Data is stored as direction of moment of the free layer.

Apart from its potential applications, spin orbit torque driven magnetic switching is interesting from a fundamental physics perspective. Spin orbit torque occurs at the interface of a heavy metal and a ferromagnet. Electrons flowing through such a heterostructure experience spin orbit coupling and apply a torque on the magnetization of the ferromagnet. When the first experimental demonstrations of spin orbit torque based magnetic switching were reported [9,10] the physics behind such switching was largely unexplored and hence it became a topic of great interest and debate in the community of physicists and device physicists. In this thesis, in addition to demonstrating applications of spin orbit torque, we report our experiments and simulations that throw light on the physics of spin orbit torque driven magnetic switching.

The thesis is divided into 7 chapters.

i. *Chapter 1*: This chapter briefly surveys the current trends in computing and memory technology and states the application areas where spin orbit torque driven magnetic switching can be useful.

ii. *Chapter 2*: This chapter discusses the origin of spin orbit torque in ferromagnet-heavy metal heterostructures and reports the experimental results of other research groups that demonstrate spin orbit torque driven magnetic switching and magnetic domain wall motion. This puts our experimental and simulation results, discussed in the following chapters, in the proper perspective.

ii. *Chapter 3*: In this chapter, we report our experimental demonstration of magnetic switching driven by spin orbit torque and discuss the mechanism of the switching in details in the light of the single domain and micromagnetic simulations we performed to support our experimental results. We also report a new kind of domain wall motion, where the domain wall moves orthogonal to the current, which is only possible due to the unique symmetry of spin orbit torque.

iv. *Chapter 4*: In this chapter, we experimentally demonstrate that spin orbit torque can be used in nanomagnetic logic, an example of “beyond CMOS” logic, to reduce the power consumption by orders of magnitude and can thus provide a low power alternative to conventional CMOS based computing.

v. *Chapter 5*: In this chapter, we show micromagnetic simulations that explain the recent experimental results of our group, where a perpendicularly polarized ferromagnet is switched deterministically in the absence of any magnetic field altogether using spin orbit torque. This result makes spin orbit torque a potential alternative to conventional spin transfer torque for STTMRAM because it eliminates the need of an external magnetic field, which was necessary in previous experimental demonstrations of spin orbit torque driven switching.

vi. *Chapter 6*: This chapter shows that spin orbit torque experienced by a ferromagnet can be further enhanced by using a bilayer of two heavy metals with opposite polarities of spin orbit torque as opposed to one heavy metal. This new result can make spin orbit torque based switching even more energy efficient.

vii. *Chapter 7*: This chapter summarizes the key results made in the thesis and provides suggestions for future research in this area.

Chapter 2

Background Theory and Experiments

This chapter discusses the basic physics of spin orbit torque and how spin orbit torque in heavy metal/ ferromagnet heterostructures can be used to control the magnetization of the ferromagnet. It discusses relevant experiments performed by other research groups that show spin orbit torque driven magnetic switching and domain wall motion. Thus it puts our experiments on spin orbit torque driven switching, discussed in the following chapters, in perspective.

In spintronics, information is stored as the state of magnetization in ferromagnets. Application of these magnets for memory and logic applications involves switching the magnetization. If an external magnetic field is used to switch the magnetization, the power dissipation is very high because a lot of current needs to flow through a conducting material to generate a high magnetic field, thereby resulting in a large amount of Joule heating. Controlling ferromagnetic switching with spin polarized electrons through current injection has proven to be a lower power consuming and more scalable option compared to magnetic field driven switching [6]. In the last decade the conventional spin filtering and spin transfer torque mechanism have been used to manipulate the ferromagnet [6]. In a spin valve or a magnetic tunnel junction, as electrons pass through the pinned layer of the spin valve, they become spin polarized. When these electrons enter the free layer, they transfer spin angular momentum to the free layer and thus manipulate the magnetization of the free layer. This mechanism is the working principle of Spin Transfer Torque Magnetic Random Access Memory (STT-MRAM), which is expected to replace the existing semiconductor based RAM devices in near future. Spin transfer torque has also been used to move ferromagnetic domain walls with very low current pulses for racetrack memory [11]. When spin polarized electrons coming from a uniformly magnetized region impinge on a domain wall they try to align the moments of the domain wall in the direction of their own spin, resulting in domain wall motion. Either of these mechanisms needs a non-collinear configuration of the magnetic structure.

Recently an alternative mechanism of spin transfer torque is being explored where the spin orbit coupling of heavy metals or interfaces creates a non equilibrium density of spin polarized conduction electrons [9,10,12,13]. The non equilibrium spin density interacts with the magnetization of the ferromagnet through exchange coupling and thereby manipulates the magnetization for sufficiently high current density. This kind of spin transfer torque, where a non-collinear configuration of the magnetic structure is not necessary, is known as spin orbit torque. In the extensively studied system comprising a heavy metal/ ferromagnet/ oxide multilayer, spin orbit torque can have two different origins:

i. Rashba effect- When electrons flow through the ferromagnet, the presence of the heavy metal below and the oxide above creates an asymmetric crystal-field potential profile as a result of which electrons experience an electric field. From the reference frame of the electrons this electric field translates into a magnetic field due to relativistic effects. This is known as the Rashba spin-orbit interaction (SOI). Rashba SOI creates a non-equilibrium spin density of conduction electrons in the ferromagnet, which couples with the magnetic moment through exchange interaction and thus manipulate the magnetic moment of the ferromagnet.

ii. Spin Hall effect- When electrons with unpolarized spins flow through a layer of a heavy metal like platinum (Pt) or tantalum (Ta), which has a very high spin orbit coupling, electrons with spins polarized in opposite directions separate across the thickness of the layer due to spin Hall effect in the heavy metal. Thus a transverse spin current is generated from a charge current. Absorption of this spin current by the ferromagnetic layer neighboring the heavy metal results in the transfer of spin torque to the ferromagnet.

Section 2.1 of this chapter reviews the basic physics behind spin orbit torques originating from the Rashba effect and the spin Hall effect. Section 2.2 discusses the experimental measurement of magnetic switching in a heavy metal/ ferromagnet/ oxide multilayer due to the spin orbit torques and determination of the strength of the torques, performed by other research groups. This acts as a background material for the experiments and simulations we have performed in this area, which we discuss in Chapters 3,4 and 5 of this thesis. Section 2.3 discusses experiments, performed by other research groups, on spin orbit torque driven domain wall motion in magnetic wires. This puts our experiments on domain wall motion orthogonal to the current, reported in Chapter 3 of this thesis, in perspective.

2.1 Theory of spin orbit torque

When a particle travels at a speed comparable to the speed of light, an electric field in the laboratory frame transforms to a magnetic field in the rest frame of the particle [14]. The electric field in the laboratory frame of reference is $\vec{E}$ and the magnetic field is 0. Then the second-rank, antisymmetric field-strength tensor corresponding to $\vec{E}$ is:

$$F^{\alpha\beta} = \begin{bmatrix} 0 & -E_x & -E_y & -E_z \\ E_x & 0 & 0 & 0 \\ E_y & 0 & 0 & 0 \\ E_z & 0 & 0 & 0 \end{bmatrix}$$

Let a particle move at a velocity v in the x-direction in the laboratory frame of reference. Transformation from the laboratory frame of reference (K) to the rest frame of the moving particle (K') is given by the following Lorentizian transformation matrix:

$$A = \begin{bmatrix} \gamma & -\gamma\beta & 0 & 0 \\ -\gamma\beta & \gamma & 0 & 0 \\ 0 & 0 & 1 & 0 \\ 0 & 0 & 0 & 1 \end{bmatrix}$$

, where $\beta = \frac{v}{c}$ and $\gamma = \frac{1}{(1-\beta^2)^{\frac{1}{2}}}$ (c is the speed of light). The field strength tensor in reference frame K' is:

$$F'^{\alpha\beta} = AFA \begin{bmatrix} 0 & -E'_x & -E'_y & -E'_z \\ E'_x & 0 & -B'_z & -B'_y \\ E'_y & B'_z & 0 & -B'_x \\ E'_z & -B'_y & 0 & -B'_x \end{bmatrix} = \begin{bmatrix} 0 & -E_x & -\gamma E_y & -\gamma E_z \\ E_x & 0 & \gamma\beta E_y & \gamma\beta E_z \\ \gamma E_y & -\gamma\beta E_y & 0 & 0 \\ \gamma E_z & -\gamma\beta E_z & 0 & 0 \end{bmatrix}$$

Thus B'_x=0, B'_y=$\gamma\beta E_z$, B'_z=-$\gamma\beta E_y$ or the effective magnetic field experienced by the moving particle at its own reference frame is given by $\vec{B'} = -\frac{\gamma}{c}(\vec{v} \times \vec{E}) \simeq \frac{1}{c}(\vec{v} \times \vec{E})$ neglecting $(\frac{v}{c})^2$ term. If that particle is an electron, energy of the electron in this effective magnetic field is given by $-\vec{\mu}\vec{B'} = \frac{e}{mc}(\vec{s}.\vec{B'}) = \frac{\hbar e}{2mc}\vec{\sigma}.(\vec{v} \times \vec{E}) = \frac{\hbar^2 e}{2m^2c^2}\vec{\sigma}.(\vec{k} \times \vec{E})$, where $\vec{\mu}$ is the magnetic moment of the electron, $\vec{s}$ is the spin angular momentum of the electron, $\vec{\sigma}$ is the vector of the Pauli sigma matrix, m is the mass of the electron and $\vec{k} = \frac{m\vec{v}}{\hbar}$. The spin-orbit interaction term in the Hamiltonian (H_{SO}) is is this energy term with a correction factor of 2 known as the Thomas factor [15]. Thus,

$$H_{SO} = \frac{\hbar^2 e}{2m^2c^2}\vec{\sigma}.(\vec{k} \times \vec{E}) = -\eta_{SO}\vec{\sigma}.(\vec{k} \times \nabla V(r)) \tag{2.1}$$

where $\eta_{SO} = (\frac{\hbar}{2mc})^2$ is the SOI coefficient for vacuum and $V(r)$ is the potential acting on the electron. This SOI term is responsible for both Rashba effect and spin Hall effect in a heavy metal/ ferromagnetic metal/ oxide trilayer, the difference being that in the former case the electrons that experience the effective magnetic field from spin orbit coupling are the conduction electrons in the ferromagnet and in the latter case they are the conduction electrons in the heavy metal.

i. Rashba effect- When current passes through a heavy metal/ferromagnetic metal/ oxide trilayer, e.g. Pt/Co/AlOx, conduction electrons flowing through the ferromagnet experience an electric field perpendicular to the film plane (along z-axis) due to structural inversion asymmetry (SIA) [9,13]. In the rest frame of the electron the electric field transforms to a Rashba magnetic field (H_R), which is the cross product of the velocity of the electron ($\vec{k}$) and the electric field (Fig. 2.1a). The spin orbit coupling term in this case, known as the Rashba Hamiltonian, is given by: $H_{SO} = \alpha_r(\hat{z} \times \hat{k}).\vec{\sigma}$ (α_r is the spin orbit coupling efficiency) The conduction electrons also experience exchange interaction with the local moments of the ferromagnet. Thus the Hamiltonian of a conduction electron can be written as $H = \frac{\hbar^2 k^2}{2m} + H_{SO} + H_{ex}$ where H_{SO} corresponds to the spin orbit coupling and H_{ex} corresponds to the exchange interaction.

$$= \frac{\hbar^2 k^2}{2m} + \alpha_r(\hat{z} \times \hat{k}).\vec{\sigma} - J_{ex}\vec{M}.\vec{\sigma} \tag{2.2}$$

,where $\vec{M}$ is the magnetization of the ferromagnet and $J_e x$ is the exchange coupling coefficient. For a conventional 3d ferromagnetic metal $J_e x >> \alpha_r \hbar k_F$ where k_F is the Fermi momentum. As a result, spin of the conduction electron is parallel to the magnetization ($\vec{M}$) and thus effect of the Rashba term is equivalent to an effective magnetic field $\vec{H_{eff}} = -\alpha_r(\hat{z} \times \hat{k}) \propto \alpha_r(\hat{z} \times \vec{J})$ where $\vec{J}$ is the current density [16]. Thus the magnetic moment of the ferromagnetic metal experiences a Rashba effective field perpendicular to the current direction and the normal to the plane of the layers, which can help in switching the magnetic moment. A more exact solution of the system using the Boltzmann transport formalism also shows the existence of this Rashba field [13].

ii. Spin Hall effect- Apart from the Rashba effective field experienced by the ferromagnetic layer in the heavy metal/ ferromagnetic metal/ oxide trilayer, switching of the magnetic moment of the ferromagnetic layer can also be caused by the spin current injected into the ferromagnet from the heavy metal due to the spin Hall effect [10]. The origin of the spin Hall effect in the heavy metal is again due to spin orbit coupling experienced by the conduction electrons, but the source of the potential V(r) in equation (1) can be different. In extrinsic spin Hall effect, the potential of the impurities in the metal is the source of spin-orbit coupling [12,17]. If the impurity potential of a non-magnetic impurity in a metal is $u(\vec{r})$, it gives rise to an electric field $\vec{E} = \frac{1}{e}\vec{\nabla} u(\vec{r})$. An electron passing through this field with velocity $\vec{v} = \frac{\hbar}{im}\vec{\nabla}$ experiences spin orbit coupling: $\eta_{SO}\vec{\sigma}.(\nabla u(\vec{r}) \times \frac{\nabla}{i})$ (from equation (1)). In the presence of this spin orbit coupling it can be shown that an electron picks up an anomalous velocity ($\vec{\omega}^{\sigma}_{\vec{k}}$), which is spin dependent [17]. So the electron velocity is:

$$\vec{v}^{\sigma}_{\vec{k}} = \vec{v}_{\vec{k}} + \vec{\omega}^{\sigma}_{\vec{k}} = \frac{\hbar\vec{k}}{m} + \frac{\hbar}{2e}\theta_{SHE}(\vec{\sigma} \times \vec{v}_{\vec{k}}) \tag{2.3}$$

,where $\vec{v}$ is the usual velocity, $\vec{(\sigma)}$ is the spin polarization, and θ_{SHE} is the spin Hall angle. When electrons with unpolarized spins pass through the metal, due to the anomalous velocity

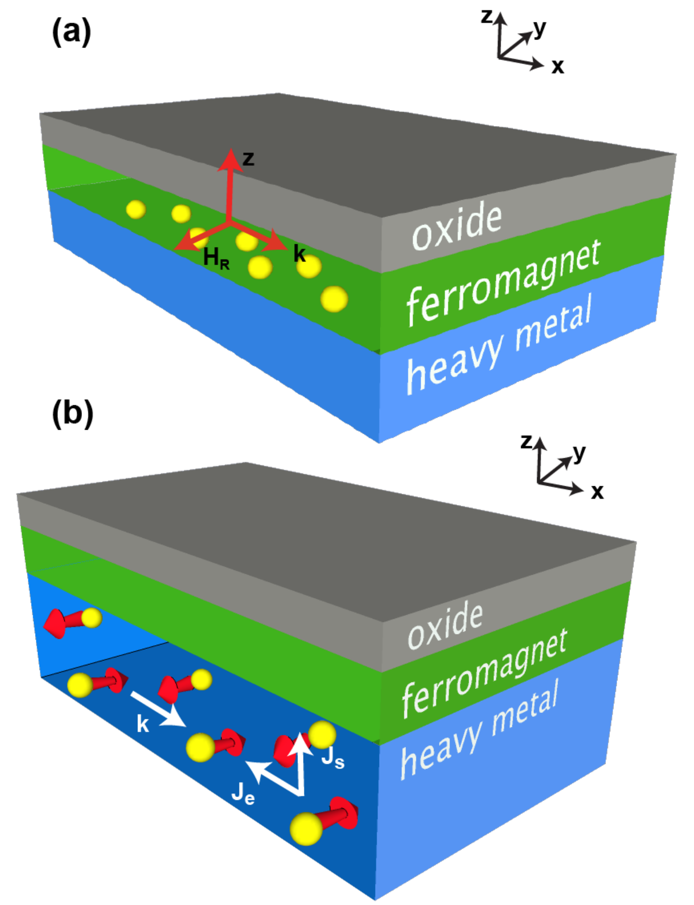

Figure 2.1: (a) Rashba effect- Conduction electrons in the ferromagnet moving with a velocity proportional to $\vec{k}$ (in +x direction here) experience an electric field along the z-axis due to structural inversion asymmetry at the interface, which transforms to an effective magnetic field $\vec{H_R}$ in the rest frame of the electron. (b) Spin Hall effect- Conduction electrons in the heavy metal moving with a velocity proportional to $\vec{k}$ (in +x direction here) drift either in +z or -z direction based on their direction of spin polarization. This results in creation of a spin current perpendicular to the charge current in the heavy metal.

term, the electrons will deflect one way or the other depending on the spin of the electrons (Fig 2.1b).Thus, the spin current is given by: $\vec{J_S} = \frac{\hbar}{2e}\theta_{SHE}(\hat{y} \times \vec{J_e})$, where $\vec{J_e}$ is the charge current density, proportional to $\vec{v_{\vec{k}}}$ of the electrons and $\hat{y}$ is the direction of spin polarization of the electrons at the top surface of the layer of heavy metal . Thus spin Hall angle is essentially the ratio of spin current to charge current and hence a measure of the efficiency of the material to generate spin polarized electrons from a charge current with unpolarized spins.

The spin Hall effect in metals can also be intrinsic in nature. It has been observed experimentally that the spin Hall angle of 4d and 5d transition metals like Nb, Ta, Mo, Pd and Pt changes sign based on the number of d electrons [18]. This is consistent with the theory of intrinsic spin Hall effect where the spin hall effect depends on the L-S coupling in the material [19,20]. The expectation value of the L-S coupling changes sign based on whether the d-shell of the atom is less than half filled or more than half filled, resulting in the change of sign of the spin Hall angle. In a stack of just the heavy metal with S.H.E. on the substrate, when current passes through the heavy metal spin current is generated in the bulk due to S.H.E. but boundary condition dictates that the spin current is zero at the top and the bottom surface. This implies that the spin Hall component of the spin current needs to be cancelled by another spin current. This other component is the spin diffusion current which flows opposite to the spin current as a result of a net spin accumulation across the thickness of the material given by: $\mu^{\uparrow}(z) - \mu^{\downarrow}(z) = D j_x \frac{C_h}{C^2} \frac{sinh(\frac{z}{D})}{cosh(\frac{w}{2D})}$, where $\mu^{\uparrow}(z)$ is the chemical potential for electrons with spin in +x direction and $\mu^{\downarrow}(z)$ is the chemical potential for electrons with spin in -x direction [21]. The spin diffusion current is proportional to $\vec{\nabla}(\mu^{\uparrow}(z) - \mu^{\downarrow}(z))$. Thus the total spin current is:

$$\vec{J_S} = \frac{\hbar}{2e}\theta_{SHE}(\hat{y} \times \vec{J_e}) + \vec{\nabla}(\mu^{\uparrow}(z) - \mu^{\downarrow}(z)) \tag{2.4}$$

If a layer of ferromagnetic metal exists on the top of the heavy metal, the spin current is not zero at the interface of the two metals. Rather the spin current is absorbed by the ferromagnetic metal. The spin-polarized electrons diffuse into the ferromagnet and align with the magnetization of the ferromagnet owing to its strong exchange coupling. This results in a spin torque on the ferromagnet equal to the spatial change of the spin current inside the ferromagnet compensated by the spin relaxation term: $\frac{1}{V}\int dV(-\vec{\nabla}.\vec{J_s} - \frac{1}{\tau_{SF}}\vec{M})$ where V is the volume of the ferromagnetic layer, $\vec{J_s}$ is the spin current, $\vec{M}$ is the magnetization of the ferromagnet and τ_{SF} is the spin relaxation time [22].

Thus, the Rashba effect at the interface and the spin Hall effect in the heavy metal are the two possible origins of the spin orbit torque experienced by a ferromagnetic layer when in-plane current flows through a heavy metal/ferromagnet/ oxide trilayer.

2.2 Experiments on spin orbit torque driven magnetization switching

Miron and colleagues reported the first observation of spin orbit torque experienced by a ferromagnet in a heavy metal/ferromagnet/ oxide trilayer [9,23]. A 0.6 nm thick Co layer was used as the ferromagnet and it was sandwiched between a 3 nm thick Pt layer (heavy metal) and a 1.6 nm Al layer, which was oxidized to form AlOx (oxide). Structural inversion asymmetry (SIA) due to the presence of Pt and AlOx on either side of the Co layer results in an electric field to be experienced by the Co layer. Due to the Rashba spin orbit interaction (SOI) effect discussed in Section I, the magnetic moments of the Co layer experience an effective Rashba magnetic field when an in-plane current flows through the Co layer (Fig. 2.1a). 0.5 μm wide and 5 μm long nanowires are fabricated from the Pt/Co/AlOx stack, which exhibits perpendicular magnetic anisotropy. Starting from a saturated state of the magnet in the out of plane direction, application of a current pulse at a zero magnetic field nucleates reverse polarized domains in the magnet. This is because the current pulse applies a field like torque on the magnet given by $\vec{M} \times \vec{H_R} = \vec{M} \times (\hat{z} \times \hat{j})$, where $\vec{H_R}$ is the effective in-plane Rashba field, $\hat{z}$ is the out of the plane z direction and $\hat{j}$ is the direction of the current. The in-plane $\vec{H_R}$ cannot break the symmetry and switch the magnet from out of the plane to into the plane but it can lower the barrier between the two states resulting in switching of some moments in the nanowire by thermal activation. Miron and colleagues further applied an external magnetic field perpendicular to the direction of the current pulse. They showed that the nucleation gets enhanced or suppressed based on the polarity of the applied field because the applied field adds to or subtracts from the Rashba effective field (Fig. 2.2b).

Miron and colleagues further demonstrated deterministic switching between up and down states of the magnet in a 500 nm by 500 nm square Co dot made from the same stack by applying current pulses parallel to an externally applied in-plane magnetic field Fig. 2.3) [24]. When the applied magnetic field is positive (along +x), a negative current pulse of magnitude 2.6 mA switches the magnet up while a positive current pulse of the same magnitude switches the magnet down. When the applied field is negative (along -x), a negative current pulse switches the magnet down and a positive pulse switches the magnet up (Fig. 2.3). They explained their result using an anti-damping torque experienced by the magnet, which has the form: $\vec{M} \times \vec{M} \times \vec{H_R} = \vec{M} \times (\vec{M} \times (\hat{z} \times \hat{j}))$, as opposed to the field like torque they used to explain their previous experimental results [9,23]. Since the efficiency of the bipolar switching increased with the increase of perpendicular anisotropy of the Co layer and the oxidation of the Al layer on top, they argued that the field like torque is an interface contribution and originates from the Rashba effect.

Liu and colleagues also obtained the same deterministic switching on microns wide Hall bars fabricated from the Pt (2 nm) /Co (0.6 nm) / AlOx stack but they explained their result using the concept of the spin Hall effect induced spin orbit torque [25]. Similar to the experiment by Miron et al., in the presence of an external magnetic field, a current pulse in the direction of the field generates hysteric magnetic switching between up ($M_z > 0$) and down states ($M_z < 0$) based on the polarity of the field. Switching the direction of the field changes the sense of the switching. In Fig.2.4 current pulse in +y direction creates an accumulation of electrons with spins polarized in the +x direction at the interface of the Pt layer with the Co layer. Under the assumption that the Co layer is uniformly magnetized (single domain assumption or the Stoner Wolfarth model) [25] and has a magnetization $\vec{M}$, the spin torque acting on the ferromagnet (Co layer) is given by: $\frac{\hbar}{2eM_st} J_s \vec{M} \times (\vec{M} \times \vec{\sigma})$ where

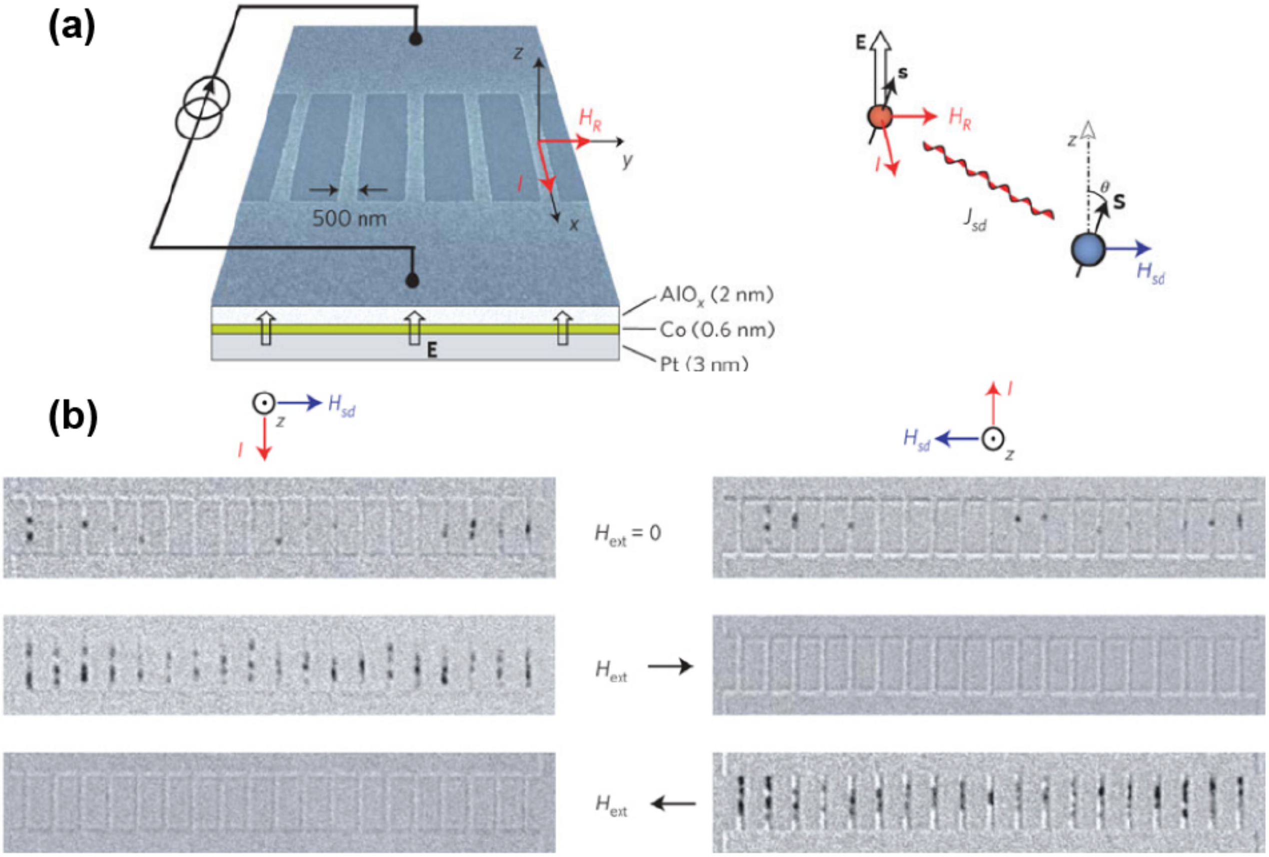

Figure 2.2: (a) When current flows through the 500 nm wide nanowires made from the Pt/Co/AlOx stack the conduction electrons experience a Rashba magnetic field $\vec{H_R}$ due to the electric field at the interface. Due to s-d exchange coupling between the conduction electrons and the local moments of the ferromagnet, the ferromagnet experiences an effective magnetic field $\vec{H_s}d$. (b) When a current pulse is applied on the nanowires at zero magnetic field, the $\vec{H_s}d$ experienced by the magnet nucleates reverse polarized domains in them (black patches in the images obtained by differential Kerr microscopy). The nucleation of reverse domains can be enhanced or suppressed by applying an external magnetic field $\vec{H_e}xt$ parallel or anti-parallel to $\vec{H_s}d$. (Reproduced from Miron *et al.* *Nature Mater.* 9, 230-234 (2010) [9].)

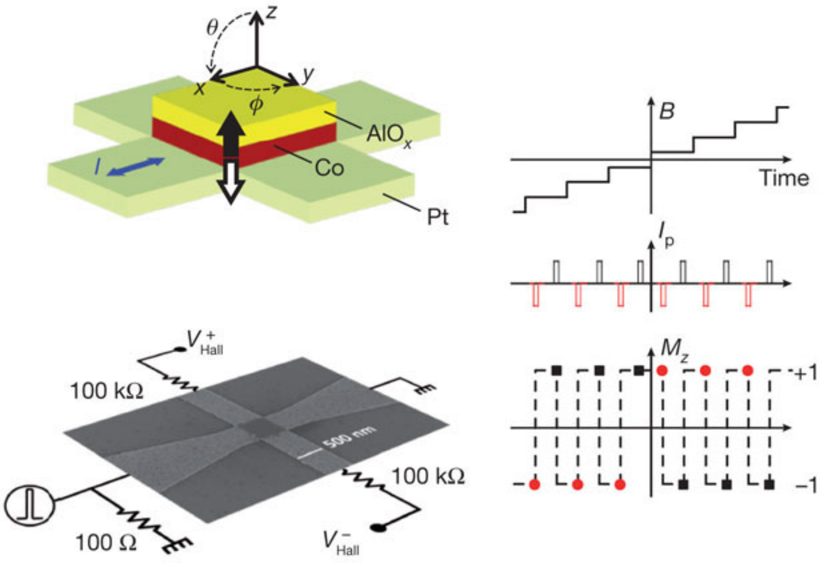

Figure 2.3: Current pulses are applied on a 500 nm by 500 nm dot made from the Pt/Co/AlOx in the presence of an externally applied magnetic field along the direction of the current. When the current pulse Ip is negative and the field is positive, the final magnetization is in the upward direction (M_z=1). When the current pulse Ip is positive, the final magnetization is in the downward direction (M_z=-1). When the current pulse Ip is negative and the field is negative, the final magnetization is in the downward direction (M_z=-1). When the current pulse I_p is positive, the final magnetization is in the upward direction (M_z=1). (Reproduced from Miron, I. M. *et al.* *Nature* 476, 189-194 (2011) [24].)

M_s is the saturation magnetization of the ferromagnet, t is the thickness of the ferromagnet, J_s is the spin current and $\vec{\sigma}$ is the direction of spin polarization of the electrons accumulated at the Pt-Co interface. If an external magnetic field ($\vec{H}$) is applied the torque due to the magnetic field is given by $\vec{M} \times \vec{M} \times \vec{H}$. Overall, the dynamics of the magnetization under the influence of the external magnetic field and the spin torque is given by the modified Landau Lifschitz Gilbert equation [25]:

$$\frac{d\vec{M}}{dt} = -\gamma(\vec{M} \times \vec{H}) - \frac{\gamma\alpha}{M}(\vec{M} \times \vec{M} \times \vec{H}) - \gamma\tau(\vec{M} \times \vec{M} \times \vec{\sigma}) \qquad (2.5)$$

When current flows in the +y direction creating spin polarization ($\vec{\sigma}$) in the +x direction, the magnetic field ($\vec{H}$) is in the +y direction and the magnetization is in +z direction, $\vec{M} \times \vec{\sigma}$ and $\vec{H}$ are of the same polarity (+y) and thus the two torque terms [$\vec{M} \times \vec{H}$ and $\vec{M} \times \vec{M} \times \vec{\sigma}$] add up resulting in making the magnetization orientation unstable. On the other hand, when the magnetization direction is -z direction, $\vec{M} \times \vec{\sigma}$ and $\vec{H}$ are of two opposite polarities and the two torque terms cancel making the orientation of the magnetization stable. Thus in presence of a magnetic field in +y direction a sufficiently high positive current pulse will switch the magnetization from up ($M_z > 0$) and down ($M_z < 0$). This intuitively explains the hysteric magnetic switching observed experimentally. Solving the modified LLG equation under the single domain assumption for the ferromagnet (equation 5) provides qualitative matching with the experimental result.

Liu and colleagues followed their experiments on Pt/Co/AlOx with similar experiments on microns wide Hall bars fabricated from the Ta (4 nm)/CoFeB (1 nm)/MgO (1.6 nm)/ Ta (1 nm) stack, which also exhibit perpendicular magnetic anisotropy [10]. Similar deterministic switching is also observed for Ta/CoFeB/MgO, but the handedness of the current induced hysteresis is opposite to that of Pt/Co (Fig. 2.5) and the switching current density is lower than Co/Pt. It made them conclude that the spin Hall angle (θ_{SHE}), or the ratio of the spin current to the charge current, for Ta is larger in magnitude and opposite in sign compared to Pt. The authors quantified the spin Hall angle of Ta by three different techniques, which yielded consistent results: spin torque driven ferromagnetic resonance on Ta/CoFeB ($|\theta_{SHE}| = 0.15$) current dependent shift in the magnetization versus magnetic field curves (Fig. 5) when the magnetic field is applied in-plane on perpendicularly polarized Ta/CoFeB/MgO Hall bars ($|\theta_{SHE}| = 0.12$) and spin torque switching of in-plane polarized Ta/CoFeB/MgO/CoFeB/Ta/Ru three terminal device ($|\theta_{SHE}| = 0.12$).

All these experiments show that when current $\vec{j}$ flows through a heavy metal/ferromagnet/ oxide multilayer, the magnetization of the ferromagnet $\vec{M}$ experiences a field like torque of the form $\vec{M} \times (\hat{z} \times \hat{j})$ and damping like torque, also called Slonczweski torque, of the form $\vec{M} \times \vec{M} \times (\hat{z} \times \hat{j})$ where $\hat{z}$ is the out of the plane z direction and $\hat{j}$ is the direction of the current. If $\vec{M}$ does not change significantly, the two torques can be expressed in the form of $\vec{M} \times \vec{H_{eff}}$ where $\vec{H_{eff}}$ is the effective field. Following that the field like torque can be expressed as a transverse effective field $\vec{H_T} = \hat{z} \times \hat{j}$ and is independent of the magnetization direction while the damping like torque can be expressed as a longitudinal effective field $\vec{H_L} = \vec{M} \times (\hat{z} \times \hat{j})$ and flips sign with switching of the magnetization. Kim and colleagues performed vector measurement of the longitudinal and transverse effective fields due to in-plane current in the Ta/CoFeB/MgO stack using the low frequency harmonic Hall voltage measurement technique [26,27]. They varied the thickness of the Ta layer below the CoFeB layer and showed that when the thickness of the Ta layer is higher than 1 nm, the transverse field $\vec{H_T}$ is around 3 times larger than $\vec{H_L}$. Emori and colleagues also measured $\vec{H_T}$ (400 Oe per 10^7 A/cm^2) to be larger than $\vec{H_L}$ (200 Oe per 10^7 A/cm^2) in Ta/CoFe/MgO multilayer [28]. In the Pt/CoFe/MgO stack, $\vec{H_T}$ is measured to be 20 Oe per 10^7 A/cm^2 and is lower than $\vec{H_L}$, which is measured to be 50 Oe per 10^7 A/cm^2.

As discussed before, Rashba effect at the interface and spin Hall effect in the bulk of the heavy metal are the two possible origins of the field like torque and the damping like torque, or the transverse and longitudinal effective fields. However which effect has the dominant

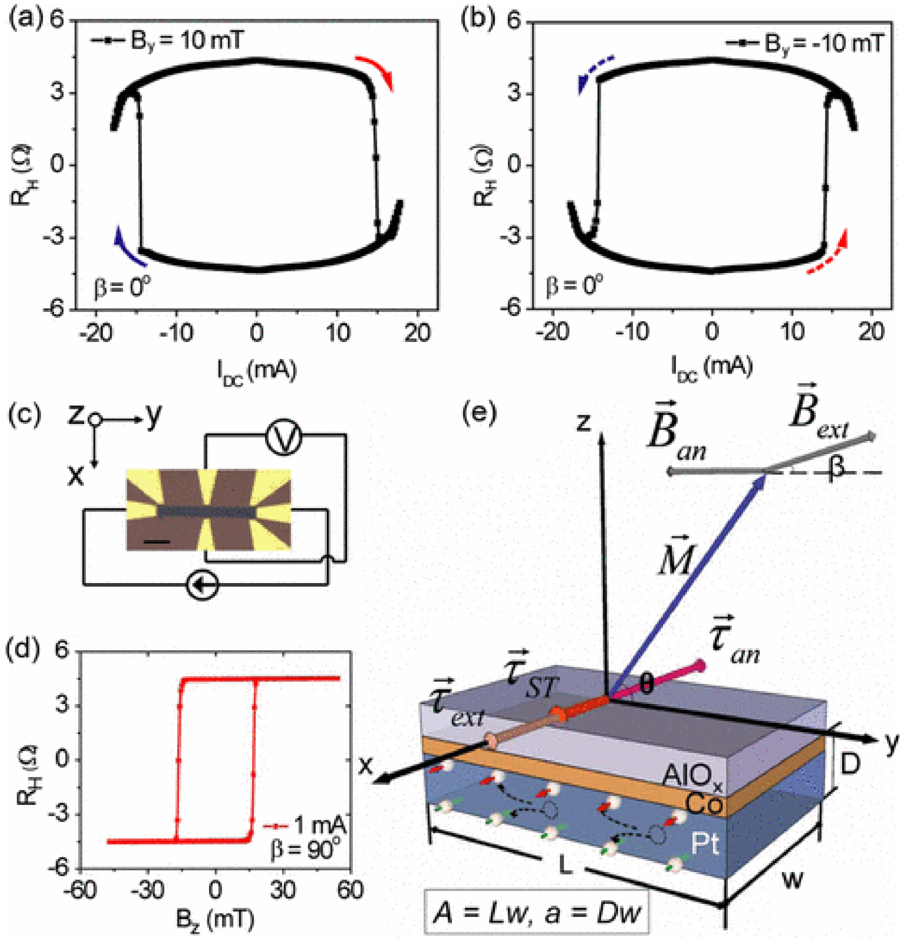

Figure 2.4: Hall bars are fabricated from the Pt/Co/AlOx stack, exhibiting perpendicular anisotropy. The ratio of the Hall voltage measured to the current applied gives the anomalous Hall resistance R_H, which is 4.5 Ω when the magnetization of the Co layer is up (M_z = 1) and -4.5 Ω when the magnetization of the Co layer is down (M_z = -1) (c,d). Plot of RH versus current flowing through the Hall bar (I_{dc}), in the presence of external magnetic field, shows a hysteresis behaviour. For a positive field of 10mT in +y direction, positive current supports negative (in z) magnetization and negative current supports positive magnetization. For a field of 10mT in -y direction, positive current supports positive (in z) magnetization and negative current supports negative magnetization (a,b). This result is consistent with the result obtained by Miron *et al.* (Figure 3). Current flowing through Pt creates an accumulation of spin-polarized electrons at the Pt/Co interface. The final direction of the magnetization is the cross-product of the externally applied magnetic field ($\vec{B_{ext}}$) and the spin polarization of the electrons at the interface ($\vec{\tau_{ext}}$). (Reproduced from Liu *et al.* *Phys. Rev. Lett.* 109, 096602 (2012) [25].)

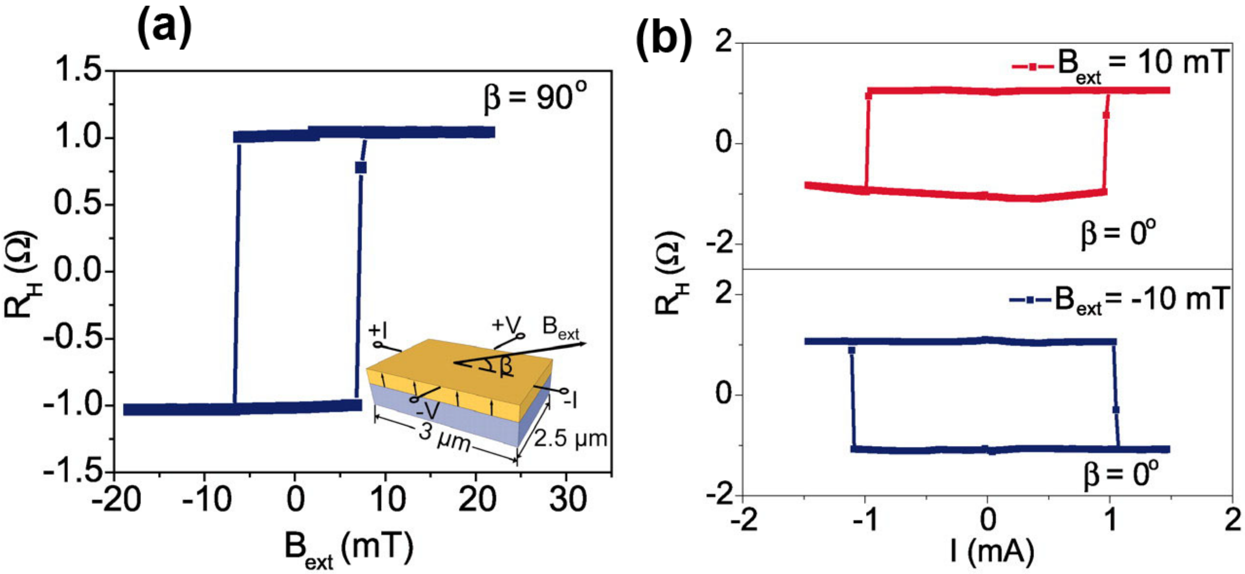

Figure 2.5: (a) Hall bars are fabricated from the Ta/CoFeB/MgO stack, exhibiting perpendicular anisotropy. The ratio of the Hall voltage measured to the current applied gives the anomalous Hall resistance R_H, which is 1 Ω when the magnetization of the CoFeB layer is up ($M_z = 1$) and -1 Ω when the magnetization of the CoFeB layer is down ($M_z =$ -1). (b) Plot of R_H versus current flowing through the Hall bar (I_dc), in the presence of external magnetic field, shows a hysteresis similar to the Co/Pt/AlOx stack, but the sense of the hysteresis is reversed because the direction of spin polarization of the electrons at the Ta/CoFeB interface is opposite to that of Pt/Co interface for the same polarity of current. Thus even in this case, the final direction of the magnetization= externally applied magnetic field × direction of spin polarization at the interface. (Reproduced from Liu *et al.* *Science* 336, 555-558 (2012) [10].)

contribution to the field like torque and which effect gives rise to the damping like torque is still a subject of debate and needs further investigation [29,30,31,32,33]. Haney *et al.* use the Boltzmann equation and drift-diffusion formalism to calculate the spin orbit torques in a bilayer system of a ferromagnetic metal and a non- magnetic metal [22]. When they include only the spin Hall effect from the non-magnetic/ heavy metal in their calculation, they obtain the damping like torque to be high and the field like torque negligible (Fig. 6). When they only include the Rashba interaction at the interface between the ferromagnetic metal and the non-magnetic metal in their calculation, they obtain the damping like torque to be negligible and the field like torque to be high (Fig. 2.6). However they also argue that the Rashba effect and the spin Hall effect can coexist in these systems without interfering with each other thus giving rise to field like torque and damping like torque terms simultaneously, both of which have been measured experimentally by Kim et al. [27] and Emori et al. [28].

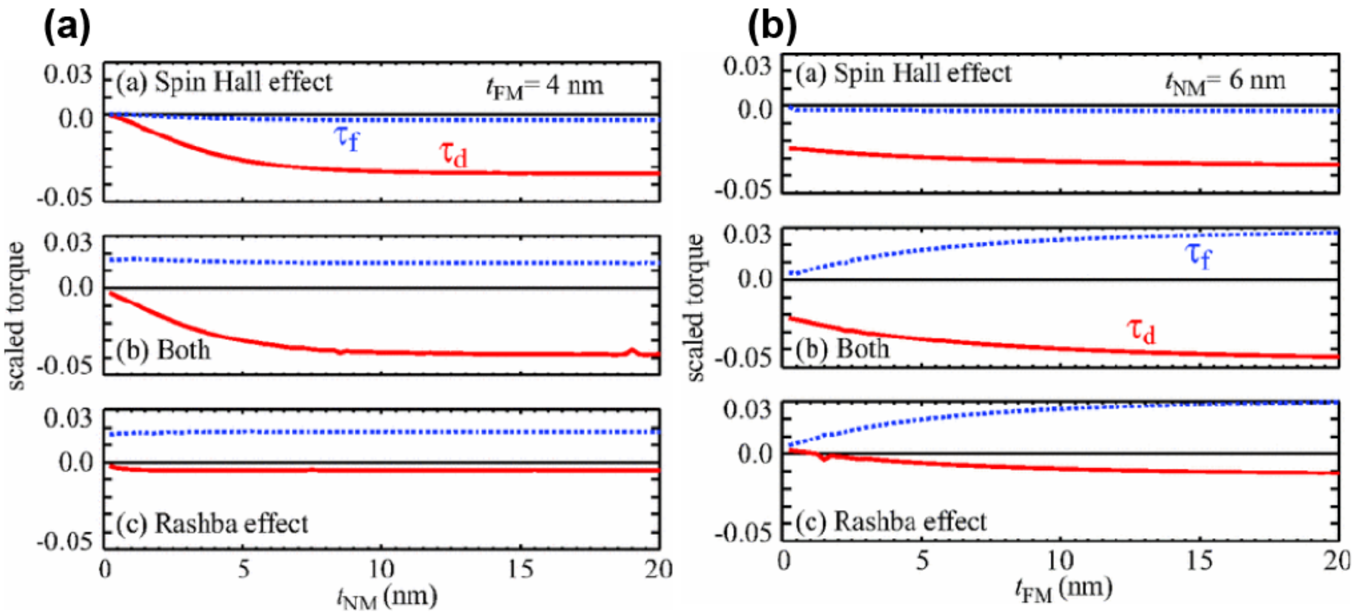

Figure 2.6: (a) Calculations performed by Haney *et al.* show that for different thicknesses (t_{NM}) of the normal metal (also called heavy metal in literature) in the normal metal/ferromagnetic metal system, the damping like torque (τ_D) is high while the field like torque (τ_F) when the spin Hall effect of the normal metal is only considered. When the Rashba effect at the interface is considered only and spin Hall effect is neglected, the damping like torque (τ_D) is negligible while the field like torque (τ_F) is high. (b) Calculations for different thicknesses (tFM) of the ferromagnetic metal also show similar results. (Reproduced from Haney, P. M. *et al. Phys. Rev. B.* 87, 174411 (2013).[29])

But Garello et al. [30] recently showed experimentally that the spin orbit torque terms in these systems are more complicated than the $\vec{M} \times (\hat{z} \times \hat{j})$ and $\vec{M} \times \vec{M} \times (\hat{z} \times \hat{j})$ terms, obtained by Rashba effect and spin Hall effect models considered this far. Thus they find a calculation on the torques based on a more realistic description of the electron structure necessary.

Though the macroscopic/ single domain model proposed by Liu *et al.* [10,25] provides a qualitative match with the experimental results, it does not provide a quantitative match. This is because magnetic switching in this kind of heterostructures that exhibit perpendicular magnetic anisotropy usually occurs via a complex mechanism that involves nucleation of reverse domains followed by domain wall motion. Spin orbit torque controls such domain wall motion, thereby controlling the switching. In Chapter 3 we will provide our own experimental results connected to magnetic switching in Ta/CoFeB/MgO heterostructures and a detailed microscopic analysis of the switching. Also, Liu *et al.* [10,25] and Miron *et al.* [9,24] show magnetic switching in the presence of spin orbit torque and in-plane magnetic field. In

Chapter 3, we will also report switching in the presence of spin orbit torque and out of plane magnetic field.

2.3 Experiments on spin orbit torque driven domain wall motion

A domain wall formed in a ferromagnetic layer exhibiting perpendicular magnetic anisotropy is of two types- Bloch wall and Neel Wall. In a Bloch wall, the magnetic moment rotates from +z to -z by curling towards +y axis or -y axis when one travels across the domain wall (x-axis) (Fig. 2.7a). In a Neel wall magnetic moment goes from +z to -z by rotating in the x-z plane (Fig. 8a). Bloch walls avoid magnetostatic charge ($\vec{\nabla}.\vec{M} = \frac{\nabla M}{\nabla x} = 0$) other than on the surface. So Bloch walls are energetically more favorable than Neel walls in wide structures made from the multilayer stack exhibiting perpendicular anisotropy but probably not in nanostrips where the ratio of the surface to the bulk is significantly higher than wide structures. Recently an asymmetric exchange interaction term, known as the Dsyaloshinskii- Moriya Interaction (DMI) has been proposed to contribute to the energy of this kind of systems- a ferromagnetic layer sandwiched between a heavy metal and an oxide [28,34,35,36,37]. For the heavy metal/ ferromagnet interface considered here, the DMI term adds to the total energy of the system in the following form: $-\vec{D_{ij}}.(\vec{M_i} \times \vec{M_j})$, where $\vec{M_i}$ and $\vec{M_j}$ are the magnetization vectors of two adjacent moments in the ferromagnetic layer and $\vec{D_{ij}}$ is the vector on the plane of the film, shown in Fig. 2.7b [35]. As a result of this term, a Neel wall of a specific handedness (left or right, based on the sign of $\vec{D_{ij}}$) may end up having lower energy compared to a Bloch wall in magnetic nanowires and become the dominant domain wall in the system.

To investigate the nature of the domain walls in the heavy metal/ferromagnet/oxide system, Emori and colleagues fabricated 500 nm wide and 40 μm long wires from a Pt/CoFe/MgO and a Ta/CoFe/MgO stack, both exhibiting perpendicular magnetic anisotropy, injected a domain wall locally in the wires and observed its motion under the application of current pulses with a polar MOKE microscope (Fig. 2.8a) [28]. They observed that the domain wall propagation is hindered in the electron flow direction in Pt/CoFe/MgO and assisted along the electron flow direction in Ta/CoFe/MgO (Fig.2.8a). They argue that the domain wall moves under the influence of an effective out of plane field experienced by the domain wall, which is given by the cross-product of the average magnetization in the domain wall $\vec{M_{avg}}$ and the spin polarization at the interface due to spin Hall effect $\vec{\sigma}$. Since the current flows across the domain wall, the domain wall needs to be a Neel wall for the average magnetization to be perpendicular to the spin polarization vector $\vec{\sigma}$ resulting in a non-zero out of plane effective field. DMI makes Neel wall energetically stable and provides a handedness to the rotation of the magnetic moments within the domain wall, as a result of which both up/down and down/up domain walls move in the same direction (Fig.2.8b). Since the

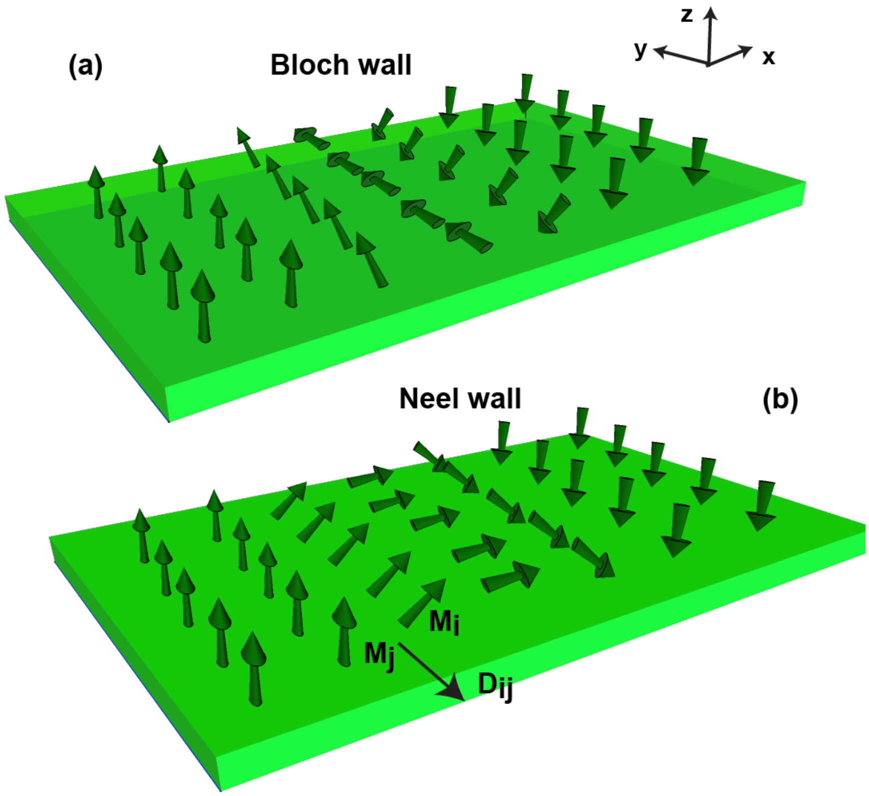

Figure 2.7: (a) Configuration of the magnetic moments inside a ferromagnetic domain wall of the Bloch type is shown. As one moves across the domain wall (in +x direction) the moment transitions from out of plane (+z) to into the plane (-z) by rotating in the yz plane. (b) For the Neel wall, the moment transitions from +z to -z by rotating in the xz plane. The chirality of the domain wall is determined by the direction of the vector ($\vec{D_{ij}}$) where i and j refer to two adjacent sites for magnetic moments. This is because Dzyaloshinskii Moriya interaction dictates ($\vec{M_i} \times \vec{M_j}$ to be parallel to $\vec{D_{ij}}$).

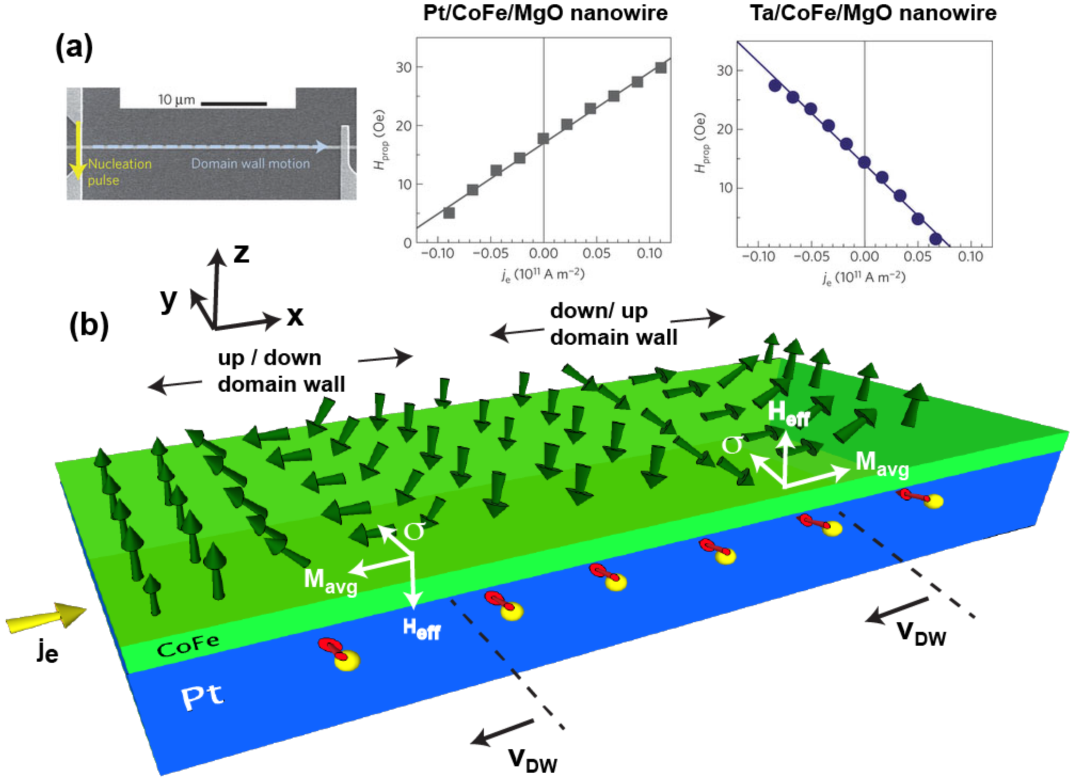

Figure 2.8: (a)A domain wall is injected at the end of 500 nm wide nanowires made from Pt/CoFe/MgO and Ta/CoFe/MgO stack exhibiting perpendicular magnetic anisotropy. The out of plane magnetic field needed to propagate the domain wall along the wire (H_{prop}) is measured as a function of the electron current (j_e) along the wire. For Pt/CoFe/MgO nanowire a higher field is needed to propagate the wall when j_e is positive (electrons flow along the direction of propagation of the wall) and lower field is needed to propagate the wall when j_e is negative. Thus the domain wall is hindered in the electron flow direction for a Pt/CoFe/MgO nanowire. On the other hand for a Ta/CoFe/MgO nanowire, the propagation field is lower for positive j_e , which means domain wall motion is assisted in the direction of electron flow. (b) For a Pt/CoFe/MgO nanowire, the domain wall is of Neel type and the moment rotates inside the domain wall following a left handed chirality. Electron current j_e in +x direction causes accumulation of electrons with spin polarization ($\vec{\sigma}$) in +y direction. For the up/down domain wall, the average magnetization of the wall ($\vec{M_{avg}}$) is in -x direction. So the wall experiences an effective out of plane field ($\vec{H_{eff}}$), given by $\vec{M_{avg}} \times \vec{\sigma}$ in -z direction which moves the domain wall in -x direction. Similarly for the down/up domain wall, $\vec{M_{avg}}$ is in +x direction and $\vec{H_{eff}}$ is in +z direction, which makes the wall move in the -x direction. (Reproduced from Emori *et al.* *Nature Mater.* 12, 611-616 (2013) [28].)

direction of spin polarization of the electrons accumulated at the Ta/CoFe and Pt/CoFe interfaces is opposite, the direction of effective field is opposite and hence the domain wall moves in opposite directions for Ta/CoFe and Pt/CoFe for the same direction of the current pulse. Ryu and colleagues also measured the domain wall velocity in nanowires fabricated from Pt/Co/Ni/Co and ascribed the domain wall motion to a combination of DMI and spin orbit torque due to spin Hall effect [34].

The domain wall, controlled by spin orbit torque, in the experiments performed by Emori *et al.* [28] and Ryu *et al.* [34] is transverse in nature, i.e., it lies along the width of the magnetic nanowire and current flows across the domain wall. Conventional spin transfer torque acts on such a domain wall apart from spin orbit torque. In order to isolate conventional spin transfer torque from spin orbit torque and make sure that only spin orbit torque acts on the domain wall, we have created longitudinal domain walls in microns wide bars made from Ta/CoFeB/MgO stack that exhibits perpendicular magnetic anisotropy. We have shown a new kind of domain wall motion where current flows along the domain wall and the longitudinal domain wall moves orthogonal to it. We report our experiments and micromagnetic simulations on such domain wall motion in Chapter 3 of the thesis.

Chapter 3

Microscopic mechanism of spin orbit torque driven magnetic switching and domain wall motion

In this chapter, we discuss the magnetic switching and domain wall motion experiments we performed in our laboratory and compare them with the experiments performed by other groups, which we discussed in the previous chapter. Experiments reported by other groups showed magnetic switching in the presence of spin orbit torque and in-plane magnetic field. Here we report spin orbit torque driven switching results in the presence of in-plane magnetic field as well as out of plane magnetic field. We use a simple macrospin/ single domain model to explain the result qualitatively. Then we explain why such a simple model cannot explain the physics of the switching and develop a micromagnetic model of the switching that captures the physics better and provides a much better quantitative match with the experiments than a single domain analysis. We also show a new kind of domain wall motion utilizing the unique symmetry of the spin orbit torque where a longitudinal domain wall moves orthogonal to the direction of current flow. We explain such domain wall motion with our micromagnetic model.

3.1 Spin orbit torque driven magnetic switching in the presence of out of plane magnetic field

In a Ta-CoFeB-MgO heterostructure, in plane current flowing through Ta in +y direction separates electrons with +x and -x directed spins across the thickness of Ta (Fig. 3.1) [10]. This causes accumulation of electrons with +x spin polarization (red arrows) at the Ta-CoFeB interface, which applies a spin orbit torque on the magnetization and drive the magnetizations in-plane from out of the plane (+z) direction. As a result a smaller -z directed field is needed to switch the magnetization from +z to -z in the presence of spin orbit torque compared to in the absence of spin orbit torque. Thus flow of current through the Hall bar

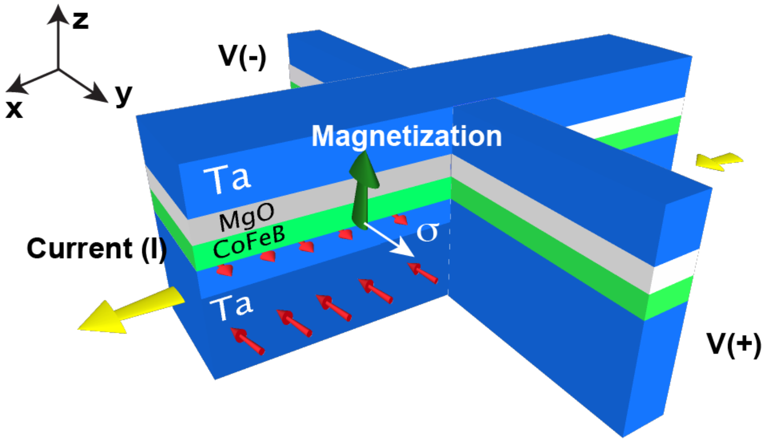

Figure 3.1: Schematic shows the origin of spin orbit torque due to flow of current in perpendicularly polarized ferromagnet (CoFeB) / heavy metal (Ta) heterostructures. It also shows the device geometry for anomalous Hall effect (AHE) measurements on these thin film stacks.

reduces the coercivity of the CoFeB layer. We next show experiments that demonstrate the reduction of the coercivity.

Thin films of thermally oxidized Si substrate/Ta (10 nm)/CoFeB(1 nm)/MgO(1 nm)/Ta(10 nm) (from bottom to top) are deposited through sputtering on Si substrates. The bottom Ta layer acts as the heavy metal layer, CoFeB acts as a ferromagnet, CoFeB-MgO interface provides perpendicular magnetic anisotropy to the ferromagnet [38,39] and the top Ta layer acts as a capping layer. Hall bars of length 500 microns and width 20-40 μm for wider bar and 5 μm for narrower bar are fabricated from that stack (Fig. 3.1). Magnetic properties of the devices are characterized through anomalous Hall effect (AHE) measurement. Current is injected into the wider Hall bar and voltage is measured from narrower bar (Fig 3.1), the ratio between voltage and current being the anomalous Hall resistance ($R_{AHE} = (V_+ - V_-)/I$) which is proportional to the out of plane magnetization of CoFeB.

When the current flowing through the device is very small and magnetic field is varied in the out of plane direction, we observe square hysteresis loop with coercivity of 60 gauss. It shows that the magnetic thin film exhibits perpendicular magnetic anisotropy [38]. When more current flows through the device coercivity of the magnet is reduced. Coercivity can be modulated from 60 gauss to 2 gauss by varying the current density from 0.25×10^6 A/cm^2 to 3.75×10^6 A/cm^2 at room temperature (Fig. 3.2a). The effect is independent of direction of current (+x or -x) as shown in Fig. 3.2b. We observe similar effect in various devices with different areas of cross section. From an average linear fit of plots of coercivity vs current

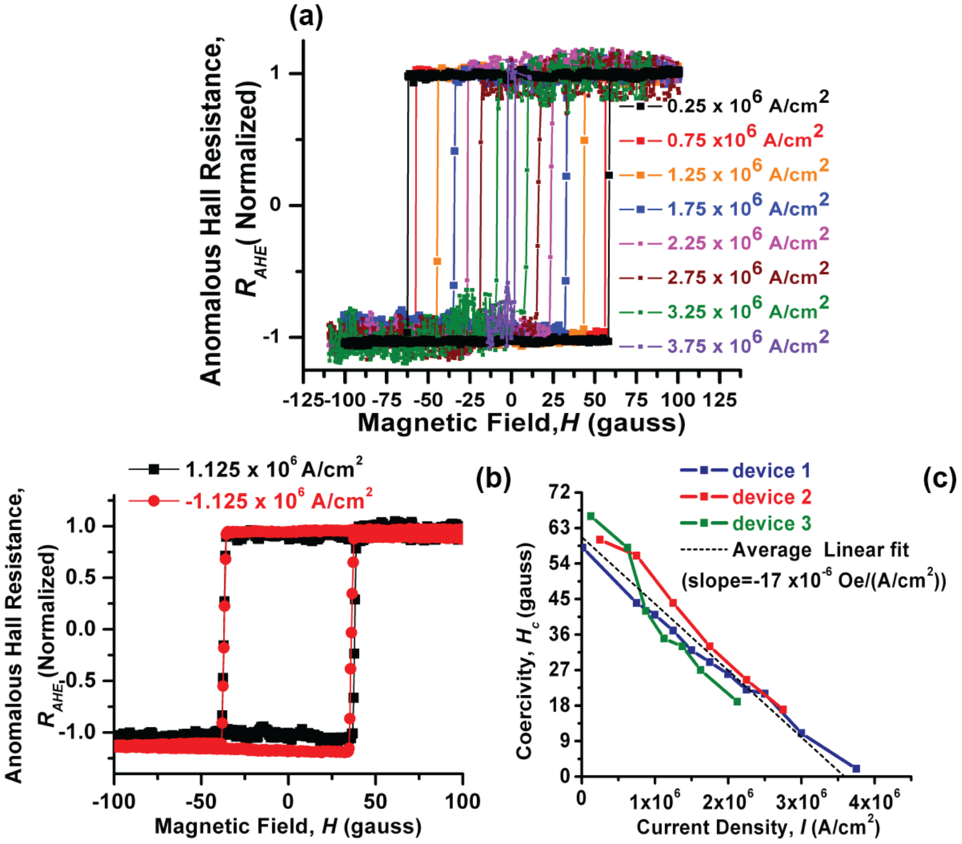

Figure 3.2: (a) Anamolous Hall Resistance is normalized to correspond to the out of plane magnetization component of CoFeB and plotted against the magnetic field applied in perpendicular direction. At very low current density, the AHE response shows that the magnet has its easy axis out of plane with coercivity of 60 Oe. As more current flows through Ta, coercivity of CoFeB is reduced. (b) Reversing the direction of current reverses the direction of spin torque, but does not break any symmetry in out of plane direction. So coercivity change should be similar for positive and negative currents as observed in our experiments. (c) For an average of three devices, coercivity of 1 nm layer of CoFeB decreases linearly with increase in current density following a slope of -17×10^{-6} Oe/(A/cm^2) or -17 gauss per 10^6 A/cm^2 through Ta.

density for three such devices, we find out that for increase of current density in Ta by 10^6 A/cm^2 coercivity decreases by approximately 17 gauss (Fig. 3.2c).

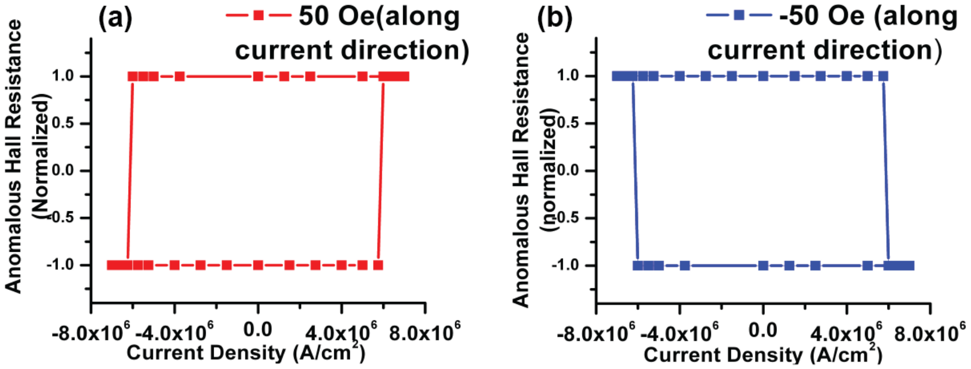

Figure 3.3: In-plane magnetic field breaks the symmetry with respect to spin torque and its direction determines whether up or down magnetization would be stabilized for given polarity of spin torque. So we observe experimentally through AHE measurements a hysteric magnetic switching for applied in-plane current and the curve is either left handed (a) or right handed (b) based on direction of magnetic field.

3.2 Spin orbit torque driven magnetic switching in the presence of in plane magnetic field

To verify that the modification of magnetic properties observed is not an effect of Joule heating or Oersted field, generated by the current, we observe the dependence of magnetization on the polarity of current in the presence of an in-plane magnetic field along the direction of current. We observe a hysteric switching of magnetization with current when 50 gauss of magnetic field is applied along the direction of current (+x direction in Fig. 3.1). Positive polarity of current (+x direction in Fig.3.1) beyond a certain magnitude ($5 \times 10^6 A/cm^2$) switches the magnet upward ($R_{AHE} = 1$) while negative polarity of current (-x) beyond that magnitude switches the magnet downward ($R_{AHE} = -1$) (Fig. 3.3a). On the other hand when -50 gauss of magnetic field is applied along the direction of current (-x direction in Fig. 3.1) , negative current switches the magnet upward while positive current switches the magnet downward (Fig. 3.3b). Thus in-plane magnetic field breaks the symmetry of the system and causes deterministic switching due to spin orbit torque. This peculiar nature of magnetic switching, based on the polarity of current and the polarity of the magnetic field applied along current direction, cannot be an effect of thermal or Oersted field based switching. It is to be noted that the direction of the switching is consistent with the results obtained by Liu *et al.* on Ta/CoFeB/MgO samples ([10] which we have reported in the previous chapter (Fig. 2.5).

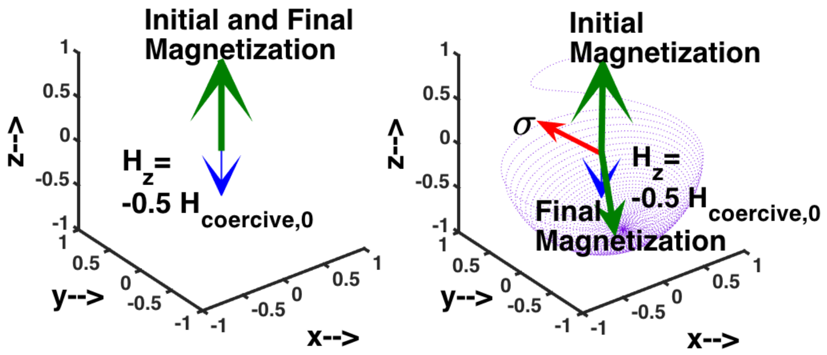

Figure 3.4: (a)The magnetization being initially upward (+z), in the absence of spin torque, application of downward magnetic field equal to half the coercive field ($H_{coercive,0}$) is unable to switch the magnet to down(-z) as expected. (b) However in the presence of in-plane spin torque with strength half that of $H_{coercive,0}$ the same value of applied magnetic field can switch the magnet from +z to -z direction.

3.3 Macrospin modeling of spin orbit torque driven magnetic switching

We verify our experimental results through Landau Lifschitz Gilbert equations based modeling of the system where we assume that the CoFeB layer is uniformly magnetized or is a giant macrospin (single domain assumption or the Stoner Wolfarth model) [40] has a magnetization $\vec{M}$. Spin orbit torque acting on the ferromagnet (CoFeB layer) due to current flowing through the heavy metal (Ta layer) is given by: $\tau\vec{M}\times(\vec{M}\times\vec{\sigma}) = \frac{\hbar}{2eM_s t}J_s\vec{M}\times(\vec{M}\times\vec{\sigma})$ where M_s is the saturation magnetization of the ferromagnet, t is the thickness of the ferromagnet, J_s is the spin current and $\vec{\sigma}$ is the direction of spin polarization of the electrons accumulated at the Pt-Co interface. If an external magnetic field ($\vec{H}$) is applied the torque due to the magnetic field is given by $\vec{M}\times\vec{M}\times\vec{H}$. Overall, the dynamics of the magnetization under the influence of the external magnetic field and the spin torque is given by the modified Landau Lifschitz Gilbert equation [25]:

$$\frac{d\vec{M}}{dt} = -\gamma(\vec{M}\times\vec{H}) - \frac{\gamma\alpha}{M}(\vec{M}\times\vec{M}\times\vec{H}) - \gamma\tau(\vec{M}\times\vec{M}\times\vec{\sigma}) \tag{3.1}$$

where γ is the gyromagnetic ratio and α is the damping factor.

We first explain the spin orbit torque driven switching result in the presence of an out of plane magnetic field (Fig. 3.2) with our simplistic single domain based analysis. We assume that the single domain magnet has a perpendicular anisotropy, equivalent to 60 gauss, i.e. 60 gauss of in-plane magnetic field is needed to drive the magnet in-plane and 60 gauss of

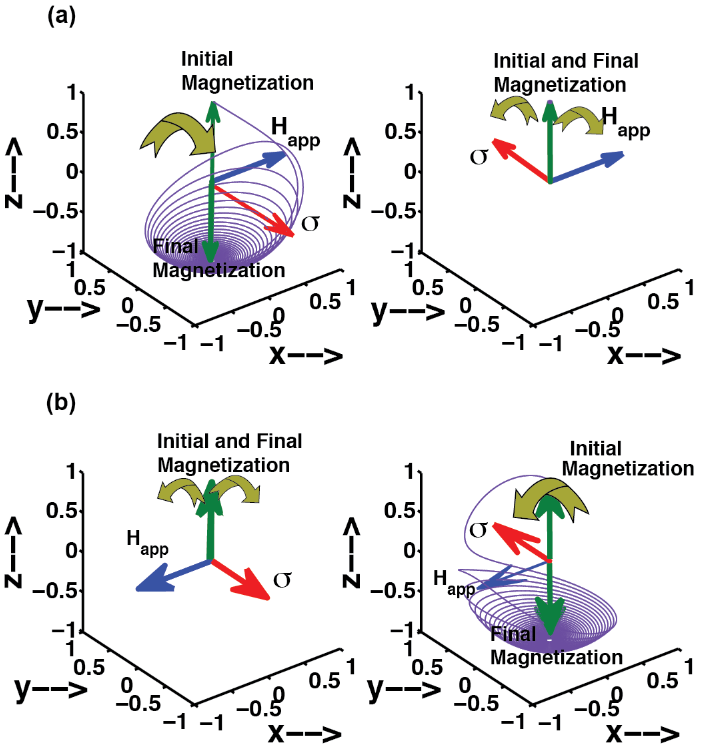
(a)
Initial Magnetization
H app
σ
Final Magnetization
Initial and Final Magnetization
H app
σ
(b)
Initial and Final Magnetization
H app
σ
Initial Magnetization
σ
H app
Final Magnetization
z-->
y-->
x-->
1
0.5
0
−0.5
−1

Figure 3.5: (a) With magnetization initially in +z state (M_z=1), torque generated by -y directed spin accumulation (σ) and torque generated by +x directed magnetic field add up to cause rotation from +z (M_z=+1) to -z (M_z=-1) while torque generated by +y directed spin accumulation and torque generated by +x directed magnetic field counteract to keep the magnet in +z state (M_z=+1). (b) When magnetic field is -x direction, +y directed spin accumulation switches the magnet from +z to -z while -y directed spin accumulation keeps the magnet in +z state

down (-z) directed magnetic field is needed to switch the magnet from up (+z) to down (-z). Thus coercivity of the magnet ($H_{coercive,0}$) is 60 gauss. We observe in our simulations (Fig. 3.4) that in the absence of spin orbit torque, a -z directed magnetic field with magnitude half that of the coercivity cannot switch the magnet from +z to -z as expected. However, in the presence of spin orbit torque, the same magnetic field (half that of the coercive field) can switch the magnet. Thus our simulations show that the coercivity of the magnet is reduced in the presence of spin orbit torque, just as we observe in the experiments (Fig. 3.2).

Next we explain the spin orbit torque driven switching result in the presence of in-plane magnetic field with our macrospin model. We observe in our simulations that in the presence of an in-plane magnetic field in +x direction and spin accumulation $\vec{\sigma}$ in +y direction, generated by +x directed current (Fig. 3.1) the final state of the magnetization is up (+z) while in the presence of an in-plane magnetic field in +x direction and spin accumulation $\vec{\sigma}$ in -y direction, generated by -x directed current (Fig. 3.1) the final state of the magnetization is down (-z) (Fig. 3.5a). Similarly, in the presence of an in-plane magnetic field in -x direction and spin accumulation $\vec{\sigma}$ in +y direction, generated by +x directed current (Fig. 3.1) the final state of the magnetization is down (-z) while in the presence of an in-plane magnetic field in +x direction and spin accumulation $\vec{\sigma}$ in -y direction, generated by -x directed current (Fig. 3.1) the final state of the magnetization is up (+z) (Fig. 3.5a).

3.4 Micromagnetic analysis of spin orbit torque driven magnetic switching

The analysis we have performed so far has assumed the magnetization of the ferromagnetic layer to be uniform. This model, known as the Stoner Wolfarth model or single domain model, does not give correct quantitative result for the spin orbit torque driven magnetic switching experiments performed by Liu *et al.* [10,25] as well as that performed by us (Fig. 3.2 and Fig. 3.3). A simple calculation shows why a single domain analysis yields incorrect quantitative result. Though we have assumed an energy barrier equivalent to 60 gauss between up (+z) and down (-z) directed states in our single domain simulations ($H_{coercive,0}$=60 gauss), if we perform Vibrating Sample Magnetometry (VSM) on the thin film stack or anomalous Hall effect (AHE) measurements with the magnetic field in-plane we see that $\sim$ 2kG of magnetic field is needed to saturate the magnet in-plane (Fig. 3.6a). This means that for every moment in the ferromagnetic layer, an energy barrier of $\sim$ 2kG exists between up (+z) and down (-z) directed states. Under the single domain assumption, for spin orbit torque to bring the magnet in-plane (Fig. 3.4) or switch the magnet (Fig. 3.5), the magnitude of spin torque has to be comparable to this strong in-plane energy barrier equivalent to $\sim$ 2kG. Thus, for spin torque strength $\tau = \frac{\hbar}{2eM_st}J_s = 2$ kG where M_s= saturation magnetization of the ferromagnet= 8×10^5 A/m and t = thickness of the ferromagnetic layer= 1 nm, $J_s \sim 5 \times 10^7$ A/cm ^{2}. When current (current density is given by J_c) flows through the heavy metal layer, spin current (spin current density J_s) is generated at the top surface of the heavy metal which gets injected into the ferromagnet due to spin Hall effect in the heavy metal. The ratio of J_s to J_c is called the spin Hall angle (θ_{SHE}). Spin Hall angle determines the spin orbit torque efficiency of the system. If the spin current density needed for the switching is 5×10^7 A/cm^2 then for a spin Hall angle equal to 0.1 of Ta (values around 0.1 have been reported by most groups) the calculated switching current density (J_c) is 5×10^8 A/cm^2 which is two orders of magnitude higher than what we need in our experiments ($\sim 3 \times 10^6$ A/cm^2). Similarly, if we take the switching current density J_c to be 3×10^6 A/cm^2 as in our experiments and calculate the spin Hall angle (θ_{SHE}) from the calculated spin current density ($J_s = 5 \times 10^7$ A/cm^2), θ_{SHE} turns out to be 17 which is two orders of magnitude higher than the expected value ($\sim$ 0.1). Thus single domain analysis does not provide quantitative match for spin orbit torque driven magnetic switching experiments.

Hence the assumption that the entire ferromagnet can be treated as a single domain magnet does not hold. Another evidence that the magnet is not a single domain or one giant macrospin during the switching is as follows: The ferromagnetic layer in the Ta/CoFeB/MgO stack exhibits perpendicular magnetic anisotropy with an anisotropy field H_k of around 2kG needed to align the magnetic moment in-plane (Fig. 3.6a). Thus if the ferromagnetic layer is considered as a giant macro-spin in the Stoner Wolfarth model an energy barrier equivalent to 2kG exists between the up (+z) and down state (-z) (Fig. 3.6b). Yet measurement shows that the magnet can be switched by a field, called the coercive field, as small as ∼50 G, which is 2 orders of magnitude smaller than the anisotropy field H_k, as observed in the Vibrating Sample Magnetometry measurement on the stack (Fig. 3.6a) and anomalous Hall effect measurement on the Hall bars made from the stack (Fig. 3.1a). This significant deviation from the Stoner Wolfarth model is known as Brown's paradox in magnetism literature [41,42]. Within the Stoner Wolfarth model the magnet needs to cross the in-plane (x-y plane) energy barrier $\frac{H_k}{2}$ to switch by 180^0 from up (+z) to down (-z) and as a result a switching field close to H_k will be necessary (Fig. 3.6b). However if a domain wall is introduced in the system the magnet can switch through domain wall motion at a switching field much smaller than H_k. This is because across the width of the domain wall the magnetic moment changes gradually from up to down. For the wall to move, each moment inside the wall needs to turn only by a small angle, which needs much lower energy than H_k (Fig. 3.6c). Starting from the magnet saturated in the up (+z) direction such a domain wall can be introduced by applying a magnetic field in the negative direction much smaller in magnitude than H_k. The ferromagnetic layer has several defects where the anisotropy is much lower than rest of the magnet. So reverse domains nucleate at these defects with domain walls surrounding them. Theoretically if the applied magnetic field is infinitesimally small but negative the domain wall can move such that the reverse polarized domains expand and the entire magnet switches from up (+z) to down (-z). However in reality the domain wall gets pinned at defects where the domain wall sits at a local energy minimum and an external field is needed to "depin" the domain wall. This field is called the depinning field. When the externally applied reverse magnetic field exceeds the depinning field in magnitude, the domain wall moves entirely to switch the magnet over (Fig. 3.6d). Thus under the domain wall depinning based switching mechanism, the depinning field determines the coercivity of the magnet. If the reverse magnetic field is applied at an angle θ with respect to the film normal, the magnet switches when the component of the applied magnetic field along the normal exceeds the depinning field. Thus the coercivity of the magnet varies as $\frac{1}{cos(\theta)}$. Such $\frac{1}{cos(\theta)}$ dependence of coercivity has been observed in anomalous Hall effect measurements we performed on Hall bars made from the Ta/CoFeB/MgO stack (Fig. 3.6e), confirming that the magnetization of ferromagnetic layer in these stacks indeed switch under a magnetic field by nucleation of reverse domain followed by motion of depinned domain walls.

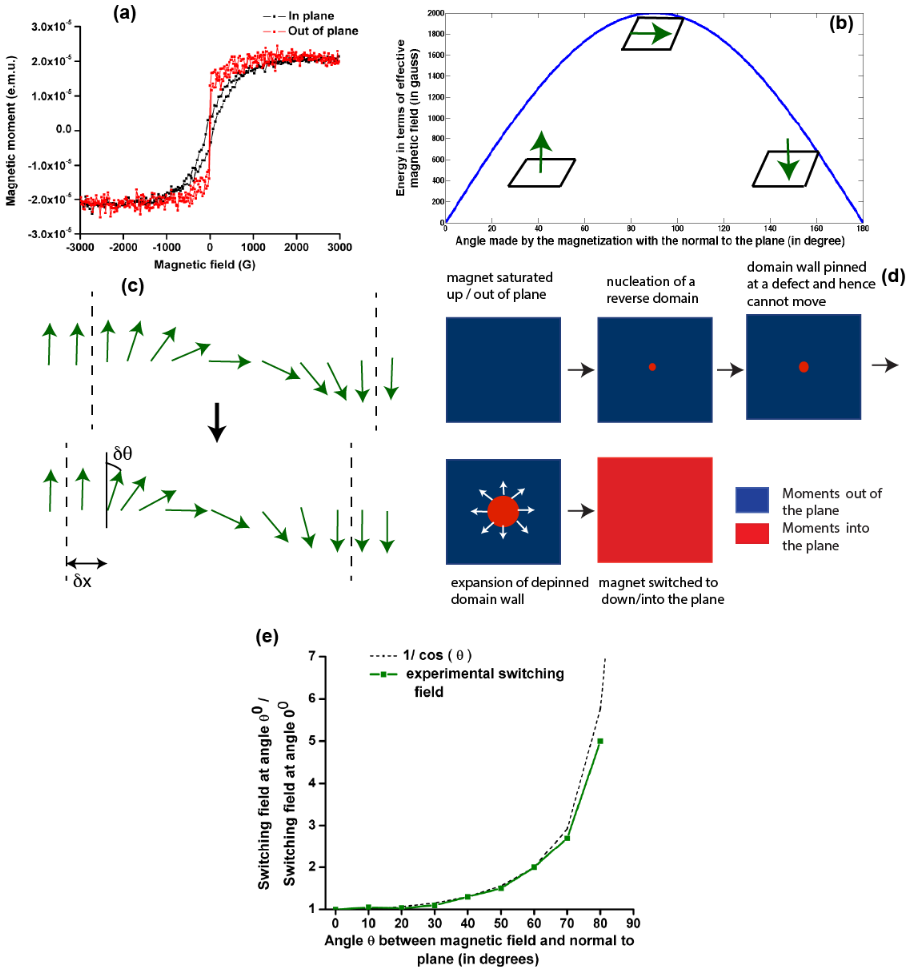

Figure 3.6: (a)Vibrating Sample Magnetometry (VSM) measurement on thin films of Si (substrate)/ SiO_2 (100 nm)/ Ta (10 nm)/ CoFeB (1 nm)/ MgO (1 nm)/ Ta (2 nm) shows that the stack exhibits perpendicular magnetic anisotropy. As a result, a large field (∼2000 gauss here) is needed to saturate the magnet in the in-plane direction (red plot). However the out of plane hysteresis loop shows that a very small field can switch the magnet in the out of plane direction (black plot). This behavior is observed for any Co/Pt/AlOx stack or Ta/CoFeB/MgO stack that exhibits perpendicular magnetic anisotropy. (b) Energy landscape of a single domain magnet shows that an anisotropy field of ∼2000 gauss is needed to switch the magnet by 180^0 in the out of plane direction. (c) The ferromagnetic domain wall moves by a distance $\delta\theta$ through the rotation of each moment in the domain wall by an angle $\delta\theta$. (d) Switching of a magnet with perpendicular anisotropy from up/ out of the plane (blue color) to down/ into the plane (red color) is shown schematically. Starting from a saturated state (all blue), reversed domain (red circle) nucleates with a small magnetic field into the plane. However, the domain wall is pinned at defects and hence cannot move. When the field is high enough to depin the domain wall, it moves and the reverse domain (red circle) expands to switch the magnet to into the plane (red square). (e) Minimum magnetic field needed to switch the magnet is plotted as a function of the angle between the direction of the applied magnetic field and normal to the surface of the film.

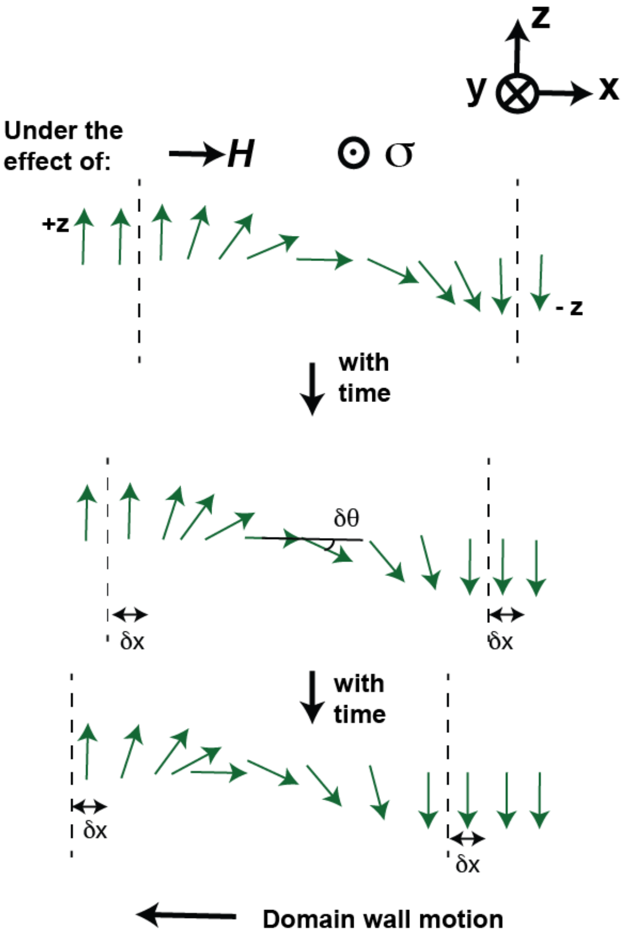

Figure 3.7: A domain wall, under the influence of a magnetic field (H) in x direction and spin accumulation ($\vec{\sigma}$) in -y direction, moves to the left (-x) such that the entire magnet switches from +z to -z

An argument, similar to that we just used to explain why a single domain magnet cannot be switched with a small out of plane magnetic field but a domain wall can move under a small magnetic field to switch the entire magnet, can also be used to explain the low current density and hence low spin orbit torque magnitude needed to switch magnets in experiments. We have shown in Fig. 3.5 that in the presence of +x directed magnetic field a -y directed spin accumulation ($\vec{\sigma}$) can switch a single domain magnet from +z to -z. However for a ferromagnet with perpendicular magnetic anisotropy (in-plane energy barrier equivalent to $\sim$ 2kG) a very large spin orbit torque comparable to such energy barrier is needed for the switching. So a spin orbit torque of two orders lower magnitude acts on a single domain magnet, it cannot switch the magnet. In Fig. 3.7, we show that under the effect of +x directed magnetic field and -y directed spin accumulation (σ), a ferromagnetic domain wall can move to switch the magnet even if the spin orbit torque is orders of magnitude lower than that needed for single domain switching. If a small spin orbit torque acts on the domain wall then the moments which are totally up (+z) cannot switch to down (-z) because the spin orbit torque is orders of magnitude smaller than that needed to switch an individual moment directly from +z to -z. However the moment in the middle of the domain wall, which is in-plane, tilts a little bit down (-z) by an angle θ due to the small spin orbit torque and the moment to the left of it becomes in-plane due to exchange interaction. Next that moment also tilts a little bit down (-z). Thus the domain wall moves to the left and eventually the entire magnet switches from up(+z) to down (-z) similar to Fig. 3.6c.This explains why a current density, two orders of magnitude smaller than that needed in the single domain model, can switch the magnet in actual experiments. Thus a micromagnetic model can provide a better qualitative match with experiments compared to single domain wall. We present some more details of the switching process next. In the following section, we show a new kind of domain wall motion, driven by spin orbit torque, following the same physics we just described here. The current density needed to move the domain wall is of the order of 10^6 A/cm^2 instead of 10^8 A/cm^2 in both experiments and simulations, as expected.

3.5 Deterministic Domain Wall Motion Orthogonal To Current Flow Due To Spin Orbit Torque

According to the conventional spin transfer torque model, when spin polarized electrons coming from a magnetized region impinge on the spins in a domain wall, they exert a torque that tries to orient the domain wall spins in the direction of the incoming spins [11,36,43,44]. The strength of the torque is proportional to the relative angle between the incoming spins and domain wall spins. If a domain wall is formed along the width of a perpendicularly polarized magnetic wire (transverse domain wall) as shown in Fig. 3.8a, then a current flowing in the long direction can exert such a torque and move the domain wall. This has been the canonical configuration for studying current induced domain wall motion. If, on the other hand, a domain wall is formed along the length as shown in Fig. 3.8b and Fig. 3.8d, then no conventional spin transfer torque, to be referred to as the bulk spin torque, is exerted on this longitudinal wall by a current that flows along the length (longitudinal current), even in the presence of an external in-plane magnetic field. This is because the domain wall spins do not change direction along the path of the current in this case. In this section of the thesis we show that spin orbit torque due to current flowing in a heavy metal layer underneath the ferromagnetic layer can deterministically move a longitudinal domain wall in the presence of a longitudinal magnetic field, as opposed to bulk spin torque. Reversing the direction of the current flow or the direction of the field reverses the direction of the domain wall motion.

Recently, spin orbit torque (SOT) has been used by Ryu *et al.* [34] and Emori *et al.*[28] to move domain walls in a narrow wire using a current flow. Both these works show how a

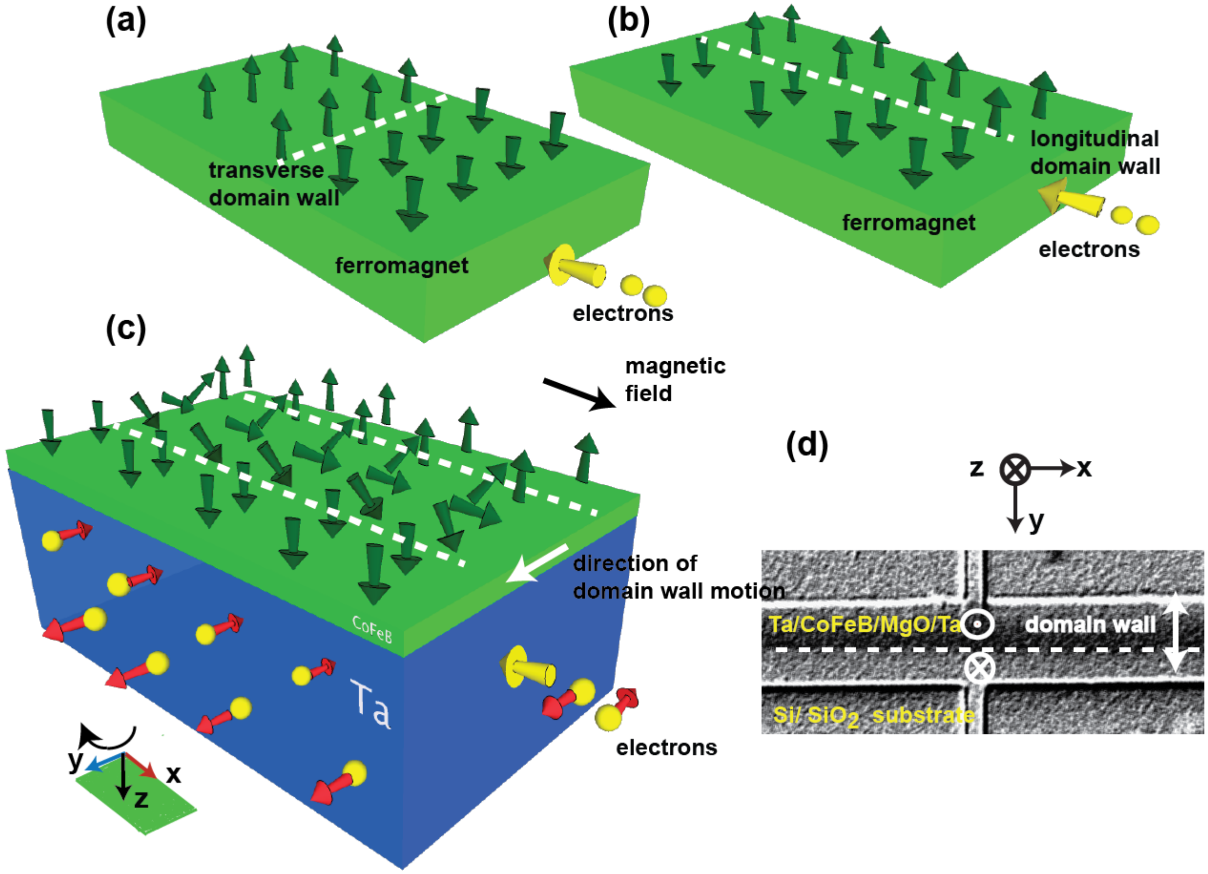
(a)
transverse domain wall
ferromagnet
electrons
(b)
longitudinal domain wall
ferromagnet
electrons
(c)
magnetic field
direction of domain wall motion
CoFeB
Ta
electrons
y
x
z
(d)
z
x
y
Ta/CoFeB/MgO/Ta
domain wall
Si/ SiO2 substrate

Figure 3.8: (a) Current flows across a transverse domain wall. Green arrows represent the magnetic moments. (b) Current flows along a longitudinal domain wall. (c) When current flows through the Ta in x direction (electrons in -x direction) electrons with spin polarization in -y direction accumulate at the interface of the Ta and CoFeB. This results in the transfer of spin orbit torque to the domain wall in CoFeB. The green parallelogram represents the plane of the sample and the three arrows show the directions of x, y and z-axes. The z-axis points in the direction of the vector product of x and y axes following the right hand rule, which is into the plane ($\otimes$). (d) The MOKE image of the 20 microns wide magnetic bar shows the formation of a longitudinal wall along it when current flows in the +x direction. The longitudinal domain wall at y=0 separates an "out of the plane" ($\odot$) polarized domain for $y < 0$ and an "into the plane" ($\otimes$) polarized domain for $y > 0$. Anomalous Hall voltage is measured across the orthogonal bar.

transverse domain wall, created in a heavy metal/ ferromagnet heterostructure, can be moved by a current flow due to a simultaneous action of spin orbit torque and Dzyaloshinskii-Moriya Interaction (DMI) at the heavy metal/ ferromagnet interface. Nonetheless, the structure of the domain wall used in these experiments is transverse which is identical to the conventional structure where a bulk spin torque could also move the wall along the direction of current flow. By contrast, we have created a longitudinal domain wall and have shown that such a wall, which cannot be moved by bulk spin torque, can be deterministically moved by the spin orbit torque orthogonal to the current flow. This is enabled by the fact that the current flowing through the structure leads to a spin accumulation at the heavy metal (Ta) / ferromagnet (CoFeB) interface, which is orthogonal to the current direction (Fig.3.8c)[10]. This is different from the case of bulk spin torque where the spins impinging on the magnetic domain wall are collinear with the source magnetization. Thus our work shows that the otherwise well-known spin orbit torque resulting from a relative mis-alignment of the magnetization and spin accumulation can be exploited in a novel geometry to demonstrate a new type of domain wall motion orthogonal to the current flow.

In the following subsections, we discuss our results in details. In Subsection 3.5.1, we show through micromagnetic simulation that conventional spin transfer torque cannot move the longitudinal domain wall even in the presence of in-plane magnetic field, thereby showing the uniqueness of the geometry we have used in these experiments. In Subsection 3.5.2, we report our experimental results showing the formation of the longitudinal domain wall. In Subsection 3.5.3, we show micromagnetic simulations that explain formation of the longitudinal domain wall. In Subsection 3.5.4 we show experimentally how spin orbit torque moves such a longitudinal domain wall deterministically in the presence of an external in-plane magnetic field. In Subsection 3.5.5 we support the experimental result with micromagnetic simulations. It is to be noted that in this section of the chapter, including all the subsections, we have a different coordinate notation, as shown in Fig. 3.8c. Still we have $\hat{x} \times \hat{y} = \hat{z}$ but positive $\hat{z}$ points into the plane of the thin film/device as opposed to previous sections of this chapter and other chapters of the thesis.

3.5.1 Micromagnetic simulation showing that conventional/ bulk spin torque can move the transverse domain wall but not the longitudinal domain wall

The domain wall studied by Ryu *et al.* [34] and Emori *et al.* [28] is transverse in nature, i.e., it runs across the width of the magnetic nanowire. As a result current flows across the domain wall. Apart from spin orbit torque, bulk spin transfer torque or conventional spin transfer torque from the current contributes to its motion. However, if a domain wall is formed along the length of the magnetic bar as in our experiments here, bulk spin transfer torque does not move such a domain wall. As a result whatever motion we observe in our experiments is due to spin orbit torque and not due to bulk spin transfer torque. Thus we can isolate the role of spin orbit torque from bulk spin transfer torque when we study the motion of a longitudinal domain wall as opposed to a transverse domain wall. To support our claim, in this subsection we show through micromagnetic simulations that bulk spin transfer torque, or conventional spin transfer torque, can move the transverse domain wall but not the longitudinal domain wall.

When current flows through a ferromagnet, conduction electrons in the ferromagnet apply a bulk spin torque on the domain wall of the ferromagnet, given by $b_J(\vec{J_c}.\nabla)\vec{m} - \beta b_J \vec{m} \times ((\vec{J_c}.\nabla)\vec{m})$ where $b_J = \frac{\mu_B P}{e M_s} J_c$; μ_B- Bohr magnetron, P- spin polarization, e- charge of an electron, M_s- saturation magnetization of the ferromagnet, β- non adiabatic parameter and J_c- charge current [8-12]. For a transverse domain wall, since the current flows across the domain wall, the magnetization has a non-zero gradient along the direction of the charge current $((\vec{J_c}.\nabla)\vec{m} \neq 0)$. So the bulk spin torque is non-zero. We perform micromagnetic simulations on Object Oriented MicroMagnetic Framework (OOMMF)[45] using the extension module for current induced domain wall motion (class spinTEevolve)[46] to show that a transverse domain wall moves due to the bulk spin torque when current flows across it. Only bulk spin torque and no spin orbit torque is present in this simulation (Fig. 3.9).

A 600 nm long, 200 nm wide and 1 nm thick magnet is used for simulations, with a mesh size of 2 nm laterally and 1 nm across the thickness. For all micromagnetic simulation figures, blue dots with red background represent moments pointing out of the plane (-z) while red dots with blue background represent moments pointing into the plane (+z). The simulation parameters are: saturation magnetization $M_s = 8 \times 10^5$ A/m (measured for our materials stack by performing Vibrating Sample Magnetometry), exchange constant $A = 3 \times 10^-11$ J/m, perpendicular anisotropy constant $K = 6 \times 10^5$ J/m^3, spin polarization P=0.5, non-adiabatic parameter β=0.04 and charge current $J_c = 10^8$ A/cm^2. Starting from a transverse domain wall at the centre of the magnet, we see that the domain wall moves with time under the application of current due to the bulk spin torque (Fig. 3.9). The domain wall moves in the direction of propagation of electrons, i.e., opposite to the direction of the current, as expected from theory [11,36,43,44]. When we simulate a longitudinal domain wall instead, current flows along the domain wall. In this case the direction, in which the gradient of the magnetization is not zero, and direction of the current are orthogonal to each other, so $(\vec{J_c}.\nabla)\vec{m} = 0$. So the longitudinal domain wall does not experience a bulk spin torque and hence it does not move under the application of a current pulse, as we verify through micromagnetic simulations using the same simulation parameters as the transverse domain wall case (Fig. 3.10). Only bulk spin torque and no spin orbit torque is present in this simulation. In our experiments we move the longitudinal domain wall with current pulses in the presence of an in-plane magnetic field along the current direction. In Fig. 3.11, we show simulations of a bulk spin torque acting on a longitudinal domain wall just like Fig. 3.10, with an in-plane magnetic field of 10 G applied in addition to it along the current direction. We see that even in this case the longitudinal domain wall does not move with time.

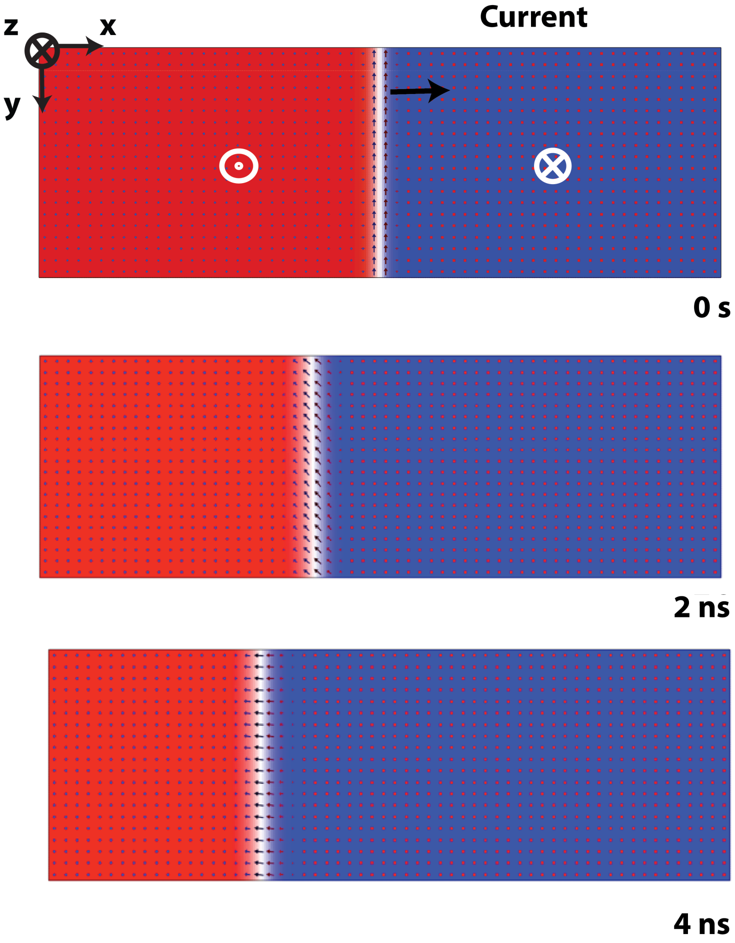

Figure 3.9: Current flows in the +x direction, i.e. electrons move in the -x direction to apply the bulk spin torque on the transverse domain wall. Blue dots with red background represent moments pointing out of the plane (-z) while red dots with blue background represent moments pointing into the plane (+z). We see that the transverse domain wall moves along the flow of electrons with time as expected.

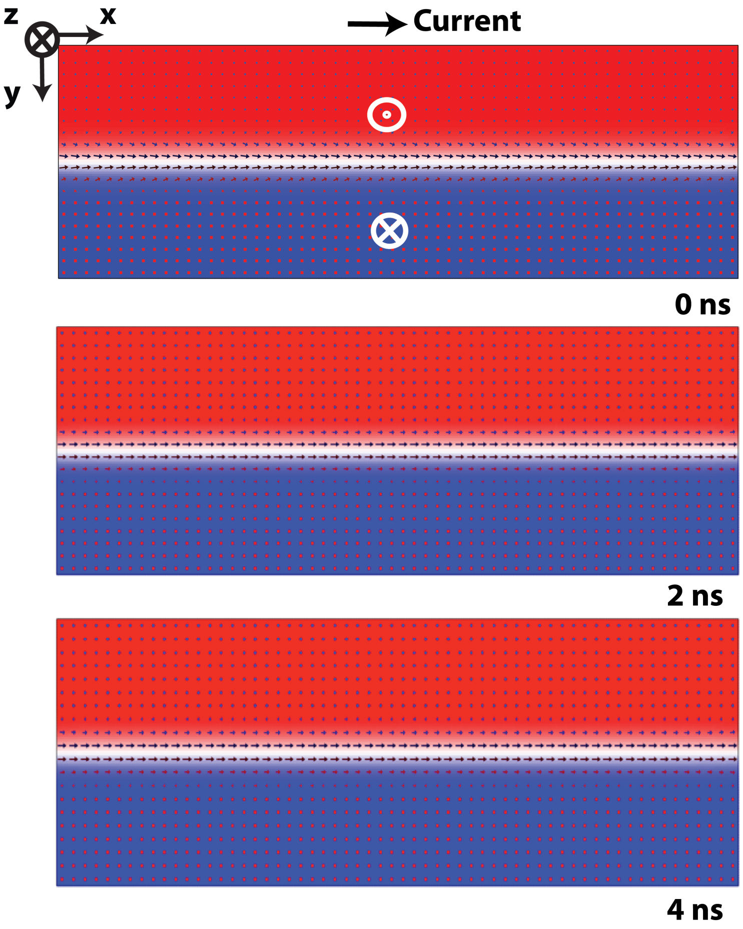

Figure 3.10: Current flows in +x direction, i.e. electrons move in -x direction, but it cannot apply a bulk spin torque on the longitudinal domain wall. No magnetic field is applied. We see that the longitudinal domain wall does not move with time.

3.5.2 Creation of a longitudinal ferromagnetic domain wall and its motion under an out of plane magnetic field

Having shown that conventional or bulk spin transfer torque cannot move a longitudinal domain wall, we now discuss how we have created a longitudinal domain wall in our devices so that we can study its motion under the application of spin orbit torque. Hall bars are fabricated from a stack of Si (substrate)/ SiO_2 (100 nm)/ Ta (10 nm)/ CoFeB (1 nm)/ MgO (1 nm)/ Ta (2 nm) (same stack as used before). Current is applied along the bar of width 20 microns, which is along the x-axis, and anomalous Hall voltage is measured in the y direction across the narrower bar of width 5 microns (Fig. 3.12a). The anomalous Hall voltage is proportional to the average out of plane magnetization at the intersection region of the two bars. Anomalous Hall resistance (R_{AHE}) is the ratio of the anomalous

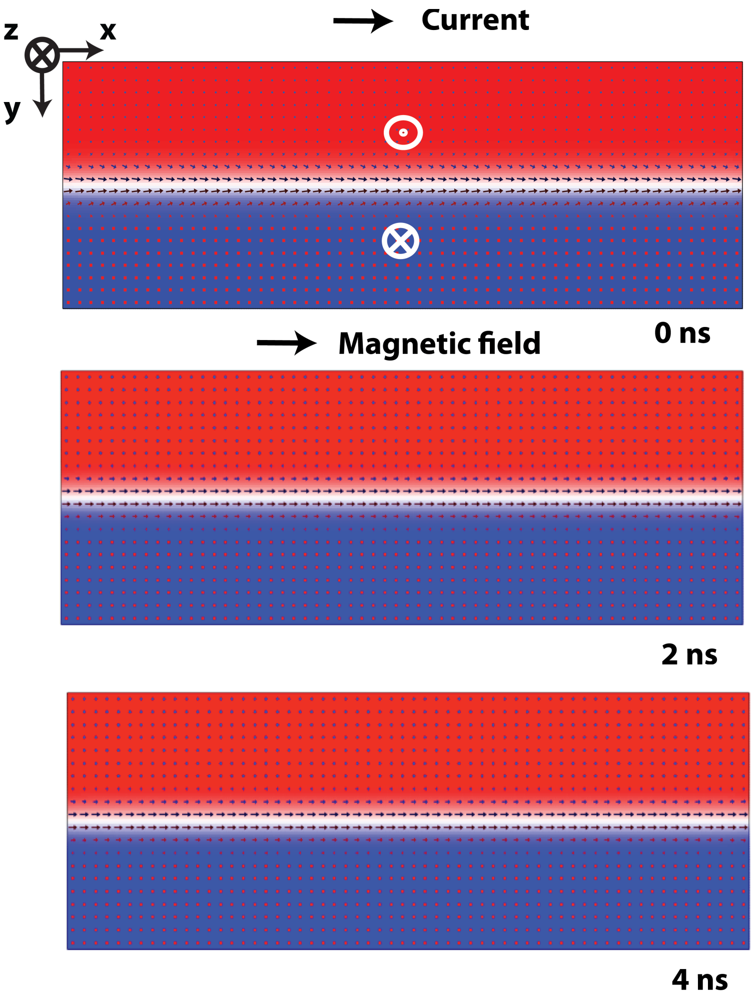
Current
z
x
y
Magnetic field
0 ns
2 ns
4 ns

Figure 3.11: Current flows in +x direction, i.e. electrons move in -x direction. An in-plane magnetic field of 10 G is applied in +x direction. We see that the longitudinal domain wall does not move with time.

Hall voltage to the small constant current applied to measure the voltage (100 μA for all our measurements). The anomalous Hall resistance (R_{AHE}) versus magnetic field plot of Fig. 3.12a shows that the CoFeB layer exhibits perpendicular anisotropy with a magnetic field of 30 G needed to switch its magnetization between the two saturated states- "into the plane" or $m_z = 1$ state ($\otimes$) with R_{AHE}=1.2 Ω and "out of the plane" or $m_z = -1$ state ($\odot$) with $R_{AHE} = -1.2\Omega$; m_z is the magnetization in z-direction, normalized by the saturation magnetization. We follow the following convention consistently throughout the paper: x and y axes are two orthogonal directions on the plane of the sample and the cross product of x axis and y axis is z axis ($x \times y$), following right hand rule. The axes are chosen such the positive z axis is "into the plane" and negative z axis is "out of the plane" (Fig. 3.8c, Fig. 3.8d).

Along with measurement of R_{AHE}, Magneto Optic Kerr Effect (MOKE) has been used to image the magnetic domains of the wider Hall bar [28,34]. To obtain the best contrast, each image has been subtracted from a reference image of a saturated "into the plane" state of the magnet. The subtracted image of the saturated "into the plane" state of the magnet shows no contrast between the magnetic bar and the background substrate material because the substrate does not contribute to a magnetic signal and the positive magnetic signal of the "into the plane" magnet when subtracted from another image of "into the plane" magnet yields zero (Fig. 3.12a). On the other hand, when an image of a saturated "out of the plane" state is subtracted from the reference image of "into the plane" state, the substrate still gives no signal, but the difference between negative signal of the "out of the plane" magnet and positive signal of the "into the plane" magnet is non-zero. So a subtracted image of "out of the plane" state shows a dark contrast between the magnetic bar and the background (Fig. 3.12b).

Starting from the magnet saturated "into the plane" ($m_z = 1$, $R_{AHE} = 1.2\Omega$), a current pulse of magnitude 7.5×10^6 A/cm^2 and duration 1s is applied along the wider Hall bar in +x direction at a zero magnetic field (Fig. 3.8d). At the end of the pulse, the steady state R_{AHE} of the final magnetic state is measured to be $\sim 0\Omega$ (Fig. 3.12a). The MOKE image of that state shows the magnet to be split into a domain of "out of the plane" or $m_z = -1$ ($\odot$)) polarized moments for $y < 0$ and a domain of "into the plane" or $m_z = 1$ ($\otimes$) polarized moments for $y > 0$ with a longitudinal domain wall separating the two, based on the chosen coordinate system (Fig. 3.12a and Fig. 3.8d). We call this state the "mixed" state (Fig. 3.12a) because the magnet has both $m_z = 1$ and $m_z = -1$ polarized domains in this state. Reversing the polarity of the current reverses the position of the two domains in the "mixed" state (Fig. 3.12c). The polarity of the domains in the "mixed" state follows the out of the plane component of the Oersted field, generated by the current pulse, at the edges of the bar. Starting from a saturated state, reverse polarized domains are nucleated at the edge of the bar due to the Oersted field of magnitude 10 G (found from analytical calculations and COMSOL simulations) from the current that flows along the bar. Since the edges have more

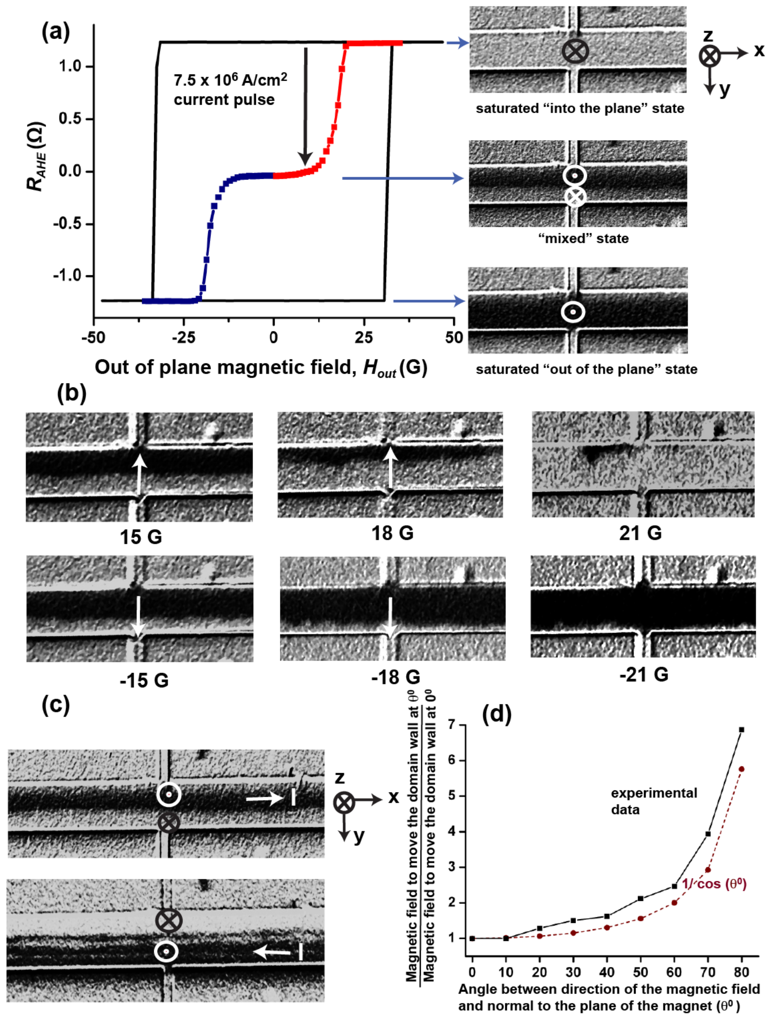

Figure 3.12: (a) Anomalous Hall resistance (R_{AHE}) measurement shows that the magnet can be switched between a saturated “into the plane” (⊗) polarized state ($m_z = 1$ or $R_{AHE} = 1.2\Omega$) and a saturated “out of the plane” (⊙) polarized state ($_= -1$ or $R_{AHE} = -1.2\Omega$) with a switching field of ∼30 gauss. Starting from the $m_z = 1$ state, a current pulse of magnitude 7.5×10^6 A/cm^2 is applied along the bar in +x direction at a zero magnetic field. At the end of the pulse R_{AHE} is measured to be 0 Ω. This corresponds to the “mixed state” of the bar. MOKE image of the “mixed state” shows a longitudinal domain wall with a $m_z = -1$ polarized domain for $y < 0$ and a $m_z = 1$ polarized domain for $y > 0$. When out of plane magnetic field is applied in z direction on the “mixed” state, R_{AHE} does not change till ∼15 G. Beyond that, R_{AHE} increases till the magnet reaches the saturated “into the plane” state ($m_z = 1$, $R_{AHE} = 1.2\Omega$) - red plot. Applying another current pulse of magnitude 7.5×10^6 A/cm^2 on the saturated state creates the “mixed state” with a longitudinal domain wall again. Now applying a magnetic field in -z direction causes reduction in R_{AHE} till the magnet gets saturated in the “out of plane” direction ($m_z = -1$, $R_{AHE} = -1.2\Omega$) - blue plot.

Figure 3.12: (b) MOKE images of the magnetic bar under the application of “into the plane” (+z) field shows the movement of the longitudinal domain wall in -y direction so that the average magnetization is aligned with the field. When “out of the plane” (-z) field is applied, the longitudinal domain wall moves in +y direction. (c) Mixed state, formed by a positive current pulse (current I along +x) has “out of the plane” ($\odot$) polarized domains for $y < 0$ and “into the plane” ($\otimes$) polarized domains for $y > 0$ whereas mixed state, formed by a negative current pulse (I along -x) has “into the plane” ($\otimes$) polarized domains for y¡0 and “out of the plane” ($\odot$) polarized domains for $y > 0$. (d) Minimum field needed to move the longitudinal domain wall from the centre of the bar is plotted against the angle of application of the field.

defects due to the fabrication process, it is easier to nucleate reverse domains at the edges. Subsequently, the domain wall moves from the edge of the bar to the center to reduce the magnetostatic energy of the system. Next we show micromagnetic simulations that explain the formation of the longitudinal domain wall.

In Figure 3.13a the magnet is initially saturated “into the plane” ($m_z = 1$; red dots in blue background). As current flows in +x direction, Oersted field generated by the current switches the moments near the upper edge of the bar ($y < 0$) to “out of the plane” ($m_z = -1$, blue dots in red background). A longitudinal domain wall is formed as a result near the upper edge of the bar (Fig. 3.13a). We simulate a 600 nm long and 200 nm wide magnetic bar using the same simulation parameters as used for Fig. 3.9, 3.10 and 3.11 with the initial condition of a longitudinal domain wall near the upper edge of the bar (Fig. 3.13a-image of the magnet at time = 0 ns). We use the standard time evolver provided by OOMMF to let the system evolve with time taking into account all the energy terms- exchange energy, anisotropy energy and magnetostatic energy. We observe that the longitudinal domain wall moves in +y direction towards the center with time to reduce the total energy of the system. This is because magnetostatic energy is minimum when the domain wall is at the center of the bar. The final steady state of the system consists of a longitudinal domain wall at the center ($y = 0$) with the upper part of the bar ($y < 0$) being polarized “out of the plane” and the lower part ($y > 0$) being polarized “into the plane”. The polarity of the domains matches with what we observe in the experiment (Fig. 3.12c). Similarly starting from a magnet saturated in the “into the plane” direction current flowing in the -x direction nucleates “out of the plane” polarized domains at the lower edge of the magnet resulting in the formation of a longitudinal domain wall near the lower edge (Fig. 3.13b- image of the magnet at time= 0 ns). As time progresses the longitudinal domain wall moves towards the center and at the steady state we get a “mixed state” with equal number of “out of the plane” and “into the plane” polarized domains. The polarity of the domains matches with what we observe in the experiment (Fig. 3.12c).

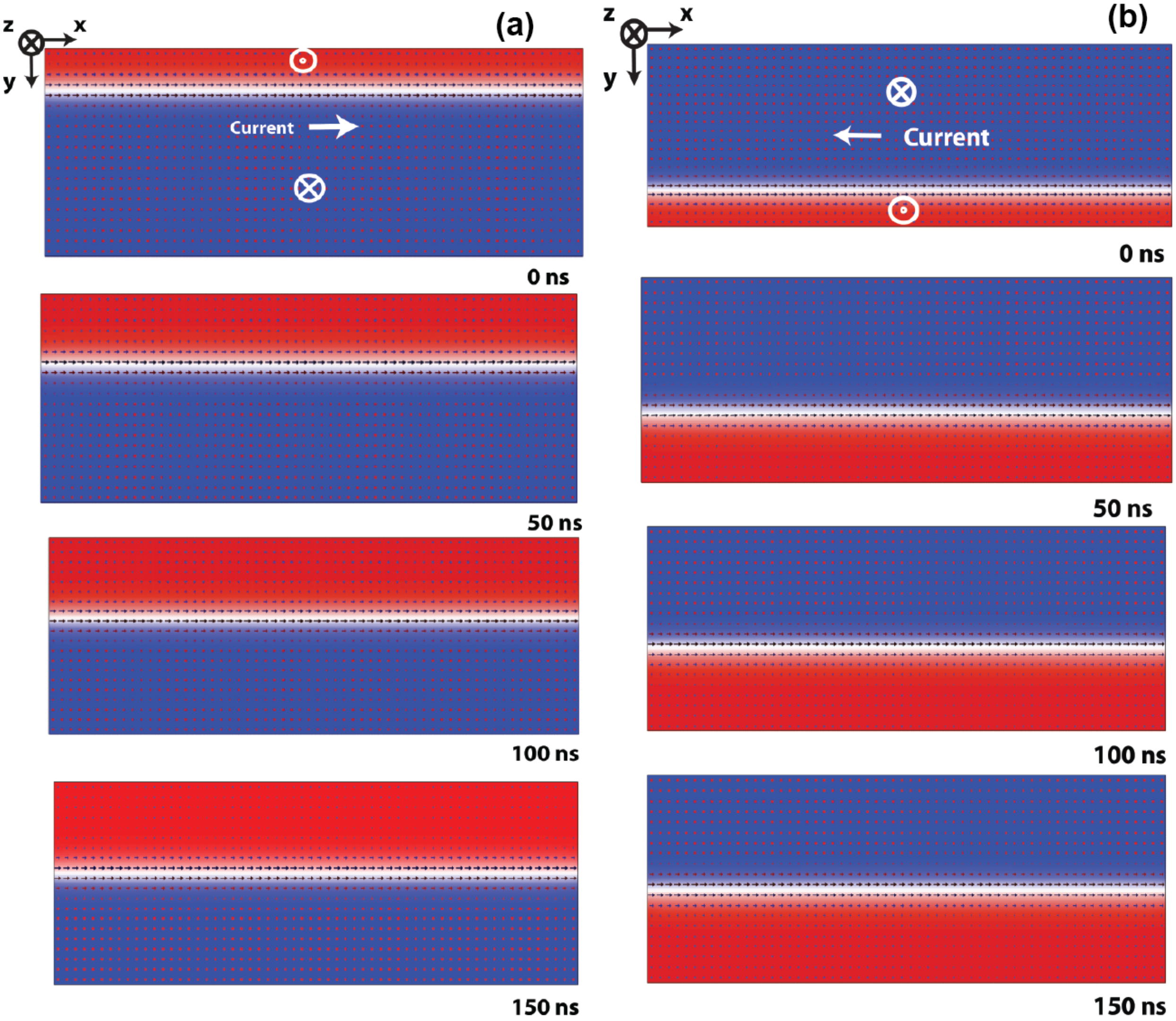

Figure 3.13: (a) Current in +x direction creates a domain wall at the upper edge of the bar ($y < 0$) because of its Oersted field. Micromagnetic simulation shows that starting from the upper edge of the bar the domain wall moves to the center of the bar at a zero magnetic field to lower its magnetostatic energy.(b) Current in -x direction creates a domain wall at the lower edge of the bar ($y > 0$) because of its Oersted field. Micromagnetic simulation shows that starting from the lower edge of the bar the domain wall moves to the center of the bar at a zero magnetic field to lower its magnetostatic energy.

Once the longitudinal domain wall is formed at the center of the bar after the application of the current pulse, application of an out of plane magnetic field moves the domain wall in one direction or another based on the polarity of the field as observed from the MOKE images (Fig. 3.12b). The displacement of the domain wall is proportional to the magnitude of the applied field, indicating that the domain wall motion is governed by pinning defects [47,48]. We also observe that the domain wall starts moving from the centre of the bar only when the out of plane field is 15 G or above. If the magnetic field is next applied at different angles (θ) with respect to the film normal, the magnetic field needed to move the domain wall follows a $\frac{1}{cos(\theta)}$ dependence as expected from the Kondorsky model of domain wall depinning field [40,41,42,47,48] (Fig. 3.12d).

3.5.3 Motion of the longitudinal domain wall orthogonal to current flow in presence of an in-plane magnetic field

Creation of such a longitudinal domain wall provides us with the unique opportunity to control its motion orthogonal to the current flow using spin orbit torque, which is not otherwise possible from a bulk spin torque. Deterministic control of the motion of this domain wall orthogonal to the current flow is the central point of the paper, which we discuss next. We first saturate the magnetic bar in “into the plane” ($m_z = 1$) state and apply a current pulse of magnitude 7.5×10^6 A/cm^2 and duration 1s along the bar in +x direction at zero magnetic field to create a “mixed state” with a longitudinal domain wall at the center of the bar just as in Fig. 3.12a. Starting from the longitudinal domain wall, a current pulse of duration 1s is applied along the bar in the +x direction in the presence of an in-plane magnetic field in the -x direction (Fig. 3.14a). This is repeated for different magnitudes of the current pulse. MOKE images of the bar taken after every current pulse show that the current pulse moves the domain wall in -y direction such that the “into the plane” or $m_z = 1$ polarized domain expands while the “out of the plane” or $m_z = -1$ polarized domain contracts. The distance moved by the domain wall is proportional to the magnitude of the current pulse. Reversing the direction of the magnetic field reverses the direction of the domain wall motion because when the magnetic field is in +x direction and the current is also in +x direction, the domain wall moves in the +y direction and the final state of the magnet is in -z direction (Fig. 3.14a). We next vary the in-plane magnetic field and apply current pulses of different magnitude starting every time from the same initial condition of a longitudinal domain wall at the centre of the bar just as in “mixed state” of Fig. 3.12a. We measure R_{AHE}, indicative of the domain wall position, after each current pulse and plot the R_{AHE} as a function of the current and the in-plane field. The contour plot obtained in that process (Fig. 3.14b) shows that when the in-plane magnetic field is positive (along +x) current along +x (positive polarity) beyond a threshold value ($\sim 5 \times 10^6$ A/cm^2) moves the domain wall in +y direction and hence the average $m_z < 0$ ($R_{AHE} < 0$, blue color in contour plot). The higher the current or stronger the field, the more negative is the average m_z and the R_{AHE}. In the presence of a positive in-plane magnetic field (along +x), current

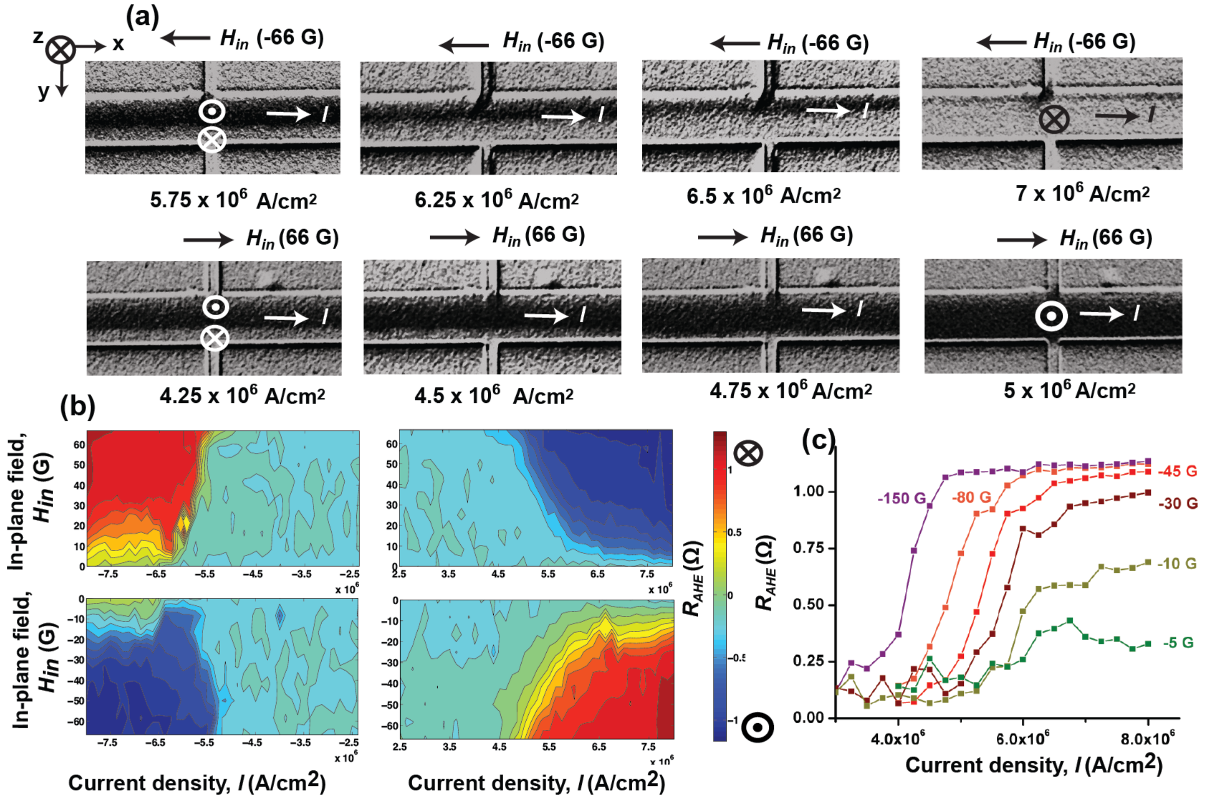

Figure 3.14: (a) MOKE images of the magnetic bar after a positive current pulse of different magnitude is applied on a longitudinal domain wall ("mixed" state of Fig. 3.12a) in the presence of an in-plane field (H_{in}) in -x and +x direction. (b) Contour plots of final R_{AHE} after application of a current pulse versus the magnitude of the current and magnitude of the applied in-plane field for different combinations of positive and negative currents and fields. (c) Plots of R_{AHE} versus magnitude of current pulse for different values of magnetic field, applied in -x direction.

in -x direction (negative polarity) moves the domain wall in -y direction and the average $m_z > 0$ ($R_{AHE} > 0$, red color in contour plot). When in-plane magnetic field is applied in -x direction (negative field), positive current pulse moves the domain wall in -y direction ($R_{AHE} > 0$, red color) and negative current pulse moves the domain wall in +y direction ($R_{AHE} < 0$, blue color). The R_{AHE} measurement results of Fig. 3.14b are consistent with the MOKE images of Fig. 3.14a in terms of the direction of domain wall motion and final state of the magnet under different combinations of current pulse and in-plane magnetic field. It is to be noted that the final state of the magnet is consistent with that for magnetic switching experiments on Hall bars in the presence of in-plane magnetic field (Fig. 3.3), just that we have changed the convention for +z and -z directions here.

3.5.4 Micromagnetic simulations showing spin orbit torque driven motion of the longitudinal domain wall

We performed micromagnetic simulations in Object Oriented Micromagnetic Framework to explain this result using a spin torque extension module- CYYSTTEvolve [49]. Starting from a longitudinal domain wall at the center of a rectangular magnet of length 600 nm, width 200 nm and thickness 1 nm, the system is allowed to evolve with time under the influence of an in-plane magnetic field along its length and a Slonczewski-like spin orbit torque orthogonal to it. Current flowing through a heavy metal-ferromagnet heterostructure is known to apply a Slonczweski-like spin orbit torque on the ferromagnet of the form $(\vec{M}\times\vec{M}\times\vec{\sigma})$ where $(\vec{M})$ is the magnetization of the ferromagnet and $\vec{\sigma}$ is the direction of spin polarization of the accumulated electrons at the heavy metal-ferromagnet interface, which is determined by the direction of the current. We consider the longitudinal wall to be a Bloch wall. Both Bloch walls and Neel walls have been observed in thin films exhibiting perpendicular magnetic anisotropy in previous studies [28,34,50-54]. Dzyaloshinskii-Moriiya Interaction (DMI) is known to stabilize Neel walls of a particular chirality in thin films. Emori *et al.*[50] and Torrejon *et al.* [54] have reported that the strength of the DMI is very low in Ta/CoFe/MgO and Ta/CoFeB/MgO heterostructures respectively. The DMI is also found to be negligible in our samples. Also, in the case of the longitudinal domain wall, which we study here, magnetostatic energy is lowered when the moments inside the domain wall are oriented along the length of the wall owing to the shape anisotropy. Thus the longitudinal domain wall formed in our system is likely to be a Bloch wall with moments inside the wall oriented along its length (Fig. 3.8c). In addition, we observe the current driven domain wall motion in the presence of an external magnetic field, applied in-plane along the length of the wall (Fig. 3.14 and Fig. 3.15). In the presence of this field, the moments inside the wall prefer to orient along the direction of the field (Fig. 3.8c).

A 600 nm long, 200 nm wide and 1 nm thick magnet is simulated with a 2 nm mesh size laterally and 1 nm mesh size along the thickness (Fig. 3.15). Thus the simulation is basically performed on a two dimensional grid. At every point in the grid (x, y), the moment is allowed to evolve under time following the Landau Lifschitz Gilbert equation with the Slonczewski spin transfer torque term:

$$\frac{d\vec{M}(x,y)}{dt} = -\gamma(\vec{M}(x,y)\times\vec{H_{eff}}(x,y)) - \frac{\gamma\alpha}{M}(x,y)(\vec{M}(x,y)\times\vec{M}(x,y)\times\vec{H}(x,y)) - \gamma\tau(\vec{M}(x,y)\times\vec{M}(x,y)\times\vec{\sigma}) \tag{3.2}$$

where $\vec{M}(x,y)$ is the magnetization at a point in the grid with coordinates (x,y) (Fig. 3.15) and can point in any direction in the (x,y,z) space,$\vec{H}(x,y)$ is the effective field experienced by the magnetization at that point (x,y), α- damping constant, γ- gyromagnetic ratio, σ- direction of spin polarization and $\tau = \frac{\hbar}{2eM_st_F}\theta J_c$, θ- spin orbit torque efficiency, J_c- charge current, e- charge of an electron, μ_0- vacuum permeability, M_s- saturation magnetization of

the ferromagnet (8×10^5 A/m or 800 e.m.u./c.c. used for simulation) and t_F- thickness of the ferromagnet (1 nm).
The effective field $\vec{H_{eff}}$ is calculated using $\vec{H_{eff}} = -(\frac{1}{M_s})(\nabla_{\vec{M}})E_{total}$ where $E_{total} = E_{anisotropy} + E_{exchange} + E_{Zeeman} + E_{Magnetoelastic}$
Anisotropy energy $E_{anisotropy} = -KM_z^2$, corresponding to the perpendicular magnetic anisotropy of the ferromagnet. K= 6×10^5 J m$^-3 = 6 \times 10^5$ erg/cc. is used in the simulation.
Exchange energy $E_{exchange} = A((\nabla M_x)^2 + (\nabla M_y)^2 + (\nabla M_z)^2)$, where A is the exchange correlation constant (3×10^{-11} J/m or 3×10^6 erg/cc.)
Zeeman energy $E_{Zeeman} = -\mu_0(\vec{M}.\vec{H_{applied}})$ where $\vec{H_{applied}}$ is the applied magnetic field.
$E_{magnetoelastic}$ is the magnetostatic energy or dipole energy of the system, calculated by the micromagnetic simulator.
The initial condition of the simulations is a longitudinal domain wall, which divides the magnet into oppositely polarized domains. To simulate that we use the function $M_z(x, y) = -M_s(cos(\Psi)), M_x(x, y) = M_s(sin(\Psi))$ [55] for $H_{applied,x} > 0$ and $M_x(x, y) = -M_s(sin(\Psi))$ for $H_{applied,x} < 0$ where $\Psi = tan^{-1}(sinh(\frac{\pi(y-y_0)}{\delta_{DW}}))$, y_0 is the position of the domain wall, which is the center of the bar initially (t=0 s) and δ_{DW}=domain wall width=$\pi(\frac{A}{K})^{\frac{1}{2}}$)=22 nm. The system is allowed to evolve using equation (3.2) under the application of a 10 G magnetic field. $\vec{H_{applied}}$ is in +x/-x direction and a spin polarization of $\tau\vec{\sigma}$ where $\tau = \frac{\hbar}{2eM_s t_F}\theta J_c$ and $\vec{\sigma} = +\hat{y}$ or $-\hat{y}$ (Fig. 3.15) with θ=0.08, $M_s = 8 \times 10^5$ A/m= 800 emu/cc, t_F=1 nm and $J_c = 3.5 \times 10^6$ A/cm^2.

Micromagnetic simulations show that when a magnetic field is applied in -x direction and a current is applied in the +x direction the domain wall moves in -y direction till the magnet is saturated into the plane (Fig. 3.15a). Reversing the direction of the magnetic field (Fig. 3.15b) or the current (Fig. 3.15c) reverses the direction of domain wall motion, just as observed experimentally (Fig. 3.14). Thus, polarity of the final state of the magnet is found to be a cross product of direction of the in-plane field and direction of accumulated spins. Notably, these simulations results, which show a one-to-one correspondence with the experimental observation, are consistent with the Slonczewski-like spin orbit torque. Oersted field or field like spin orbit torque from the current cannot explain such domain wall motion. This is because when we replaced the Slonczewski-like spin orbit torque $(\gamma\tau(\vec{M}(x, y) \times \vec{M}(x, y) \times \vec{\sigma})$ with torque due to an in-plane magnetic field, which could be Oersted field or field like term in spin orbit torque, in our simulations, the domain wall does not move at all.

To summarize this section, we showed through experiments and simulations that a longitudinal domain wall moves from the center to edge of a magnetic bar due to current flowing through the bar in the presence of an in-plane magnetic field. Thus the motion of the domain wall is orthogonal to the direction of the current flow. The domain wall moves as if it is under the influence of an effective magnetic field which is either "out of plane" or "into the plane" and is the cross product of the applied in-plane magnetic field ($\vec{H_{in}}$) and spin

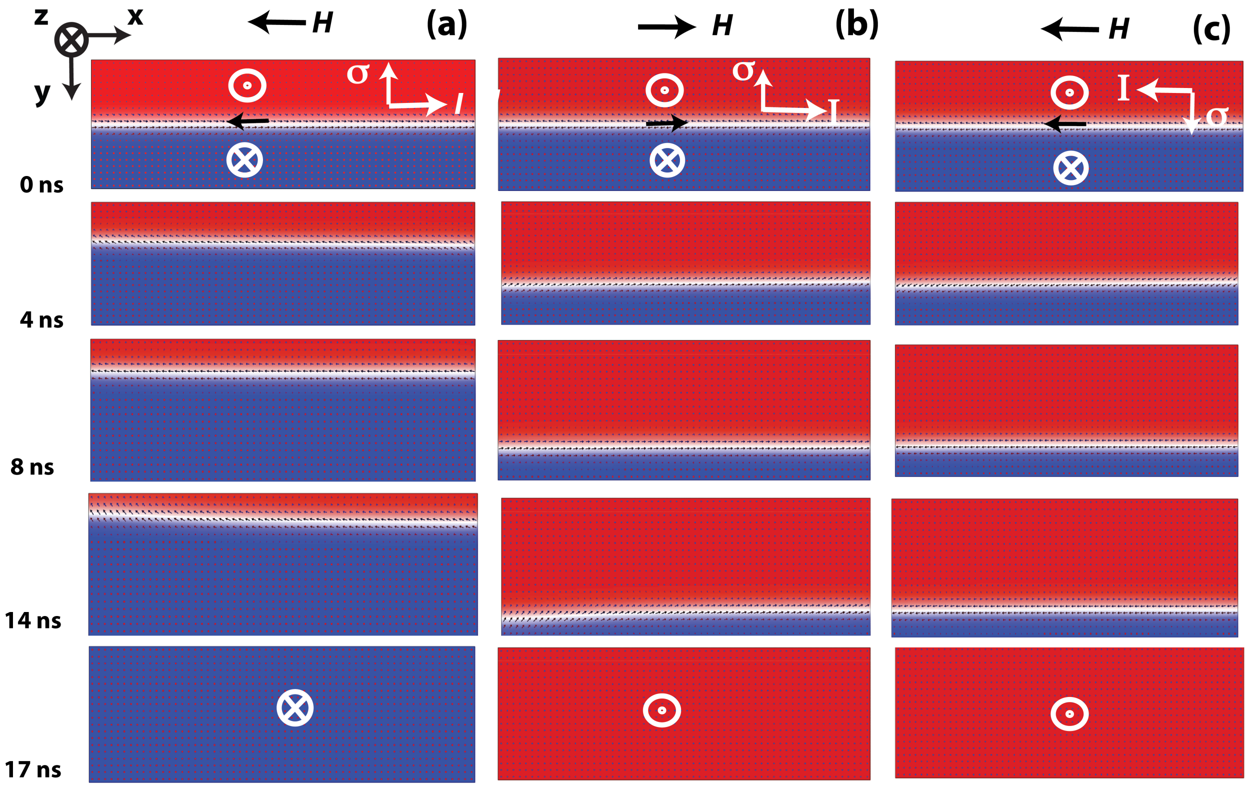

Figure 3.15: (a) (b) Micromagnetic simulation of a 600 nm long and 200 nm wide magnet shows the motion of a longitudinal domain wall under the application of a spin polarization in -y direction (current I in +x direction) and an in-plane magnetic field (H_{in}) in -x/+x direction. The direction of the net magnetic moment in the domain wall, shown by a black arrow, is initialized along the direction of applied field. (c) Micromagnetic simulation of the same magnet with spin polarization in +y direction (current I in -x direction) and magnetic field in -x direction.

accumulation from the current ($\vec{\sigma}$). Thus the final direction of the magnetization= $\vec{H_{in}} \times \vec{\sigma}$, as we see in Fig. 3.14 and Fig. 3.15.

3.6 Microscopic mechanism of spin orbit torque driven magnetic switching: A revision

In this chapter, we first reported our experiments on spin orbit torque driven magnetic switching where a magnet switches from saturated up/"out of plane" state to down/"into the plane" state due to spin orbit torque from an in-plane current flowing through the heavy metal layer underneath the ferromagnet. Then we discussed how solving the Landau Lifschitz

Gilbert equations with Slonczweski like spin orbit torque under the assumption that the ferromagnet is a single domain or one giant macrospin can provide qualitative match with the experiments, but there is a two orders of magnitude difference in magnitude of current needed to switch the magnet in experiments (of the order of 10^6 A/cm^2) and simulations ((of the order of 10^8 A/cm^2). Then we suggested that magnetic switching in this kind of ferromagnets occurs via nucleation of reverse domains, followed by domain wall motion. Thus if we can model the motion of domain wall around a reverse domain via spin orbit torque, we can provide a much better quantitative match of the current magnitudes. The spin orbit torque driven motion of longitudinal domain wall, orthogonal to the current flow, that we discussed next, needed currents in the order of 10^6 A/cm^2 both in experiments and simulations because the simulations we did in this case did not assume that the magnet is single domain. We performed a micromagnetic simulation where we calculated spin orbit torque on a domain wall. Equipped with the knowledge that current can move domain walls and a micromagnetic picture can provide a quantitative match between currents in experiments and simulations, we now explain the microscopic mechanism of magnetic switching results of section 3.2. In that regard, we also discuss here a work by Lee *et al.*, who worked on this problem independently around the same time as us [48].

Lee *et al.* provided a micromagnetic picture of the switching, reported by Liu *et al.* in Pt/Co Hall bars that exhibit perpendicular magnetic anisotropy [25]. We discussed the results of Liu *et al.* in Chapter 2 of the thesis (Fig. 2.3). The switching in Pt/Co samples depends on the polarity of the external in-plane magnetic field and the direction of the current just like our Ta/CoFeB samples just that the polarity of the switching is different because Pt/Co interface has the opposite direction of spin accumulation as that of Ta/CoFeB for the same polarity of current. Lee *et al.* [48] argue that once a reverse domain is nucleated by the current pulse due to thermal nucleation, the domain wall formed around the reverse domain is of Neel type due to DMI and has the magnetization coming outward from the center of the reversed domain at every point in the domain wall. Such a reverse domain will not expand under the spin orbit torque from the current pulse because the domain wall experiences effective magnetic field (average direction of magnetization in the wall × spin accumulation direction (σ), as discussed in Section 2.3 and Section 3.5) of opposite polarities across its diameter (Fig. 3.16a). However, when an external magnetic field is applied strong enough to overcome the DMI, the average magnetization of the domain wall is aligned along the field. The net effective field experienced by the domain wall is non-zero and so the reversed domain expands to switch the magnet. Yu *et al.* also argued based on their MOKE microscopy results that DMI and spin Hall torque together move the domain walls and switch the magnet [56]. However, in our longitudinal domain wall motion experiments reported in Section 3.5, we have argued that the domain wall is of Bloch type and not Neel type. Hence here we argue that the domain wall formed around a nucleated reverse domain is of Bloch type as well. The average magnetization of the wall follows the externally applied magnetic field and the cross product of that with the spin polarization vector (σ) gives a

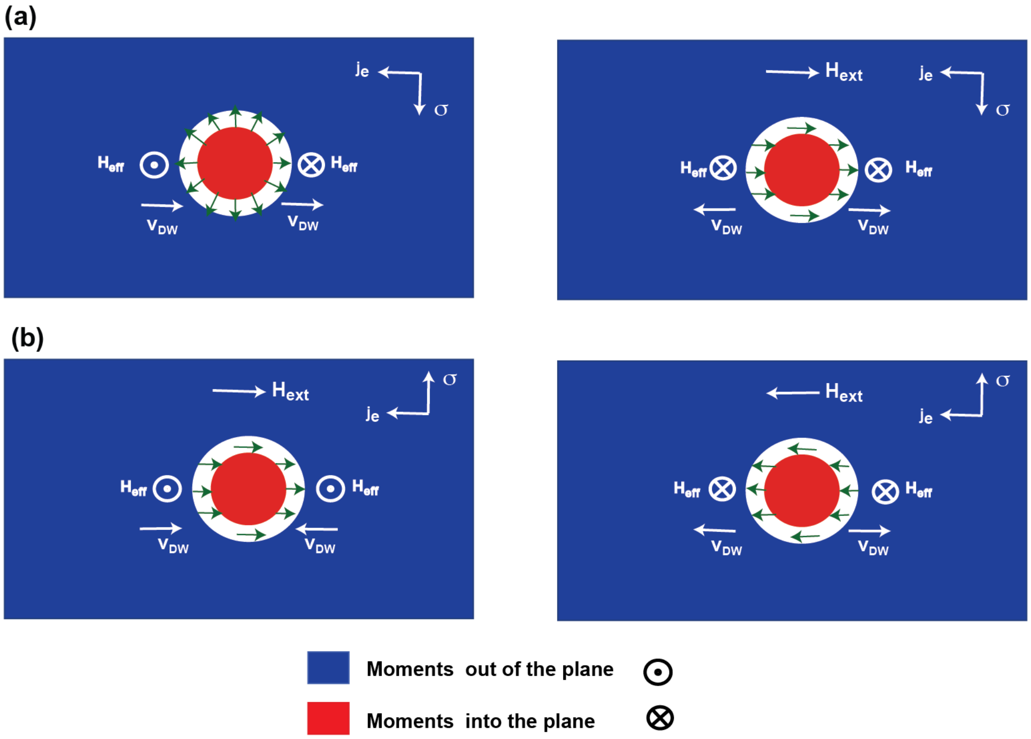

Figure 3.16: (a) The domain wall formed around the reverse domain (red circle), nucleated in the ferromagnet, is of Neel type if the DMI is strong. In the absence of an external magnetic field, the configuration of the moments (green arrows) inside the domain wall is such that the effective out of plane magnetic field H_{eff} experienced by different parts of the domain wall cancels each other (H_{eff}= average magnetization inside the domain wall $\times\sigma$, where σ is the direction of spin accumulation at the interface). So the reverse domain does not expand and the magnet does not switch. When an external magnetic H_{ext} field is applied and it is strong enough to overcome the DMI, the moments inside the domain wall orient in that direction. So H_{eff} experienced by all parts of the wall is "into the plane" and the reverse domain expands to switch the magnet into the plane. (b) In the absence of DMI, the moments of the domain wall around the reverse domain can be easily switched by an external magnetic field H_{ext} in its direction. When H_{ext} is towards the right, the domain wall experiences an effective field in "out of plane" direction, which favors out of plane directed moments. So the reverse domain shrinks and the magnet remains in "out of plane" direction (blue). When H_{ext} is towards the left, the domain wall experiences an effective field in "into the plane" direction, which favors "into the plane" moments. So the reverse domain expands and the magnet switches to "into the plane" direction (red). It is to be noted that both for (a) and (b), the final direction of the magnetization= $\vec{H_{ext}} \times \vec{\sigma}$

net out of plane magnetic field. For the right polarity of the current pulse and the magnetic field, the effective out of plane field will make the reverse domain expand and switch the magnet. The key difference between this mechanism and that discussed by Lee *et al.* [48] is that the latter needs the presence of DMI while the former doesn't, and a large external magnetic field is needed to nullify the role of DMI in the latter but not in the former. The former mechanism (proposed by us) applies better to the Ta/CoFeB heterostucture and the latter mechanism (discussed by Lee *et al.* [48]) for the Pt/Co heterostructure because Pt/Co interface has much higher DMI than Ta/CoFeB interface. However with either model the need of the external in-plane magnetic field for the switching data can be explained and the experimental switching data can be explained quantitatively to obtain the correct value of spin orbit torque efficiency which was not possible with the single domain analysis.

The circular domain wall around the reverse nucleated domain in Fig. 3.16b can be imagined as a combination of longitudinal domain walls and transverse domain walls. Both these domain walls experience an effective “into the plane” or “out of the plane” magnetic field depending on the direction of the moment inside the wall and spin accumulation (σ), which causes expansion or contraction of the domain resulting in the switching of the magnet. Thus when a magnet switches from one saturated state to another in our switching experiments (Fig. 3.3) switching can happen both by the movement of the longitudinal domain wall and transverse domain wall. Imaging experiment performed by G. Yu *et al.* shows that for Ta/CoFeB/TaOx films when the ferromagnet switches, domain wall moves diagonally which means a combination of longitudinal and transverse domain walls switches the magnet [56].

3.7 Measurement of Joule heating due to current

In order to see how much temperature of the device goes up due to the high current pulses we applied in the experiment, we have measured the resistance of a 20 μm wide magnetic bar made from the same stack of Si (substrate)/ SiO_2 (100 nm)/ Ta (10 nm)/ CoFeB (1 nm)/ MgO (1 nm)/ Ta (2 nm). Four probe measurement technique is used (Fig. 3.17a). The resistance measured at room temperature is 300 Ohm. Temperature of the sample is first increased using a heater. Change in resistance is plotted as a function of temperature in Fig. 3.17b. We see that the resistance goes down by ~6.5 Ohm as the temperature increases from room temperature (~ 290K) to 400K. This surprising result that resistance of Ta decreases with increase in temperature in this temperature range has been reported by Schwartz *et al.* [57]. Change in resistance is next plotted against dc current density through the device (Fig. 3.17c). We do four-probe measurement on the same device to measure a resistance as a function of the current through the device. Since we used 1 s current pulses for the domain wall motion reported in the paper, we need to account for the heating due to the current over the period of 1s. As a result, to obtain the plot of resistance versus current density, we first measure the resistance with a small current (5×10^4 A/cm^2). We call this the base resistance. Then high current of a particular magnitude is applied continuously

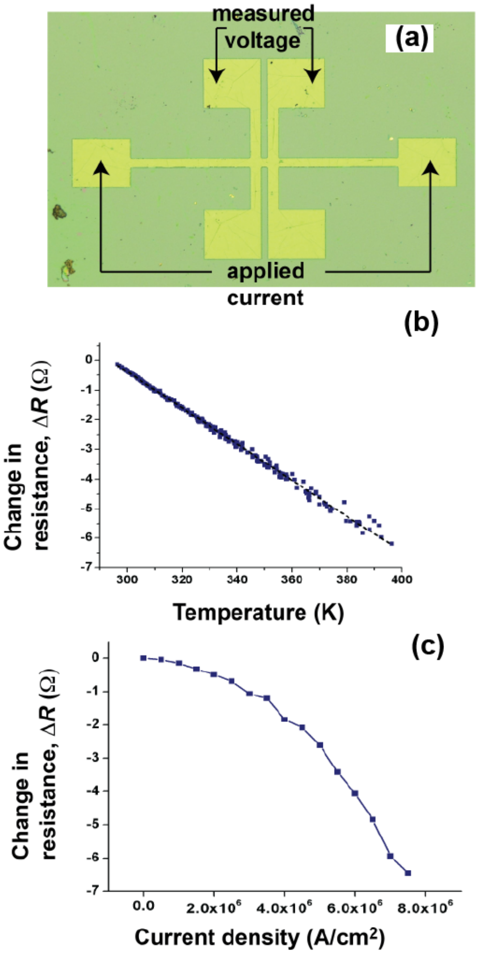

Figure 3.17: (a) Double Hall bar fabricated for four probe measurement of resistance (b) Change in resistance from resistance at room temperature plotted as a function of increase in temperature. (c) Change in resistance is plotted as a function of increase in dc current density.

for 1s and the resistance is measured at the end of 1 s with that current still on. It is then subtracted from the base resistance to get the change in resistance, corresponding to that current magnitude. The same experiment is repeated for several high current values and the change is resistance is plotted as a function of the corresponding magnitudes of current density. We see that as the current increases, resistance goes down. This is because as more current flows temperature of the device goes up due to Joule heating and resistance drops because of increase in temperature. The maximum current density used in our experiments is $\sim 7 \times 10^6$ A/cm^2. From the plots in Fig. 3.17, we infer that for such current density the temperature of the device can increase up to ~ 400 K ($\sim 127\ ^o$C).

Chapter 4

Spin orbit torque driven clocking in a nanomagnetic logic circuit

In this chapter, we discuss an application of spin orbit torque: clocking mechanism in nanomagnetic logic circuits. Spin based computing schemes can enable new functionalities beyond those of charge based counterparts [58-62]. Examples include nanomagnetic logic, where information can be processed using dipole coupled nanomagnets [63-70], as demonstrated by multi-bit computing gates [64,69]. One fundamental benefit of using magnets is the possibility of drastic reduction in the energy per bit compared to conventional transistors [57,64,70,71]. However, practical implementations of nanomagnetic logic to date have been limited by the necessity to apply a magnetic field for clocking [64,67]. While the energy associated with magnetic switching itself could be very small, the energy necessary to generate the magnetic field renders the overall logic scheme uncompetitive to CMOS counterparts. In this chapter, we demonstrate a nanomagnetic logic scheme at room temperature where the necessity for using a magnetic field clock can be completely removed by using spin-orbit torques. We construct a chain of 3 perpendicularly polarized CoFeB nanomagnets on top of a Ta wire and show that an unpolarized current flowing through the wire can "clock" the perpendicular magnetization to a meta-stable, in-plane state. Then an input magnet can drive the nanomagnetic chain deterministically to one of the two dipole-coupled states: "2 up 1 down" or "2 down 1 up" depending on its own polarization. Thus information can flow along the chain, dictated by the input magnet and clocked solely by a charge current in Ta, without any magnetic field. A three to four orders of magnitude reduction of energy dissipation is expected for our scheme as opposed to state of the art nanomagnetic logic.

4.1 Underlying physics of the clocking mechanism

The underlying physics of the clocking is that of spin orbit torque driven switching in perpendicularly polarized ferromagnet- heavy metal heterostructure, that has been described in details in the previous two chapters. We have shown that magnetization can be effectively controlled by charge current flowing in a heavy metal sitting right underneath the magnet (Fig. 4.1) [9,10]. All our previous experimental data and that of Liu *et al.*[10] and Miron *et al.*[9] were obtained from micron sized ferromagnets. In such devices, when a current pulse of sufficiently high magnitude is applied in the absence of a magnetic field, due to spin orbit torque from the current pulse, the magnet breaks into domains ("mixed state" of Fig. 3.12: previous chapter). If a small magnetic field is applied then the domain wall moves such that the magnet is in saturated up (+z) state for up (+z) directed magnetic field and down (-z) for down (-z) directed magnetic field. Similarly, if a current pulse of strong magnitude is applied in the presence of a small magnetic field, the final state of the magnet is +z if the magnetic field is in +z direction and the final state is -z if the magnetic field is in -z direction. This is because the current through the heavy metal has reduced the coercivity of the magnet to a very small value (Fig. 3.2: previous chapter). If we reduce the dimensions of the ferromagnet to few hundreds of nanometers, we observe a similar phenomenon. Independent of the initial state of the nanomagnet (+z or -z), in the presence of a small +z directed magnetic field, application of a current pulse of sufficiently high magntitude (10^7 A/cm^2) switches the magnet to +z. In the presence of a small -z directed magnetic field application of a current pulse switches the magnet to -z. This is identical to the Hall bars of dimensions in the orders of microns which we investigated previously (Fig. 3.12). However in the absence of a magnetic field, application of a current pulse of high magnitude does not create a mixed state. Instead the magnet goes to either +z state or -z state with almost a 50 percent probability (We describe the results in details in the next section). Since we do not observe domains in the case of nanomagnets, we do not use the previously used picture involving nucleation of reverse domains followed by domain wall motion to explain spin orbit torque driven switching of nanomagnets. Also the current magnitude needed for the switching is higher for nanomagnets compared to the micron sized Hall bars, further reducing the importance of domain formation to explain switching in nanomagnets. Instead we use a very simple single domain picture that we described in Section 3.3 of the previous chapter (Fig. 3.4) to explain spin orbit torque driven switching in nanomagnets.

When an in-plane current flows through a resistive bar made of Ta, electrons having spins of opposite polarities accumulate at the opposite surfaces along the thickness of the bar (Fig. 4.1a) and exert a spin orbit torque on the ferromagnet (CoFeB) sitting right on top of Ta. The CoFeB has perpendicular magnetic anisotropy. Thus the in-plane torque, if strong enough, can bring its magnetization to in-plane where it is meta-stable as it is the "hard plane" for the magnet. If the current is now turned off, the magnet, from this meta-stable state, will randomly go to an "up" (+z) or "down"(-z) state, determined by thermal noise. The ability to drive the magnet to a meta-stable state allows one to use it as an efficient clocking mechanism. For example, let us imagine a situation where there is a chain of three nanomagnetic dots, placed on the top of a Ta bar. Application of a current pulse (clock) through Ta would drive the magnets in-plane (Fig. 4.1b). Upon removal of the current, the magnets would orient themselves in their lowest energy configuration, "2 up 1 down" (↑↓↑)

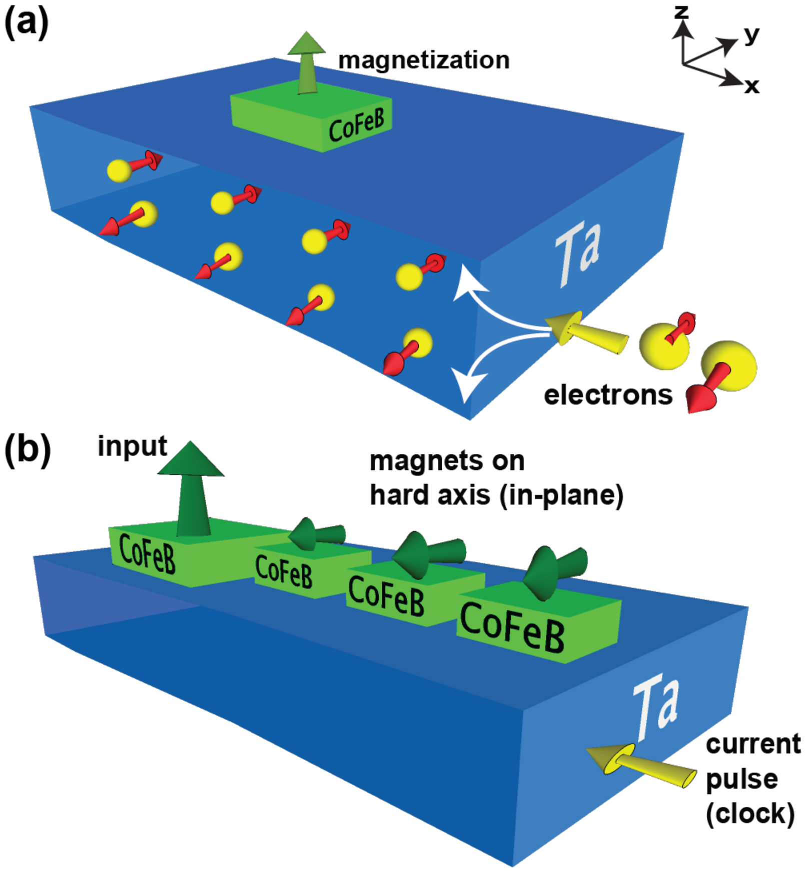
(a)
magnetization
z
y
x
CoFeB
Ta
electrons
(b)
input
magnets on
hard axis (in-plane)
CoFeB
CoFeB
CoFeB
CoFeB
Ta
current
pulse
(clock)

Figure 4.1: (a) In plane current flowing through Ta along the x direction (electrons along -x direction) causes spin separation across the thickness of Ta (z direction). It results in the accumulation of electrons with y directed spins at the Ta-CoFeB interface, which offers spin orbit torque to the magnetization (green arrow) of CoFeB. This spin torque drives the magnetization of CoFeB from its easy axis in the out of plane direction to a meta stable in-plane state. (b) When current passes through the Ta bar below the magnetic dots, magnetizations of all the dots other than the large input dot are driven in-plane to a metastable state by the spin orbit torque. Current flows in -x direction here, so electrons with -y directed spins accumulate at the Ta-CoFeB interface resulting in the magnetizations of the dots being driven to -y direction. When the current pulse is removed, the magnets go to the dipole coupled least energy configuration.

or “2 down 1 up” (↓↑↓), due to dipole coupling. Now, if the input magnet can be designed in such a way that it is not affected by the clock pulse, it will dictate the final state of the 3-dot nanomagnetic chain because the dipole field from the input magnet will switch the adjacent magnet in the direction of the dipole field (opposite to polarity of input magnet) and so on . If the input is (↑), the chain of 3 dots will go to (↓↑↓) and if the input is (↓), the chain will go to (↑↓↑). Thus the last magnet in the chain will be a function of the fixed input magnet and information will propagate along the chain. In this paper, we demonstrate that such a scheme is indeed possible.

It is to be noted that we explained the mechanism of clocking through a simple single domain model here. Spin orbit torque from a current pulse drives the magnetization of the nanomagnet in-plane, which is a “metastable” state. At the end of the current pulse the dipole field from an adjacent magnet can switch the magnet. If there is no dipole field present, the magnet goes to either up or down due to the thermal noise. However, we only measure the final state of the magnet. We do not microscopically image the “metastable” state of the magnet which is formed during the application of the current pulse. Since the coercivity of the nanomagnets is just $\sim$200 G, which is greater than that of the micron-sized Hall bars ($\sim$60 G) but still much smaller than the anisotropy field ($\sim$2000 G) the possibility of domain formation during the switching process cannot be ignored. So it might well be that in the “metastable” state the magnet is an assortment of oppositely polarized domains. After the current pulse, due to dipole field the domain wall moves to deterministically switch the magnet to “up”(+z) or “down”(-z). In the absence of dipole field, i.e., under zero magnetic field, after the current pulse the magnet does not remain in a “mixed state” with oppositely polarized domains probably because the domain wall moves in one direction or the other under thermal noise. Since the magnet is small, the full magnet is switched which is not possible in the case of the microns sized Hall bars used in the previous experiments (Fig. 3.12). In the following sections, we describe our experiments that demonstrate clocking in a nanomagnetic logic circuit using spin orbit torque. Either picture (magnetization is in-plane in the “metastable” state or the magnet broken into domains in “metastable state”) explains the results. For simplicity, we use the first picture here.

4.2 Driving a single nanomagnet to a meta-stable state

We start by investigating an individual dot. All our devices are fabricated from a stack of thermally oxidized Si (substrate)/Ta (10nm)/CoFeB (1nm)/MgO (1nm)/Ta (20 nm). First the stack of thermally oxidized Si substrate/Ta (10 nm)/CoFeB (1 nm) /MgO (1 nm) /Ta (20 nm) is processed into Hall bars by photolithography and Ar^+ ion milling. The Hall bars contain the whole thin film stack, while the region outside the Hall bars is etched till the insulating Si substrate. Next, a dot pattern of 8 nm thick Ti, which acts as an etching mask,

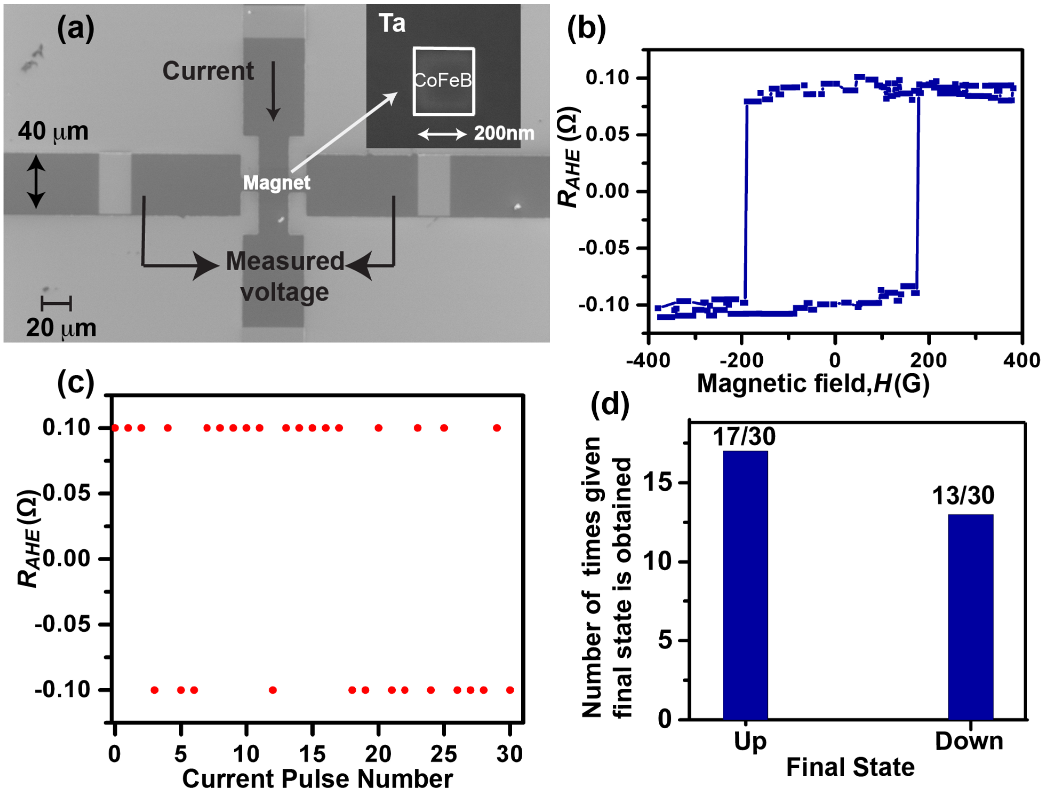

Figure 4.2: (a,b) SEM images show a Hall bar structure with a square dot of side length 200 nm at its center . The dot retains Ta (10 nm)/CoFeB(1 nm)/MgO (1 nm)/Ta(∼ 10 nm), while regions outside the dot are etched till the bottom Ta layer of the stack. (c) Anomalous Hall resistance(R_{AHE}), proportional to the out of plane magnetization of the dot, is measured using the Hall bar structure, with a varying magnetic field applied out of the plane. We obtain a square hysteresis loop, which shows that the easy axis of the magnet is out of the plane. (d) Starting from the magnet initially in the up direction, 30 successive current pulses of magnitude 1.5×10^7 A/cm^2 are applied at 0 G. R_{AHE} is measured after every current pulse and plotted against the current pulse number. (e) The histogram, obtained from the results of the same experiment, shows that the magnet is either up (+z, or $R_{AHE} = 0.1\Omega$) or down (-z or $R_{AHE} = -0.1\Omega$) after a current pulse with almost 50 percent probability. Thus spin orbit torque from the current pulse drives the magnet to a meta-stable in-plane state after which thermal noise directs it to either up or down state.

is fabricated on the Hall bar by Electron-beam lithography. Then Ar^+ ion milling is used again to etch the stack in the region, outside the dot patterns, till the bottom Ta layer. Thus the dots contain Ta (10nm)/CoFeB (1nm)/MgO (1nm)/Ta ($\sim$ 10nm) while regions of the Hall bar outside the dots are etched till the bottom Ta layer. All measurements for this work are performed at room temperature. Scanning Electron Microscopy (SEM) images of a typical Hall bar structure with a magnetic dot (200nm × 200nm) at the center are shown in Fig. 4.2. In this configuration, one could probe the magnetization by measuring the Hall resistance corresponding to Anomalous Hall Effect (AHE). The anomalous Hall resistance (R_{AHE}) is proportional to the out of plane magnetization of the dot. Fig. 4.2c shows a typical measurement. The data clearly show that the easy axis of the magnetic dot is in the out of plane direction. We initially start from a vertically up direction of the magnetization. Next, a current pulse of magnitude 1.5×10^7 A/cm^2 is applied 30 times. Among these, the final state of the magnet is found to be up ($R_{AHE} = 0.1\Omega$) 17 times and down ($R_{AHE} = -0.1\Omega$) 13 times (Fig. 4.2d, 4.2e). The near 50 percent probability of "up" and "down" states demonstrates that the current flowing in Ta is indeed putting the magnetic dot into a meta-stable state from where it is driven to up or down direction by thermal noise, following the intuitive picture presented earlier.

4.3 Dipole coupling between adjacent dots

Now that we have shown that the magnetization of a single nanomagnet can be driven into in-plane metastable state by spin orbit torque from the current pulse, we need to show that there is sufficient dipole coupling between adjacently placed nanomagnetic dots which is needed for the nanomagnetic logic scheme to work. Fig. 4.3a shows three fabricated dots, which are 200nm in diameter and separated from each other by a distance of 30nm. The distance of separation is crucial because if the displacement is high there will be no dipole coupling between the adjacent nanomagnets. The dots are placed away from the cross-center area of the Hall bars. In this configuration, the contribution to the AHE resistance from each of the dots is different and so they can be probed individually [72]. The following notation is used in text and Fig. 4.3(b-f) to represent magnetization states of the three adjacent magnetic dots - (State of the nearest magnet, State of the middle magnet, State of the farthest magnet), where state of each magnet can be up (↑) or down (↓). The dot nearest to the cross-center has the maximum contribution to the AHE signal [72] (Fig. 4.3b). When the nearest magnet switches, the change in R_{AHE} is 0.07 Ω while the same for middle magnet (middle arrow) is 0.04 Ω and for the farthest magnet (rightmost arrow) is 0.015 Ω. To verify that indeed the contribution from each dot to the total R_{AHE} signal depends on the distance of each dot from the cross-center area of the Hall bars we have fabricated another device where all the dots are at the center of the Hall bars (Fig. 4.4a). In that case we observe that the R_{AHE} signal has three jumps of equal size, suggesting that contribution from each dot is equal (Fig. 4.4b).

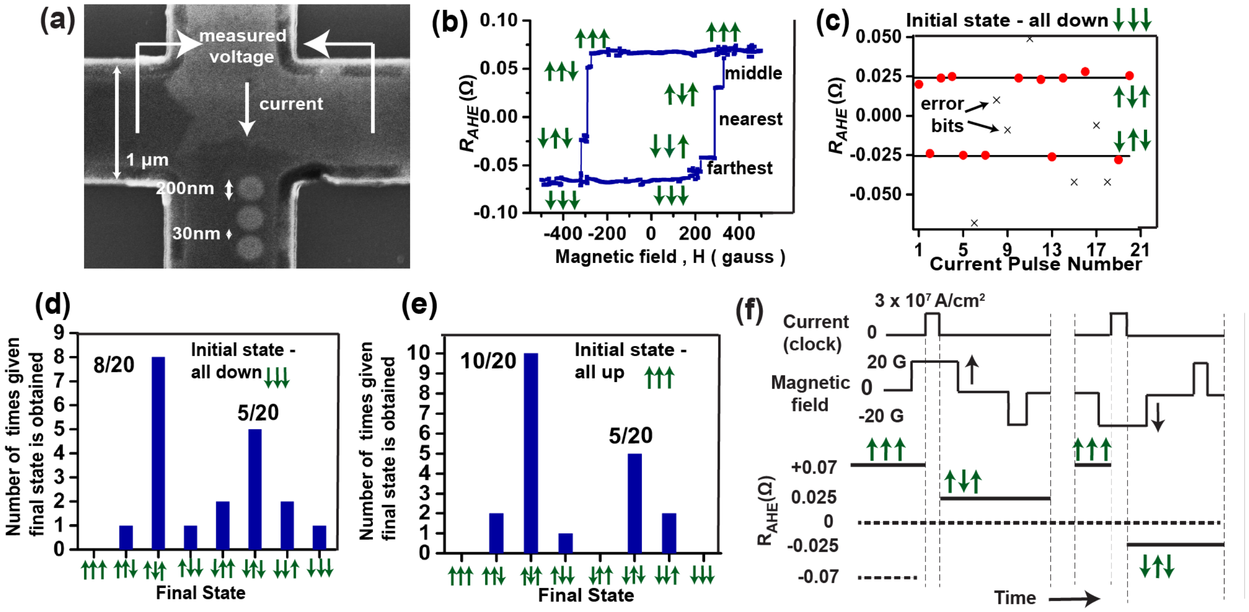

Figure 4.3: (a) SEM image shows three circular magnetic dots of diameter 200nm at a separation of 30 nm. (b) Hysteresis loop (R_{AHE} vs out of plane magnetic field) shows three discrete jumps, each jump corresponding to one magnet switching between up (↑) and down (↓). Green arrow indicates direction of magnetization of each dot. The dot farthest from the cross-center (rightmost arrow) has the lowest contribution to R_{AHE}, while the one, which is closest (leftmost arrow), has the highest contribution to R_{AHE}. (c) Starting with all three magnets initially down, current pulse of magnitude 3×10^7 A/cm^2 is applied 20 times at 0 G field. R_{AHE} of final state after current pulse is plotted against current pulse number. Bold lines are drawn through the expected final states- “2 up 1 down” (↑↓↑) and “2 down 1 up” (↓↑↓), which we obtain 13 out of the 20 times. Other 7 times we obtain states where adjacent magnets are parallel to each other. These are the error bits, represented by crosses. (d) The histogram, obtained from the results of the same experiment, show the dominance of mutually anti-parallel aligned states; (↑↓↑) - 8 times and (↓↑↓) - 5 times. This is because dipole coupling between the adjacent dots makes these two states the least energy configuration. (e) When the same experiment is repeated with all magnets initially up, (↑↓↑) state is formed 10 times and (↓↑↓) state is formed 5 times. (f) When same current pulse is instead applied in the presence of 20 G field, the magnets initially being in all up state, they always go to (↑↓↑) state. Similarly at -20 G the current pulse drive them to (↓↑↓) state. Thus the bias magnetic field controls the final state of the magnets here. Either of these states, (↑↓↑) and (↓↑↓) is stable unless another large current pulse or a magnetic field, higher than the coercivity of the dots (∼ 300G), is applied.

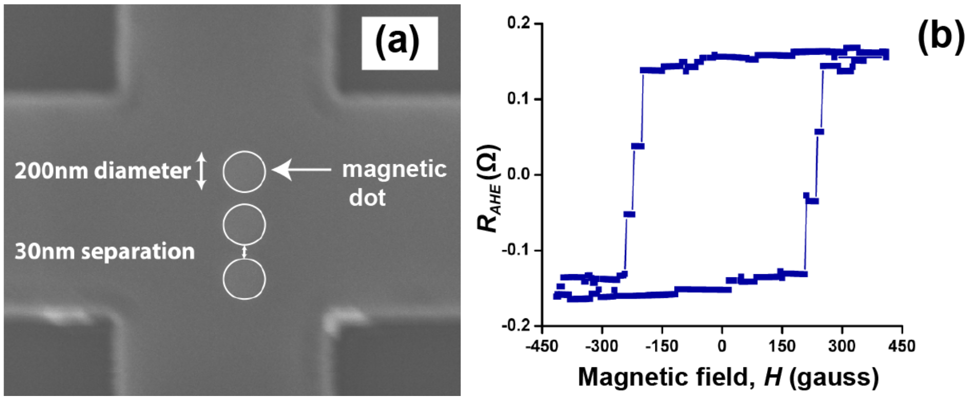

Figure 4.4: (a) SEM image of 3 dots of diameter 200nm each at a separation of 30nm, which are fabricated at the center of the Hall bars. (b) Anomalous Hall Resistance (R_{AHE}) vs magnetic field (out of plane) plot shows equal jumps in R_{AHE}, corresponding to switching of each magnet.

Getting back to the device of Fig. 4.3a, if these magnets are now driven to a meta-stable state, they are expected to go to a mutually anti-parallel state of "2 up 1 down" (↑↓↑) or "1 up 2 down" (↓↑↓) with 50 percent probability due to dipole coupling. To do this test, we first saturate the three dots in the device of Fig. 4.3a in the vertically downward direction by -400 gauss of out of plane magnetic field (positive polarity refers to upward magnetic field, negative polarity refers to downward magnetic field). Then the magnetic field is changed to 0 gauss and current pulse (clock) of magnitude 3×10^7 A/cm^2 and duration 1s is applied on the vertical Hall bar such that the same current flows through all the three dots (Fig. 4.3a). Thus all magnets experience the same spin orbit torque from the clock pulse. Once the current pulse is removed, R_{AHE} is measured by measuring the voltage across the horizontal Hall bar with a small amount of current flowing through the vertical bar to generate AHE response. The current density used for R_{AHE} measurement is two orders of magnitude lower than the magnitude of current pulse used to generate spin orbit torque.

Then the magnetic field is swept from 0 gauss to -400 gauss (saturation) and R_{AHE} is measured at every point of the sweep (Fig. 4.5). As the system goes to complete saturation (all three magnets vertically down polarized), the magnets which were vertically up polarized after the current pulse at 0 gauss show a sharp change in R_{AHE} corresponding to the their switching. On the other hand, the magnets which were down polarized after the current pulse at 0 gauss do not contribute to any change in the R_{AHE} signal. Also by looking at the size of the jump, we can conclude specifically which magnet was up polarized and which was down polarized after the current pulse. For example, when the resultant state after the current pulse at 0 gauss is (↑↓↑) state, saturation to all down takes place when the magnet, nearest to cross-center of Hall bars, switches (large jump in R_{AHE} of magnitude $\sim 0.07\ \Omega$) and magnet, farthest from cross center, switches (small jump in R_{AHE} of magnitude ~ 0.015

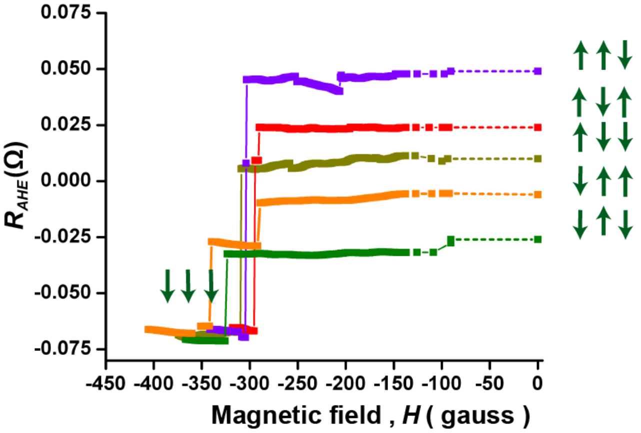

Figure 4.5: Anomalous Hall resistance (R_{AHE}) is measured while sweeping the magnetic field in the negative direction till all the three magnets become saturated in the downward magnetized state. The state of the three magnets after application of current pulse at 0 gauss is found out from the number and size of jumps in R_{AHE} on their way to saturation and is shown with respect to each R_{AHE} curve. Same notation is followed as that in text and Fig. 4.3 to represent the state of the magnets - (nearest magnet, middle magnet, farthest magnet)

Ω)(red plot in Fig. 4.5). When the resultant state after the current pulse at 0 gauss is (↓↑↓) state, saturation to all down (green plot in Fig. 4.5) takes place through only the middle magnet switching (medium jump in R_{AHE} of magnitude $\sim 0.04\ \Omega$). Thus looking at the number and magnitude of jumps, magnetization direction of each of the dots can be found out after the current pulse is applied at 0 gauss.

A current pulse of magnitude 3×10^7 A/cm^2 is applied at zero external magnetic field to drive the three magnets in a meta-stable state, starting from all the magnets in the down direction. Using this method mentioned above, we find that out of 20 repeated measurements, 8 times the magnets go to (↑↓↑) state and 5 times the magnets go to (↓↑↓) state (Fig. 4.3c, 4.3d). The same experiment is performed next with the three magnets initially in the upward direction. Out of 20 trials, on 10 occasions the final state is (↑↓↑) and 5 occasions the final state is (↓↑↓) (Fig. 4.3e). Thus indeed starting from all saturated state, the magnets are going to their lowest energy configuration (adjacent magnets anti-parallely oriented), driven by spin orbit torque. Hence adjacent magnets definitely experience significant dipole coupling. Slight deviation from 50 percent probability is possibly due to a small sample size (in terms of number of repetitions) and also due to errors that could arise in dipole coupling which have been extensively studied [73,74].

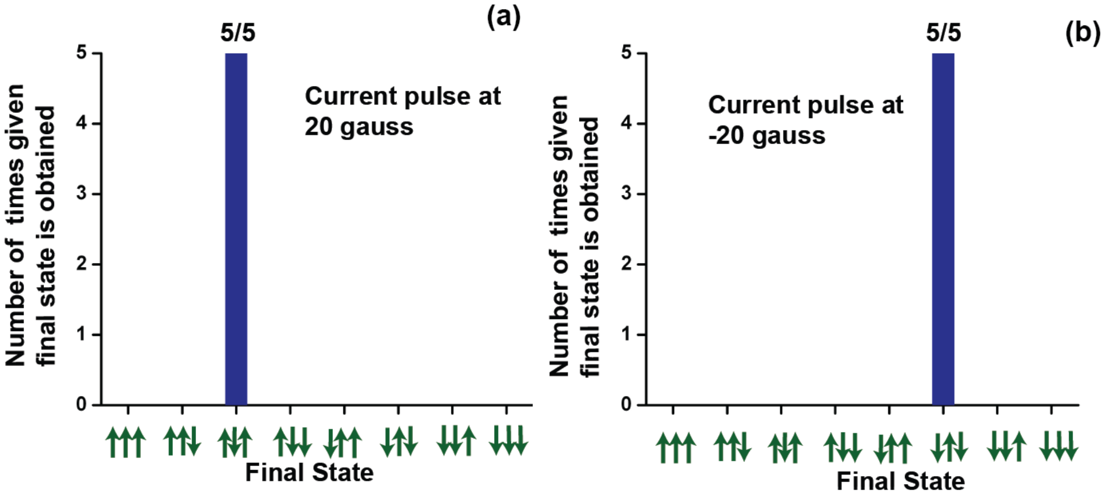

Figure 4.6: Histogram, obtained from multiple trials of the experiment in Figure 4.3f (clocking the three magnetic dots of Figure 4.3a at a bias magnetic field), shows that (↑↓↑) state is always formed when current pulse is applied at +20 gauss and (↓↑↓) state is always formed when current pulse is applied at -20 gauss.

Next the same experiment is repeated, but in the presence of a bias magnetic field. When the current pulse is applied with a 20 G field along the up direction, the magnets always go to “2 up 1 down” state (↑↓↑). Similarly when the current pulse is applied at -20 G the magnets always go to “2 down 1 up” state (↓↑↓) (Fig. 4.3f, Fig. 4.6a, Fig. 4.6b). When current pulse is applied to the three dots (all polarized upward) at +20 gauss, they go to (↑↓↑) state. We do this experiment 5 times and we always get the same result (Fig 4.6a). Similarly current pulse is applied to three dots (all polarized upward) at -20 gauss and they go to (↓↑↓) state. This experiment is also done 5 times and we always get the same result. In either case, none of the other 7 possible states is formed.Thus the external magnetic field breaks the symmetry of the system. As a result the three magnets do not go to (↓↑↓) state or ↑↓↑) state with a near 50 percent probability anymore. Instead the magnets prefer to go to one configuration compared to the other, depending on the polarity of the magnetic field. The fact that the current in Ta can drive the 3-dot chain into a meta-stable state, from where a magnetic field input, which can mimic dipole field from a fixed input magnet of Fig. 4.1b, can deterministically drive it to one of the two dipole-coupled states, clearly demonstrates that, the spin orbit torque can be used as an efficient clocking scheme for nanomagnetic logic.

4.4 Propagation of signal from an input magnet along a chain of nanomagnets

Finally, we show an implementation of an actual nanomagnetic logic circuit with spin orbit torque from a current pulse used as the clocking mechanism. We fabricate a 3-dot chain of nanomagnets (500 nm × 500 nm) together with an input magnet with the intention of showing that information propagates from the input magnet along the chain all the way to the farthest dot (Fig. 4.1b). The dots have a spacing of 30 nm between them. The input magnet in Figure 4.7a has dimensions much larger than the other magnetic dots of the 3-dot chain along which information is meant to propagate. In the AHE measurement, a larger change in R_{AHE} at smaller switching field corresponds to the switching of the large input magnet while smaller jumps at a higher switching field (Fig. 4.7b) must arise from the smaller magnetic dots because switching field reduces with increasing the size of the dot. This allows us to probe the input magnet and the 3-dot chain separately. The input magnet is a nearly rectangular dot with dimensions 2 μm by 5 μm, while the other magnets are squares of 500 nm side length. An input magnet is supposed to be unaffected by the clock pulse. Larger size of the input magnet compared to other magnets serves this purpose. Below, we explain how.

We have separately fabricated a 2 um square dot on a cross bar structure to study the properties of a large dot, like the input dot, independently (Fig. 4.8a). We start with the magnet being fully saturated in the upward direction. Application of a current pulse at 0 gauss results in the formation of a demagnetized state or “mixed” state ($R_{AHE} = 0$) with an equal number of up and down polarized domains, similar to the Hall bars measured in previous chapter (Fig. 3.12). When magnetic field is slowly increased in one direction the magnet gradually transitions from a “mixed state” to a saturated up state between 20 and 30 gauss (red plot- Fig. 4.8a).If we now apply the current pulse at 20 gauss instead, with the magnet initially up, no “mixed state” is formed. The final state of the magnet after the current pulse is same as the initial state (Fig. 4.8b). On the other hand we have already shown in Figure 4.2 that when a current pulse is applied at 0 gauss on a 200nm side square magnet, it does not break into domains. It goes to either saturated upward or downward state with 50 percent probability for each. Similarly when current pulse is applied at 0 gauss on the device in Figure 4.3 the three square magnets of 500nm size do not go to a mixed state. They rather reach dipole-coupled states with each magnet saturated up or down just like the 200nm circular dots in Fig. 4.3a.On the other hand, the larger magnet (2 by 5 μm dot) expectedly breaks into a mixed state just like the 2 μm square dot of Fig. 4.8a. Fig. 4.8c shows this happening. The larger magnet and the three other dots are all saturated upward. After application of a current pulse at 0 gauss, when the magnetic field is swept in the positive direction there is a gradual rise in R_{AHE} around 20 gauss which is the signature of a magnet transitioning from “mixed state” to the saturated state (red plot- Fig. 4.8c). We know that it is the larger magnet which is going from mixed state to saturated state and not

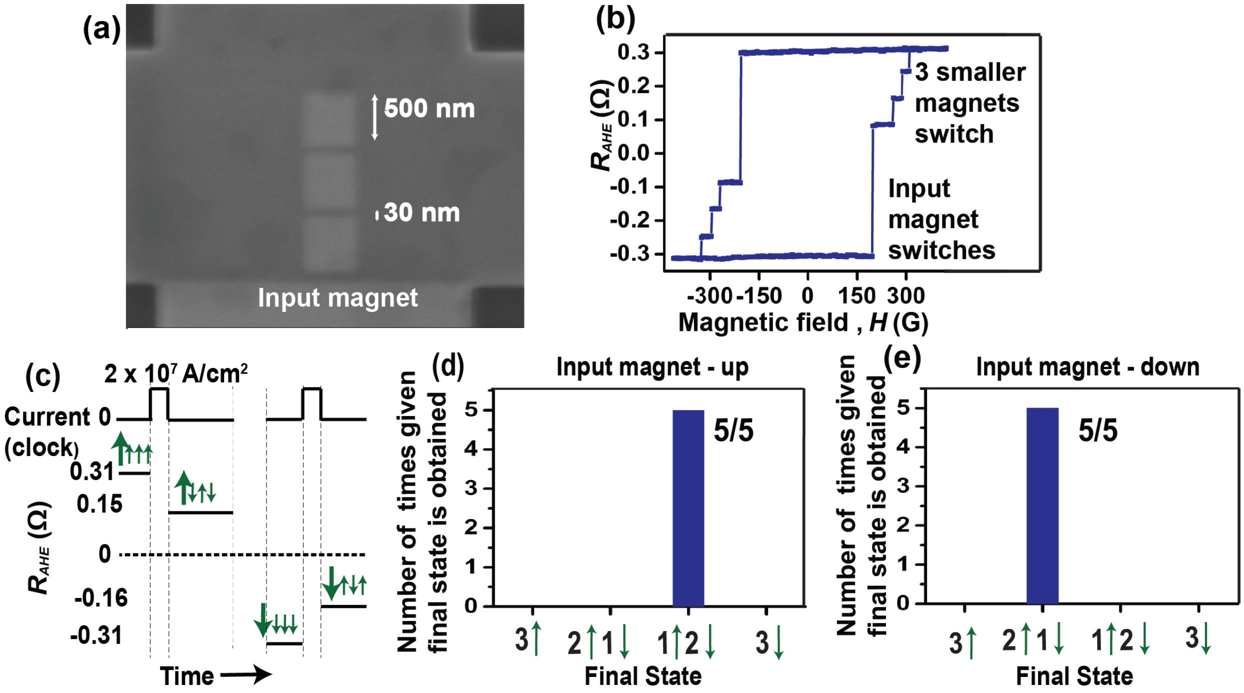

Figure 4.7: (a) SEM image shows three square magnetic dots of side length 500 nm at a separation of 30 nm, next to a larger dot with each side of a few microns length. This large magnet acts as the fixed input bit. (b) R_{AHE} measurement of the device shows two different types of jumps-larger change in R_{AHE} (0.4 Ω) corresponding to bigger input dot and three smaller jumps (0.08 Ω each) corresponding to the three smaller dots. (c) Current pulse of magnitude 2×10^7 A/cm^2 is applied at 20 G on the device with all magnets initially up. Input magnet, the magnetization direction of which is indicated by the big green arrow, remains up while other magnets (small green arrows) go to “2 down 1 up” state, thus following the input magnet. When current pulse is applied at -20 G with all magnets initially down, input magnet remains down while the other magnets go to “2 up 1 down” state. (d)(e) Histogram, obtained from multiple trials of the same experiment (c), shows that we always get “2 down 1 up” state when input magnet is up and “2 up 1 down” state when input magnet is down. Thus the magnetization state of the input magnet controls the final state of other magnets here.

the other magnets because the magnitude of the increase in R_{AHE} (0.25 Ω) is larger than the magnitude of one small jump (0.08 Ω), corresponding to the switching of each small dot (Fig. 4.7b). On the other hand, the smaller dots show sharp switching at higher magnetic fields. The change in R_{AHE} during the switching is 0.08 Ω, which corresponds to one full switch of a smaller dot between up and down (Fig 4.7b). It shows that the smaller dots were saturated in either up or down states after the application of current pulse at 0 gauss, but did not go to mixed state. If they were in mixed state, they would also have gradually saturated like the larger magnet at small magnetic fields instead of sharply switching at larger magnetic fields. If we now apply current pulse at 20 gauss instead of 0 gauss, the larger magnet (2 by 5 μ dot) should be unaffected as we have shown in Fig. 4.8b. On the other hand, Figure 4.3f shows that smaller dots form dipole-coupled states when current pulse is applied at 20 gauss. Thus for the device of Figure 4.7a, the smaller dots are affected by the current pulse at 20 gauss while the larger dot is not. Thus the larger dot acts as fixed input bit in the system.

Hence, to prepare the input state, we apply a current pulse in presence of a 20G magnetic field in the up direction. This puts the large input magnet in the up direction, which acts as an input to the chain. From Fig. 4.3e, this condition should drive the 3-dot chain to the "2 up 1 down" state (↑↓↑). On the other hand, if the input is strong, then the up-state of the input magnet should drive the 3-dot chain to a "2 down 1 up" state (↓↑↓). To test this, we start from all the magnets in the upward direction. A current pulse of magnitude 2×10^7 A/cm^2 and duration 1s is applied at 20 gauss (Fig. 4.9a). Next the magnetic field is swept in the positive direction till all dots reach saturation (red plot of Fig. 4.9a). We can see that unlike Figure 4.8c and Figure 4.8d, there is no gradual change of R_{AHE} at lower magnitudes of magnetic field, which means that the input magnet does not go to mixed state. There are only two sharp changes in R_{AHE} signal at a higher magnetic field with magnitude of each change equal to 0.08 Ω. They correspond to the switching of two smaller dots. Absence of a bigger jump ($\sim$ 0.4 Ω) means that the input magnet does not change its state when the magnetic field is increased in the positive direction, i.e, the input magnet has remained up after the current pulse at 20 gauss, which matches with our argument in the previous paragraph. Since there are two small jumps, two out of the three smaller magnetic dots were down at 20 gauss after current pulse and one was up. Also by applying the current pulse on saturated up magnets again at 20 gauss and sweeping the magnetic field negative till saturation (green plot) we observe one large jump corresponding to the input magnet switching from up to down. We also observe one small jump at higher magnetic field, which further confirms that only one of the three smaller magnetic dots was up after the current pulse at 20 gauss and it has switched down during the negative field sweep, resulting in that single sharp change in R_{AHE}. Thus we deduce that after the application of current pulse on all saturated up magnets, the input magnet is still up while the other three magnets are "2 down 1 up". The magnet next to the input magnet should be down owing to the stray field from input magnet. Thus input magnet controls the state of the other magnetic dots.

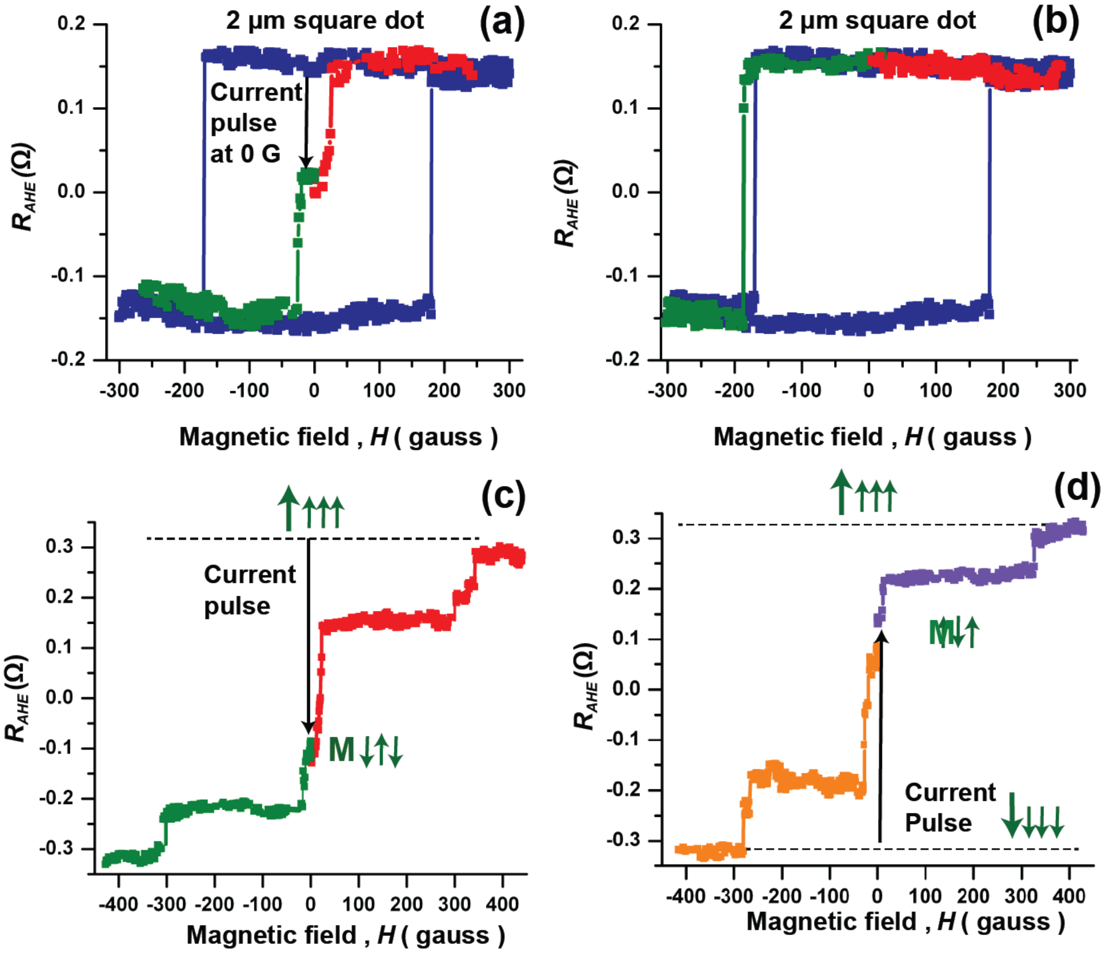

Figure 4.8: (a) Blue plot shows the hysteresis loop of a square dot of side length 2 μm obtained by R_{AHE} measurement. Current pulse with magnitude of 1.5×10^7 A/cm^2 and duration 1s applied at 0 gauss drives the magnet from a saturated up state to a mixed state of up and down polarized domains ($R_{AHE} = 0$). After that, as magnetic field is swept upward the magnet gradually goes back to saturated up state between 20 and 30 gauss, represented by a gradual rise in R_{AHE} (red plot). Similarly if magnetic field is swept downward, the magnet goes to saturated down state gradually between -20 and -30 gauss (green plot). (b) Starting with the magnet in saturated up magnetization state, application of current pulse with same magnitude and duration as before (1.5×10^7 A/cm^2, 1 s) at 20 gauss does not change the state of the magnet since no change in R_{AHE} is observed. When magnetic field is swept in the positive direction R_{AHE} does not change (red plot). When magnetic field is swept in the negative direction after current pulse at 20 gauss, R_{AHE} changes sharply at -180 gauss, corresponding to a switch from saturated up to saturated down state (green plot). This shows that when current pulse is applied at 20 gauss on a large magnet of similar dimensions (2 μm by 5 μm) saturated in one direction, the final state of the magnet is same as the initial state. So it can be used as fixed input magnet.

Figure 4.8: (c) All magnets, including the large input magnet, are saturated upward. Current pulse of magnitude 2×10^7 A/cm^2 is applied on them at 0 gauss. Next magnetic field is applied in the positive direction and the magnets are driven back to saturation (upward), with simultaneous measurement of R_{AHE} (red plot). Gradual transition for the large magnet is observed at ∼20 gauss and sharper transition for the smaller magnets is observed at higher magnetic field (∼ 300 gauss). Next, current pulse is again applied on the upward saturated magnets at 0 gauss. This time, magnetic field is next swept in the negative direction till all magnets become saturated down (green plot). Similar results are observed. (d) Same experiment as in Figure S6c is performed on the same system of magnets, only difference being both for the orange and violet plots, the state of the magnets is all down before the application of current pulse. The large magnet again shows smooth transition to saturation, while the three smaller magnets show sharp switching.

When same experiment is performed with all magnets initially down, we find out through the same procedure that the resultant state is “2 up 1 down” because the input magnet is down now and it controls its adjacent magnet to be up (Fig. 4.9b). These two results are summarized through a schematic in Fig. 4.7c.

We repeat the experiment 5 times each for the input magnet up and down, and observe the same result (Fig. 4.7d and Fig. 4.7e). Thus unlike the system of three dots without an input dot, here the three dots do not probabilistically go to either “2 up 1 down” state (↑↓↑) or “2 down 1 up” state (↓↑↓). Instead, they deterministically to one of these two states or the other based on the polarity of the input magnet. It is important to note that the 20 G magnetic field has only been used to prepare the input state and is not fundamentally necessary for the operation of the logic scheme. In a practical implementation, the input magnet will be the output of a previous stage and can be electrically isolated from the magnetic chain so that the clock current does not flow through it.

The current amplitude needed for our experimental demonstration of clocking was roughly 2 mA with a Ta wire of width of 1 μm and thickness 10 nm. This is significantly low (more than 100 times lower) compared to the current that was needed (760 mA) in the only on-chip demonstration of magnetic field based clocking for a much smaller magnet (60 nm » 90 nm), carried out by Alam *et al.* [67]. The current needed in our scheme scales linearly with the width of the magnet, making the clocking scheme scalable. More importantly, the current needed to clock the magnet scales with the thickness of the Ta. In an optimized structure for a 60 nm x 90 nm magnet where the width of the Ta wire is the same as the magnet, the current amplitude could be reduced to 120 μA. Since spin orbit torque has been demonstrated for thicknesses of Ta up to 1 nm [27], we can reduce the thickness of our Ta bars and reduce the clocking current. Thus for 2nm thickness of Ta bar, current can be further reduced to 24 μA. On the other hand, Alam *et al.* [67] performed on-chip clocking

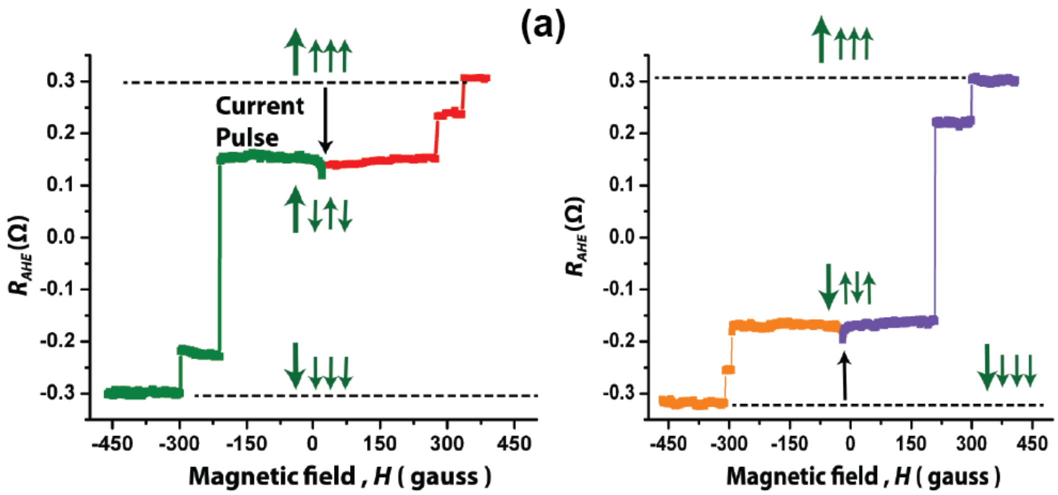

Figure 4.9: (a) All magnets, including the input magnet, are saturated upward. Current pulse of magnitude 2×10^7 A/cm^2 and duration 1s is applied on them at 20 gauss. Next magnetic field is applied in the positive direction and the magnets are driven back to saturation (upward), with simultaneous measurement of R (red plot). Two small jumps and no big jump in R_{AHE} show the formation of "2 down 1 up" (↓↑↓) state after application of the current pulse, along with input magnet remaining up. Again current pulse is applied on the upward saturated magnets at 20 gauss. This time, magnetic field is next swept in the negative direction till all magnets become saturated down (green plot). One small jump further establishes the formation of (↓↑↓) state after the current pulse. The big jump corresponds to the input magnet switching from up to down when we sweep the magnetic field in negative direction. (b) Same experiment as in (a) is performed on three dots with input magnet, only difference being both for the orange and violet plots, the state of the magnets is all down before application of current pulse and the current pulse is applied at -20 gauss. This time, saturation to all saturated up polarized state takes place through one small jump, corresponding to one small magnet switching from down to up, and one big jump, corresponding to the input magnet switching from down to up (violet plot). This shows that "2 up 1 down" (↑↓↑) state is formed after application of the current pulse at -20 gauss. It also shows that the input magnet did not change its state after the current pulse. Applying the current pulse again on downward saturated magnets at -20 gauss and sweeping the magnetic field in negative field further confirms the formation of (↑↓↑) state after the current pulse (two small jumps - orange plot).

on 60 nm × 90 nm magnets by applying 600 mA and 760 mA current pulses on Cu bars. Optimistic projections of such a scheme calculate current amplitude of 6.8 mA [67] and 4 mA [75]. Thus, both in terms of direct experimental data and projections of both schemes based on certain assumptions and idealizations, spin orbit torque driven clocking needs more than 100 times lower current than Oersted field clocking. Hence spin orbit torque driven clocking largely reduces the energy dissipated in the support circuitry to clock the nanomagnetic logic circuit.

Chapter 5

Deterministic spin orbit torque switching of a perpendicularly polarized magnet for low power memory

In the previous chapters we have already shown that spin orbit torque in heavy metal/ ferromagnet heterostructures can been used to switch the magnetization of the ferromagnet. Such spin orbit torque driven magnetic switching has been touted as a low power alternative to conventional spin transfer torque based switching for low power memory applications. Ferromagnetic structures that exhibit out of plane anisotropy are preferred for memory applications owing to their high thermal stability at ultrascaled dimensions. In a typical ferromagnet/ heavy metal heterostructure where the ferromagnet exhibits out of plane magnetic anisotropy like Ta/ CoFeB/MgO (from the bottom) in-plane current flowing in the Ta metal generates electrons with spins polarized in-plane at the Ta/CoFeB interface. Spin orbit torque resulting from the accumulation of such in-plane polarized spins cannot break the symmetry in the out of plane direction and hence cannot deterministically switch an out of plane magnet from up to down and down to up. This poses a severe challenge to the applicability of spin orbit torque for memory devices and become a viable alternative to conventional STTMRAM. However, in this chapter, we show through micromagnetic simulations that if the ferromagnet has a wedge shape then the anisotropy axis of the magnet tilts by a certain angle, which can be used to break the symmetry of the system. Then spin orbit torque can switch the magnet deterministically from up to down and down to up. Recent experimental results published by L. You. *et al.* [76] demonstrate such deterministic magnetic switching by spin orbit torque. In this paper, we present our micromagnetic simulation results in details which support and explain the experimental data. We also show that the directionality or handedness of the switching can be changed by changing the direction of the wedge.

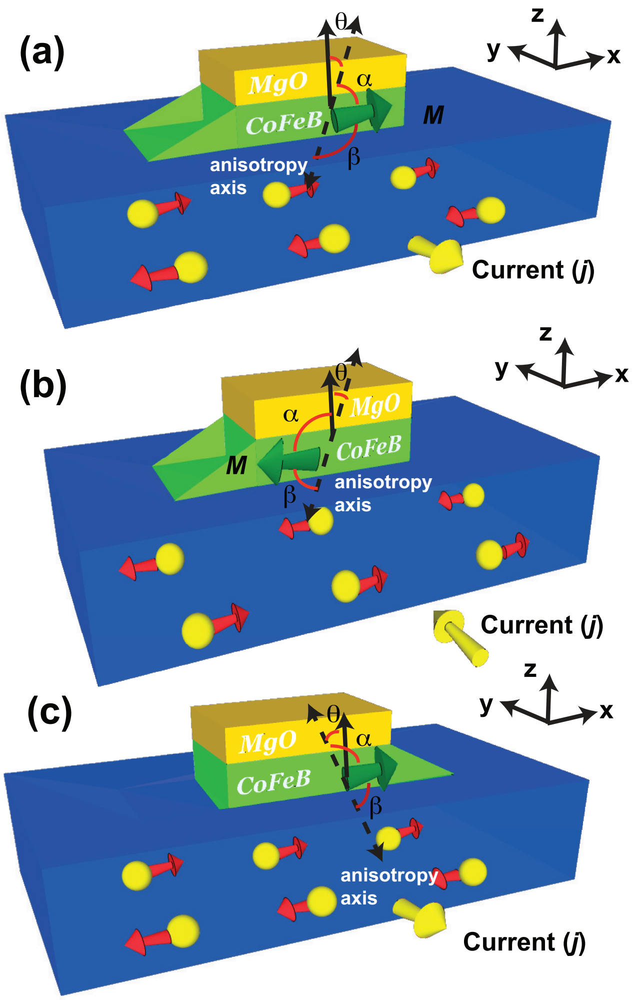
(a)
θ
α
β
MgO
CoFeB
M
anisotropy axis
Current (j)
z
y
x
(b)
θ
α
β
MgO
CoFeB
M
anisotropy axis
Current (j)
z
y
x
(c)
θ
α
β
MgO
CoFeB
anisotropy axis
Current (j)
z
y
x

Figure 5.1: (a) For a ferromagnetic (CoFeB) layer with the wedge is on the left side of the magnet looking in +y direction, the anisotropy axis tilts from the +z direction as shown. Current in -y direction results in accumulation of electrons with spins in +x direction at the interface of Ta and CoFeB. This drives the magnetization of the CoFeB layer into the +x direction. (b) Current in +y direction results in accumulation of electrons with spins in -x direction at the interface of Ta and CoFeB. This drives the magnetization of the CoFeB layer into the -x direction. (c) For a ferromagnet with wedge on the right side looking in +y direction, the anisotropy axis tilts in the opposite direction compared to the magnet with wedge on its left side.

5.1 Physical mechanism of the switching: Tilting of the anisotropy axis

Fig. 5.1 shows a typical heterostructure exhibiting perpendicularly magnetic anisotropy that has been widely used for spin orbit torque based magnetic switching experiments: Ta (10 nm)/CoFeB (1 nm) /MgO (1 nm) where Ta is the heavy metal, CoFeB is the ferromagnet and the MgO layer on the top of CoFeB is responsible for the perpendicular magnetic anisotropy exhibited by the CoFeB layer. When current flows through the heavy metal Ta in -y direction, electrons with spins polarized in +x direction accumulate at the interface of Ta and CoFeB layers. Without the wedge, the ferromagnet CoFeB has its magnetic anisotropy axis in the out of plane direction. If we assume a simple single domain picture for the ferromagnet, starting from up (+z) direction or down (-z) direction , the magnetization is driven in-plane in the +x direction by the SOT from the spin polarized electrons at the interface. Once the current pulse, and hence the SOT, is removed, the magnetization can either go to +z direction or -z direction with a 50 percent probability. In a previous experiment we have indeed reported that a 200 nm by 200 nm magnet fabricated without a wedge from a Ta/CoFeB/MgO stack exhibiting perpendicular anisotropy indeed goes to either +z or -z direction after a current pulse with near 50 percent probability [4]. However, if the ferromagnet is given a wedge shape, the anisotropy axis of the magnet gets tilted by a slight angle from the out of the plane direction. The direction of the tilt follows the direction of the sloped surface of the wedge as shown in Fig. 5.1a and 5.1b, where the wedge is on the left side of the ferromagnet (looking in the +y direction) and so the anisotropy axis tilts in the +x direction (+z quandrants). Current in -y direction (Fig. 5.1a) drives the magnetization in-plane in +x , starting from initial direction in +z or -z. Once the current pulse is removed, owing to the tilt of the anisotropy axis, the up direction along the anisotropy axis is closer to the +x direction than the down direction along the anisotropy axis (the up direction makes a smaller angle (α) with +x direction than the down direction makes (β)) (Fig. 5.1a). As a result, the magnet will go to up direction. Thus a -y directed current pulse can be used to switch the magnet from down to up, and it will not switch an up directed magnetization. If a +y directed current pulse is applied instead (Fig. 5.1b) electrons with spins polarized in the -x direction accumulate at the Ta-CoFeB interface that results in the magnetization being driven to the -x direction. Once the current is removed, the magnet now goes to the down direction because the down direction along the anisotropy axis makes a smaller angle (β) with the -x direction (direction of the magnetization when it was in-plane) compared to the angle the up direction along the anisotropy axis makes with the -x direction (α) (Fig. 5.1b) . Thus +y directed current pulse can switch a magnet from up to down and it will not switch an initially down directed magnet. Fig. 5.1c shows that if the magnet has a wedge on the right side instead (looking in +y direction) the anisotropy axis is tilted in -x direction (+z quadrants). This will change the directionality or handedness of the switch. Thus for a magnet with wedge on the right side, a -y directed current pulse (+x directed spins accumulated at the interface) will switch the magnet from up to down while a +y directed current pulse (-x directed spins accumulated at the interface) will switch the magnet from down to up.

5.2 Tilting of the anisotropy axis due to wedge shape of the ferromagnetic layer

We next show micromagnetic simulations to justify that a wedge shape of the ferromagnetic layer results in tilting of the anisotropy axis. We simulate a 300 nm long, 90 nm wide and 1 nm thick ferromagnet in micromagnetic simulation package OOMMF [45](Fig. 5.2a and 5.2b) with a wedge 60 nm long on the left side of the magnet looking in the +y direction. The mesh size is 3 nm in x and y dimensions and 0.2 nm in the z dimension. The wedge is simulated by stacking 5 rectangular layers of magnetic moments, 300 nm long and 90 nm wide, separated by a distance of 0.2 nm each. We simulate a region on the left side of each layer, looking in the +y direction, where there is no magnet or rather the magnetization at those grid points is set to 0. The length of that region increases as one goes from the bottom layer to the top layer (in +z direction). As a result the length of the region which has a magnet, or where the magnetic moment at each grid point is that of the saturation magnetization of the ferromagnet (8×10^5 A/m), goes down from bottom to top as shown in Fig. 5.2a and 5.2b. Thus we simulate a magnet with a wedge. In the region where the magnet is flat the perpendicular anisotropy constant is 6×10^5 J/m^3. On the other hand in the wedge region the perpendicular anisotropy constant is set to 0. This is because our simulated wedge structure mimics the wedge shaped nanomagnets fabricated by You *et al.* [76] where the MgO layer is present over the flat region of the CoFeB (ferromagnet) layer but it is etched off from the wedge region (Fig. 5.1). The CoFeB-MgO interface has been considered to be responsible for perpendicular magnetic anisotropy of the CoFeB layer [38, 39]. So lack of perpendicular anisotropy due to the absence of MgO layer in the wedge region can be mimicked by setting the perpendicular anisotropy of the wedge region in the simulations to be 0. The exchange correlation constant (J) has been set to be 3×10^{-11} J/m throughout the magnetic layer in the simulations. Starting from all the magnetic moments of the ferromagnetic layer in +z direction with a very small positive component in +y direction ($M_x = 0, M_y = 0.016, M_z = 0.999$ for every grid point in the magnet) the system is allowed to evolve with time in the absence of any external magnetic field. Figure 2a shows that the system relaxes to a state where the magnetic moments in the wedge tilt in the +x direction, and thus the average magnetization of the system gets a positive x component. The average M_x in the final steady state is 0.1. This shows that the anisotropy axis of the magnet has effectively tilted by an angle $\theta = \sin^{-1}0.1 = 5.73^0$ from out of plane direction (Figure 1a and 1b). The reason for this tilt is the fact that at the wedge region which has no perpendicular anisotropy the moments want to align along the sloped surface of the wedge as can be seen in Fig. 5.2a. This minimizes the magnetostatic energy of the system by reducing the quantity of magnetic surface charge. Thus the average magnetization tilts in +x direction. Starting

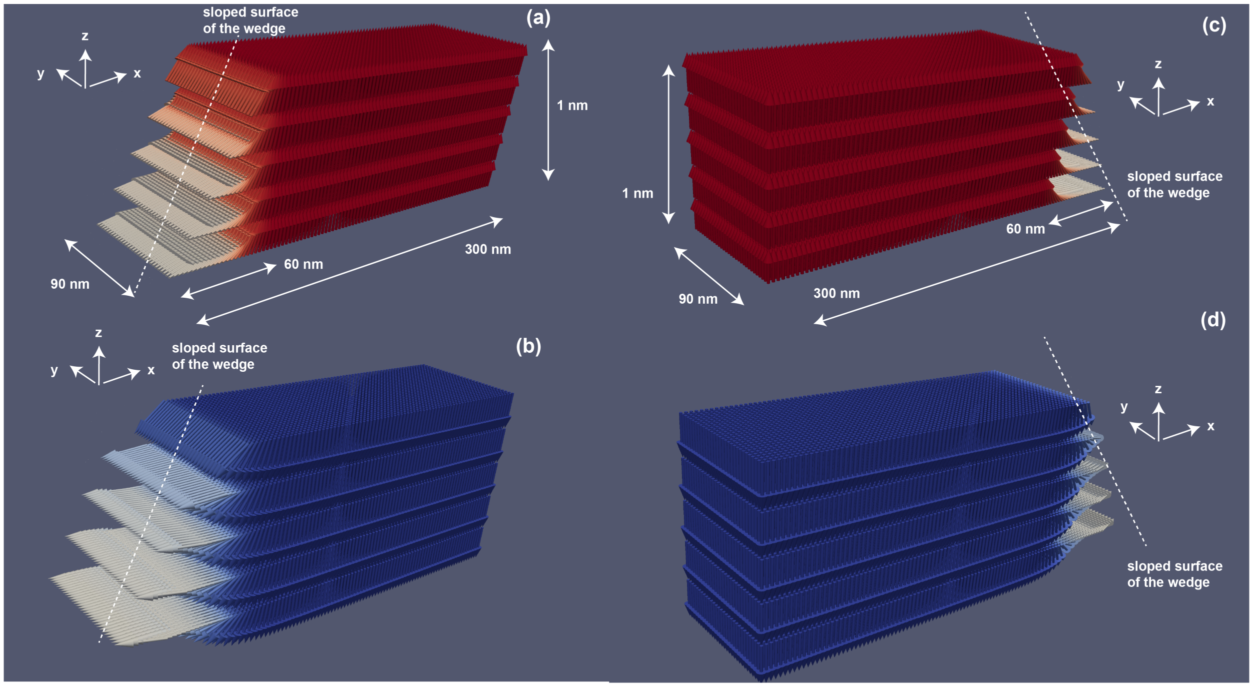
(a)
sloped surface of the wedge
z
y
x
1 nm
90 nm
60 nm
300 nm
(b)
sloped surface of the wedge
z
y
x
(c)
z
y
x
1 nm
sloped surface of the wedge
60 nm
90 nm
300 nm
(d)
z
y
x
sloped surface of the wedge

Figure 5.2: (a) For a ferromagnetic layer with the wedge on the left side of the magnet looking in the +y direction, starting from all the moments in the ferromagnetic layer pointing in the +z direction, if the system is allowed to relax, the moments at the wedge tilt towards +x direction aligning along the sloped surface of the wedge, shown by the dotted white line. The image shows the direction of the moments after the system is allowed to relax after 20 ns. (b) Starting from all the moments pointing in the -z direction, when the system is allowed to relax (for 20 ns), the moments at the wedge tilt towards -x direction again aligning along the sloped surface of the wedge. (c) For a ferromagnetic layer with the wedge on the right side of the magnet looking in the +y direction, starting from all the moments in the ferromagnetic layer pointing in the +z direction, if the system is allowed to relax, the moments at the wedge tilt towards -x direction aligning along the sloped surface of the wedge, shown by the dotted white line. The image shows the direction of the moments after the system is allowed to relax after 20 ns. (d) Starting from all the moments pointing in the -z direction, when the system is allowed to relax (for 20 ns), the moments at the wedge tilt towards +x direction again aligning along the sloped surface of the wedge. (The plots are not drawn to scale in the z dimension. The direction of the moments is suggested by the head of the arrows. Also, red color means moments are in +z direction, blue color means moments are in -z direction and white means moments are in-plane.)

from an initial state of -z directed uniform magnetization with a very small component in +y direction ($M_x = 0, M_y = 0.016, M_z = -0.999$ for every grid point in the magnet) the system is allowed to relax next. In this case, at the final steady state, the average magnetization is tilted in -x direction because again the moments in the wedge region align along the sloped surface of the wedge as shown in Fig. 5.2b. The small component of magnetization in the y direction is provided in the initial condition to prevent singularity issues in the simulation. We repeat the simulations with a small component of the magnetization in -y direction instead of +y to get the same results as Fig. 5.2a and 5.2b. Thus in this case the final direction of the average magnetization depends only on whether the magnet is in +z or -z state initially and direction of slope of the wedge. We next simulate a 300 nm long, 90 nm wide and 1 nm thick ferromagnet with a wedge 60 nm long on the right side of the magnet looking in the +y direction. In this case, starting from $M_z \sim 1$ state, the average magnetization tilts in the -x direction and starting from $M_z \sim -1$ state the average magnetization tilts in the +x direction again because the moments in the wedge region align along the sloped surface of the wedge to minimize magnetic charge at the surface (Figure 2c and 2d). Thus, the anisotropy axis tilts by an angle -θ in this case as shown in Fig. 5.1c.

5.3 Spin orbit torque from a current pulse drives the magnetic moments in-plane

Having shown that the anisotropy axis of the perpendicularly polarized magnet tilts in the direction of the sloped surface of the wedge, we now show how spin orbit torque due to current flowing through the heavy metal layer underneath the ferromagnetic layer drives the magnetization in-plane starting from +z direction. The same 300 nm long, 90 nm wide and 1 nm thick ferromagnet with a wedge 60 nm long on the left side is simulated using the same mesh as before. All the magnetic moments are initialized in the +z direction, with a very small component in y direction as before ($M_x = 0, M_y = 0.016, M_z = 0.999$). At every point in the grid, the moments are allowed to evolve in time following the Landau Lifschitz Gilbert equation modified for SOT of the Slonczweski type in OOMMF using the spin transfer torque extension module [45,49] :

$$\frac{d\vec{M}}{dt} = -\gamma(\vec{M} \times \vec{H}) - \frac{\gamma\alpha}{M}(\vec{M} \times \vec{M} \times \vec{H}) - \gamma\tau(\vec{M} \times \vec{M} \times \vec{\sigma}) \tag{5.1}$$

where γ is the gyromagnetic ratio, α is the damping constant (0.02 in this case), $\vec{H}$ is the effective field experienced by the magnetic moment due to anisotropy energy, exchange energy and magnetostatic energy of the system, $\vec{\sigma}$ is the spin accumulation at the interface of the ferromagnet and the heavy metal layer underneath the ferromagnet layer and

$$\tau = \frac{\hbar\theta_{SO} J_c}{2e\mu_0 M_s t_F} \tag{5.2}$$

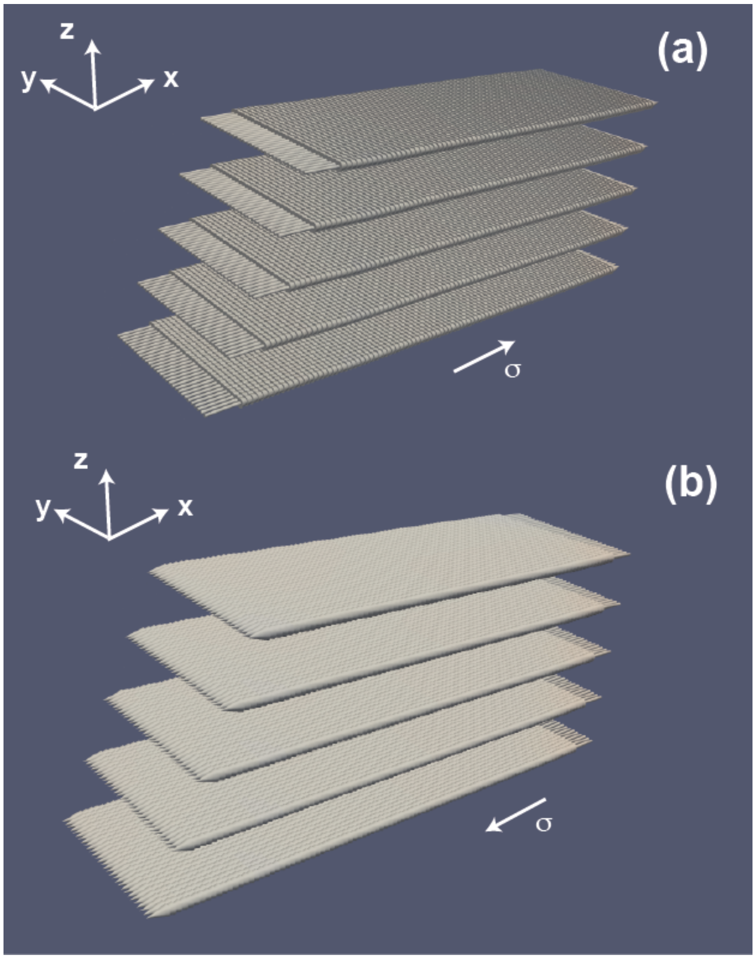

Figure 5.3: (a) Spin accumulation in +x direction (σ) at the interface of the ferromagnetic layer (CoFeB) and heavy metal (Ta) drives the magnetic moments of the ferromagnetic layer in-plane pointing in the +x direction. This image shows the direction of the magnetic moments after they are allowed to evolve in the presence of spin torque due to the spin accumulation for 1 ns. (b) Spin accumulation in -x direction at the interface drives the magnetic moments in -x direction (Image taken after 1 ns). (The plots are not drawn to scale in the z dimension. The direction of the moments is suggested by the head of the arrows. Also, red color means moments are in +z direction, blue color means moments are in -z direction and white means moments are in-plane.).

where $\hbar$- Plank's constant, μ_0- vacuum permeability, M_s- saturation magnetization (8×10^5 A/m for the simulation), t_F- thickness of the ferromagnetic layer (1 nm), J_c is the current density through the heavy metal underneath the ferromagnetic layer that cause the spin accumulation at the interface and θ_{SO} is the spin orbit torque efficiency of the heavy metal Ta considered in this case (0.12) [10]. We observe that a current density of 5×10^8 A/cm^2 or above is needed to drive the magnet in-plane. If $\vec{\sigma}$ points in the +x direction, i.e., electrons with spin polarization in +x direction accumulate at the interface of the ferromagnet and the heavy metal, the magnetic moments are driven in-plane and they point in the +x direction (Fig. 5.3a). Similarly if $\vec{\sigma}$ points in the -x direction, i.e., if electrons with spin polarization in -x direction accumulate at the interface of the ferromagnet and the heavy metal then the magnetic moments point in -x direction (Fig. 5.3b). A current pulse of magnitude 1×10^9 A/cm^2 or above through the heavy metal also drives the moments of a similar magnet, having a wedge on the right side, in-plane in the direction of the spin polarization of the accumulated electrons at the interface.

5.4 Deterministic evolution of the magnet to up or down state after the current pulse

After the spin orbit torque has driven the magnet in-plane, the current pulse is removed and we simulate how the magnetic moments evolve in the absence of spin orbit torque and zero external magnetic field. We observe that starting from the moments in +x direction, the moments evolve in time such that they are in the up direction (+z) in the final state as expected from the schematic in Fig. 5.1a. Starting from +x direction the moments in the wedge orient along the surface of the wedge ($M_z \sim 1$ with a component in +x direction) because the +x,+z direction along the surface of the wedge makes a smaller angle (α_1) with the +x direction compared to the the -x,-z direction along the surface of the wedge (β_1) (Fig. 5.4a). The moments in the flat region of the wedge then orient in the +z direction because that region has a significant perpendicular magnetic anisotropy and the +z direction is more energetically favorable compared to -z direction. This is because the exchange correlation energy between the moments in the flat region pointing in the +z direction and the moments in the wedge region pointing in the +x,+z direction ($-Jcos(90^0 - \alpha_1) = -Jsin(\alpha)$) is lower than the exchange correlation energy between the moments in the flat region pointing in the -z direction and the moments in the wedge region pointing in the +x, +z direction ($-Jcos(90^0 + \alpha_1) = Jsin(\alpha)$) , where J is the exchange correlation constant (3×10^{-11} A/m).

Similarly, starting from the initial -x direction, driven by -x spin polarized electrons accumulated at the interface (+y directed current pulse), the magnetic moments evolve to down direction (-z) (Fig. 5.4b). Thus for a wedge on the left side of the magnet, -y directed current pulse can switch magnet from down to up while +y directed current pulse switches the magnet from up to down, consistent with the schematic of Figure 1. For a magnet with a wedge on the right side of the magnet, starting from all the moments initially in the +x direction driven by -y directed current pulse, when the system is allowed to evolve, the final state of the magnet is in the -z direction with the moments in the wedge following the +x,-z direction along the surface of the wedge, following the same logic as the case for the left wedge. When the moments are allowed to evolve starting from the initial state of -x direction (driven by +y current pulse) they go to +z direction in the flat region and -x,+z direction in the wedge region following the surface of the wedge. Thus for a wedge on the right side of the magnet, -y directed current pulse switches the magnet from up to down while +y directed current pulse switches the magnet from down to up. It is to be noted that in all the four cases (Fig. 5.4) there is a reverse polarized domain at the other edge of the magnet (no the edge with the wedge). This is because the moments in the wedge determine the switching direction of the magnet, and the moments adjacent to it follow them, but beyond a certain length dipole energy wins over exchange interaction and so reverse domains are formed at the other edge of the magnet.

5.5 Comparison with experiment

Current density of 5×10^8 A/cm^2 through the heavy metal (Ta) is needed in our simulations to drive the moments of the ferromagnetic layer in-plane and thereby cause the switching. However, in the experiments performed by You *et al.* [76], the magnitude of the current pulse through Ta needed for the switching is 2.5×10^7 A/cm^2. Our simulations are performed at zero temperature while the experiments by You *et al.* are performed at room temperature. Temperature increase in Ta/CoFeB/MgO heterostructures due to application of current pulses of similar magnitude at room temperature has been measured to be about 100 K (Section 3.7). As a result, we calculate the current density that will be needed to switch the magnet we have simulated here if the switching takes place at 400 K instead of 0 K using the following expression [77,78]:

$$J_T = J_0(1 - \frac{k_B T}{E} ln(\frac{\tau}{\tau_0})) \tag{5.3}$$

where J_0 is the switching current density at 0 K (our simulations), J_T is the extrapolated current density for switching at 400K, k_B is the Boltzmann constant, T is the temperature (400 K here), τ is the time duration of the current pulse (1 s in the experiments by You *et al.*[76]), τ_0 is the natural frequency of the system ($\tau_0 = \gamma \mu_0 M_s$) and E is the energy of the switching barrier between up and down directed magnetization states. Energy E is calculated as:

$$E = K_{eff} V = (K - (\frac{1}{2}\mu_0 M_s^2))V \tag{5.4}$$

where K_{eff} is the effective anisotropy constant, K is the perpendicular anisotropy constant (6×10^5 J/m^3 in our simulations), M_s is the saturation magnetization (8×10^5 A/m in our

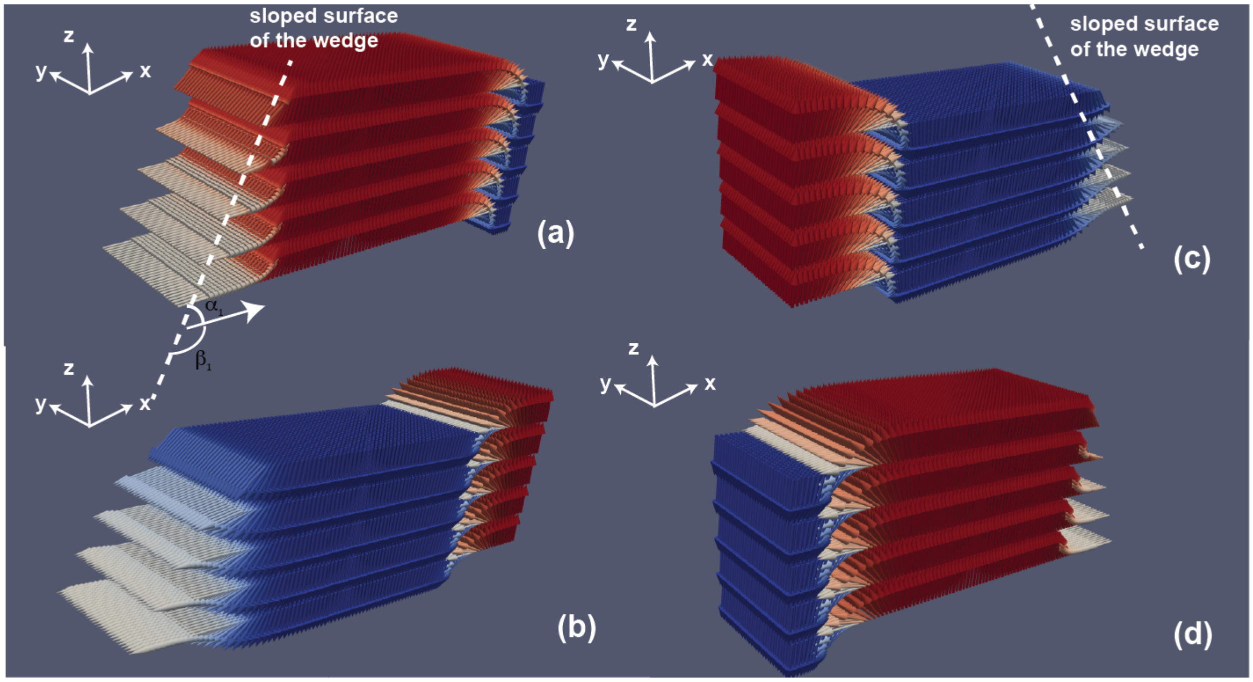

Figure 5.4: (a) For a ferromagnetic layer with a wedge on the left side of the magnet (looking in the +y direction) starting from the magnetic moments in the +x direction, driven by +x directed spins at the interface (Fig. 4.3a) if the system is allowed to evolve in the absence of spin torque (current pulse removed) the moments evolve such that in the majority of the magnet they point in the +z direction with the moments in the wedge aligned along the slope of the wedge in +x,+z direction as shown. This image shows the directions of the moments after the system was allowed to evolve for 1 ns after the removal of the spin torque (current pulse). (b) If the moments are allowed to evolve starting from -x direction, driven by -x polarized spins at the interface, (Fig. 4.3b) they finally point in the -z direction with moments in the wedge aligned along the surface of the wedge in -x,-z direction. (c) For a ferromagnetic layer with a wedge on the right side of the magnet (looking in the +y direction) starting from the magnetic moments in the +x direction, driven by +x directed spins at the interface, if the system is allowed to evolve in the absence of spin torque (current pulse removed) the moments evolve such that in the majority of the magnet they point in the -z direction with the moments in the wedge aligned along the slope of the wedge in +x,-z direction as shown. This image shows the directions of the moments after the system was allowed to evolve for 1 ns after the removal of the spin torque (current pulse). (d) If the moments are allowed to evolve starting from -x direction, driven by -x polarized spins at the interface, they finally point in the +z direction with moments in the wedge aligned along the surface of the wedge in -x,+z direction. (The plots are not drawn to scale in the z dimension. The direction of the moments is suggested by the head of the arrows. Also, red color means moments are in +z direction, blue color means moments are in -z direction and white means moments are in-plane.)

simulations) and V is the volume of a nucleated domain. $V = \pi((\frac{\delta}{2})^2)t_F$ where δ=diameter of nucleated domain=domain wall width=$\pi(\frac{A}{K_{eff}})^{\frac{1}{2}}$. The thermal stability factor $(\frac{E}{k_BT})$ calculated this way is 42.13 and the current density needed for switching at 400 K (J_T) is 3×10^8 A/cm^2. It is to be noted that our simulations do not model nucleation of reverse domains at defect sites as a part of the switching mechanism, which we have discussed in Chapter 3 of the thesis. Accounting for such a physical mechanism can lower the switching current density in our simulations and provide a better quantitative match between simulations and experiments.

Thus we have shown that a perpendicularly polarized magnet can be switched with a current pulse through the heavy metal underneath it. The directionality of the switching matches with the recent experimental findings of You *et al.* [76]. Though we have considered the Slonczweski type spin orbit torque to be responsible for driving the magnet in-plane in our simulations, the field like spin orbit torque from the current pulse can also be responsible for driving the magnet in-plane after which the moments can relax to either up or down following the same physics as described before. It is to be noted that recently Yu *et al.* [79] performed spin orbit torque driven deterministic switching of perpendicularly polarized magnet, but they used a physical mechanism which is different from ours. They created a thickness gradient over the entire film and showed that a vertically oriented Rashba field, due to structural symmetry breaking, switches the magnet. On the other hand, in our case, nanomagnets have a wedge shape and the effective anisotropy axis of the magnet gets tilted from the out of the plane direction to minimize magnetic charges on the surface of the wedge. This breaks the symmetry of the system and causes the deterministic switching of the magnet due to spin orbit torque. This result makes spin orbit torque driven switching a viable alternative to conventional spin transfer torque driven switching in STTMRAM. Thus here we have demonstrated the usefulness of spin orbit torque in memory applications just as we demonstrated the usefulness of it in computing applications in the previous chapter.

Chapter 6

Enhancement of spin orbit torque in bilayers of two metals with opposite polarities of spin orbit torque

We have seen in the previous chapters that the critical current needed to switch the ferromagnet in a ferromagnet-heavy metal heterostructure depends on the spin orbit torque efficiency of the heavy metal. In order to reduce the switching current for low power memory and logic applications, a possible research effort can be to enhance the spin orbit torque efficiency of the heavy metal. Keeping that in mind, we have deposited bilayers of two heavy metals, Ta and Pt, that are known to generate opposite polarities of spin orbit torque, and deposited a ferromagnetic layer (CoFeB) on top. We show experimentally that the current density through Ta that switches the ferromagnet goes down with decreasing the thickness of the Ta layer and increasing the thickness of the Pt layer. This goes against the intuitive picture where spin orbit torques from Ta and Pt should cancel. We perform analytical calculations based on spin transport theory which support the intuitive picture and contradict our experimental results.

6.1 Device Structure and Experimental Results

Different thin film stacks with the following composition are deposited using room temperature sputtering: Si(substrate)/ SiO_2/ Ta(2 nm)/ Pt(W_2 nm)/ Ta(W_1 nm)/ CoFeB(1 nm)/MgO(2 nm)/Ta(2 nm) (from bottom to top), where W_1 and W_2 are variables such that $W_1 + W_2 = 10$ nmFig. 6.1a). The 1 nm thick CoFeB layer is the ferromagnet that exhibits perpendicular magnetic anisotropy, which is considered to originate from the Ta-MgO interface. That is the role served by the MgO layer. The top layer of Ta of 2nm thickness serves as the capping layer. The difference between these stacks and that used in the previous three chapters (Si(substrate)/ SiO_2/ Ta(10 nm)/ CoFeB(1 nm)/MgO(2 nm)/Ta(2 nm)) is that here we have a bilayer of two heavy metals underneath the ferromagnetic layer. The thickness of the two heavy metal layers is varied keeping the summation of the two thickness values constant ($W_1 + W_2 = 10$) nm. Hall bars of 20 microns width are fabricated from these different stacks and the magnetization of the CoFeB layer is measured using anomalous Hall resistance measurement similar to previous chapters, Section 3.1 particularly. A square loop is obtained for R_{AHE} versus out of plane magnetic field (H_{out}) for all the stacks, which shows that the CoFeB layer always exhibits perpendicular magnetic anisotropy. Fig. 6.1b shows such a plot for Hall bars made from (Si(substrate)/ SiO_2/ Ta(2 nm)/Pt (7 nm)/ Ta (3 nm)/ CoFeB(1 nm)/MgO(2 nm)/Ta(2 nm)). Similar plots are obtained from other stacks. Next, for devices made from all these stacks, spin orbit torque driven switching experiment is performed under the application of an in-plane magnetic field along the direction of the current (current and in-plane magnetic field both applied in +x direction), similar to that described in Section 3.3 of the thesis. We find that the switching always follow the polarity or handedness same as that of Si(substrate)/ SiO_2/ Ta(10 nm)/ CoFeB(1 nm)/MgO(2 nm)/Ta(2 nm)) samples used before. For example, in Fig. 6.1c, current pulses of high magnitude are applied on a Hall bar fabricated from Ta(2 nm)/Pt (7 nm)/ Ta (3 nm)/ CoFeB(1 nm)/MgO(2 nm)/Ta(2 nm)) sample in the presence of in-plane magnetic field. Starting from initially -z state (R_{AHE} = -0.045 Ω) 100G is applied in +x direction and +x directed current pulses are applied of varying magnitude. We observe that current pulse for which current density through Ta is higher than 9×10^5 A/cm^2 switches the magnetization to +z state ($\Delta R_{AHE} \sim 0.045 - (-0.045) = 0.9\Omega$). +x directed current pulse and +x directed magnetic field switching the magnet from -z to +z is consistent with the switching direction for Ta-CoFeB interfaces found in our previous experiments (Fig. 3.3) and experiments by other groups [10]. Thus the presence of the Pt layer underneath the Ta layer in these new samples does not change the direction of the spin orbit torque at the Ta-CoFeB interface. Not only that, we also observe that the current density through the Ta layer that is needed to switch the ferromagnet is lower if the thickness of the Ta layer is decreased and the thickness of the Pt layer is increased (Fig. 6.4d). Thus spin orbit torque efficiency is improved as we transition from a monolayer of Ta to a bilayer of Ta and Pt.

In Chapter 2, we have discussed spin Hall effect as a possible origin of spin orbit torque in ferromagnet/ heavy metal heterostructure. Within the spin Hall physics, when current flows through the heavy metal layer, electrons with oppositely polarized spins drift in opposite directions. Thus a spin current is generated in the vertical direction, the ratio of spin current to charge current being called spin Hall angle. It results in the accumulation of electrons with spins polarized in one direction at the interface of the heavy metal layer and the ferromagnetic layer above it. This applies a spin orbit torque on the magnetization of the ferromagnet. Previous experiments have shown that Ta and Pt have opposite polarities of spin Hall angle [10,25], i.e. for the same direction of charge current flowing through the two metals, spins separate in opposite directions or spin currents are generated in the opposite directions as shown in Fig. 2. As a result, it is expected that for the same density of current flowing through the Ta layer, lower spin current and hence lower spin orbit torque

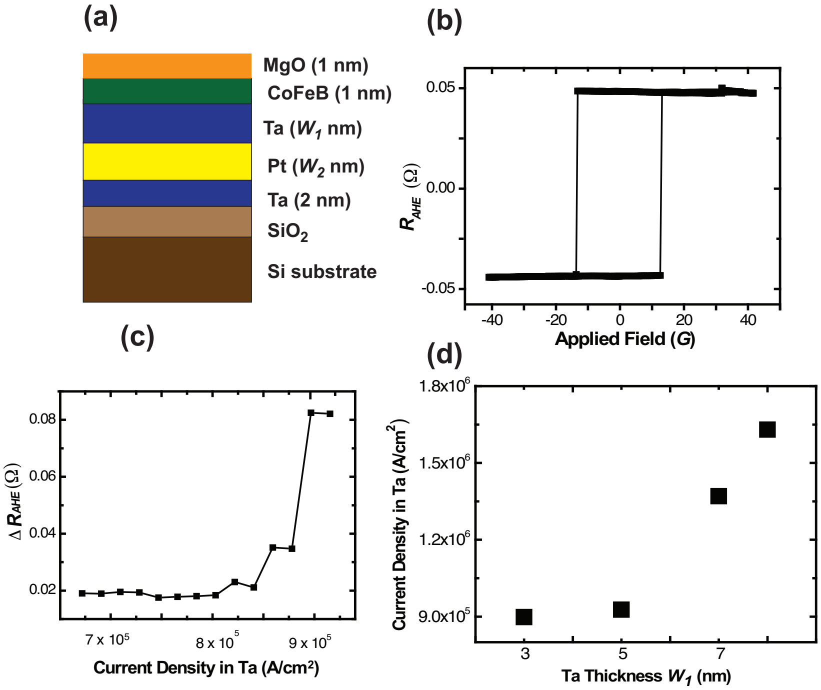

Figure 6.1: (a) The schematic describes the different stacks we used. Thickness of Ta layer below the ferromagnetic layer (CoFeB) is W_1 nm and thickness of Pt layer below it is W_1 nm, such that $W_1 + W_2 = 10$. (b) R_{AHE} versus out of plane magnetic field plot for Hall bars made from Si(substrate)/ SiO_2/ Ta(2 nm)/Pt (7 nm)/ Ta (3 nm)/ CoFeB(1 nm)/MgO(2 nm)/Ta(2 nm)) shows evidence of out of plane magnetic anisotropy. (c) Starting from an initial -z directed state (R_{AHE} = -0.045 Ω) a current pulse of a certain magnitude is applied in the presence of 100 G magnetic field in +x direction. The final R_{AHE} is measured. Then $\Delta R_{AHE} = R_{AHE,final} - R_{AHE,initial}$ and current density through Ta for the given current pulse flowing through the cross-section of the entire Hall bar are calculated.The magnet is reinitialized to -z state, another current pulse of different magnitude is applied and the same process is repeated. Finally, ΔR_{AHE} for the different current pulses is plotted against the current density through Ta for the current pulses. (d) We repeated the current pulsing experiment for different samples that had different widths of Ta and Pt layers, keeping the sum of the two constant ($W_1 + W_2 = 10$ nm). We observe that if the thickness of the Ta layer goes down or thickness of the Pt layer goes up, lower current density is needed to switch the magnet.

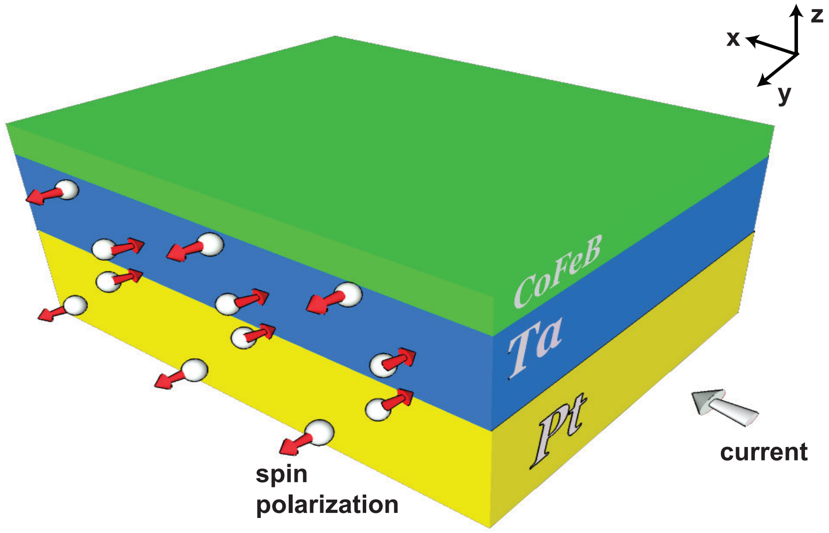

Figure 6.2: Current flowing in +x direction causes electrons with +y directed spins to go towards +z and -y directed spins to go towards -z. The opposite happens for Pt. Current flowing in +x direction drives electrons with -y directed spins to +z and +y directed spins to -z.

will be generated at the interface of Ta-CoFeB if we have a lower thickness of Ta layer and higher thickness of Pt layer because electrons with spins in opposite direction will diffuse from the Pt layer into the Ta layer and reduce the spin current at Ta-CoFeB interface. So higher switching current density through Ta should be needed to switch the magnetization of the CoFeB layer if the thickness of the Ta layer is reduced and thickness of the Pt layer is increased, but our experimental results show the opposite trend.

6.2 Spin diffusion based modeling

In order to verify the intuitive picture presented above (Fig. 2) we have modeled the Ta-Pt bilayer using spin diffusion theory. For a single layer of heavy metal 1 (say Ta) below the ferromagnet (Fig. 6.3), following the spin diffusion approach laid out by Zhang [21], spin dependent chemical potential is given by:

$$\mu_1^{\uparrow}(z) = \frac{1}{2}(A_1 e^{\frac{z}{D_1}} + B_1 e^{-\frac{z}{D_1})}; \mu_1^{\downarrow}(z) = -\frac{1}{2}(A_1 e^{\frac{z}{D_1}} + B_1 e^{\frac{z}{D_1}}) \tag{6.1}$$

such that

$$\mu_1^{\uparrow}(z) - \mu_1^{\downarrow}(z) = A_1 e^{\frac{z}{D_1}} + B_1 e^{-\frac{z}{D_1}}; \frac{d^2}{dz^2}(\mu_1^{\uparrow}(z) - \mu_1^{\downarrow}(z)) = \frac{(\mu_1^{\uparrow}(z) - \mu_1^{\downarrow}(z))}{D_1^2} \tag{6.2}$$

, where z is along the dimension of the thickness, D_1 is the spin diffusion length of the heavy metal, and A_1 and B_1 are coefficients for spin potential. Spin potential, and hence subsequently spin current, is considered to vary only in the thickness dimension (z) and not in the lateral dimensions (x and y). ↑ refers to electron with spin in +y direction and ↓ refers to electron with spin in -y direction. Spin current for electrons, spin polarized in +y and -y directions, is given by:

$$J_1^{\uparrow}(z) = -(\frac{C_1}{2})\frac{d\mu_1^{\uparrow}(z)}{dz} - (\frac{C_{h1}}{2})E_x = -(\frac{C}{4})(\frac{A_1}{D_1}e^{\frac{z}{D_1}} - \frac{B_1}{D_1}e^{-\frac{z}{D_1}}) - (\frac{C_{h1}}{2})E_x;$$

$$J_1^{\downarrow}(z) = -(\frac{C_1}{2})\frac{d\mu_1^{\downarrow}(z)}{dz} + (\frac{C_{h1}}{2})E_x = (\frac{C_1}{4})(\frac{A_1}{D_1}e^{\frac{z}{D_1}} - \frac{B_1}{D_1}e^{-\frac{z}{D_1}}) + (\frac{C_{h1}}{2})E_x \quad (6.3)$$

where C_1 is the conductivity of the heavy metal and C_{h1} is spin Hall conductivity of the heavy metal with $C_{h1} = \theta_{SHE,1}C_1$, $\theta_{SHE,1}$ is the spin hall angle of the heavy metal. Since we are considering only one layer of metal here with a ferromagnetic layer on top, the boundary conditions as follows: At the bottom surface of the heavy metal layer ($z = 0$) the net spin current (J_s) is 0 and at the top surface of the heavy metal ($z = W_1$, where W_1 is the width of the heavy metal layer) the net spin potential is 0 under the assumption that the ferromagnet absorbs all the spins at the interface.

$$J_1^{\uparrow}(z = 0) - J_1^{\downarrow}(z = 0) = 0; \mu_1^{\uparrow}(z = W_1) - \mu_1^{\downarrow}(z = W_1) = 0 \quad (6.4)$$

Solving equations1.2 and1.3 under boundary condition 1.4, spin current at the upper surface of the heavy metal layer which gets absorbed into the ferromagnet turns out to be:

$$J_s = -C_{h1}E_x(1 - sech(\frac{W_1}{D_1})) = -\theta_{SHE,1}J_{x,1}(1 - sech(\frac{L}{D})) \quad (6.5)$$

where $J_{x,1} = C_1E_x$ is the charge current density through the heavy metal. For the heavy metal Ta, $\theta_{SHE,1} = -0.12$. For a current density of 3×10^6 A/cm^2 flowing through 10 nm thick Ta, the spin current generated at the top surface which gets injected into the ferromagnetic layer above it $J_s = 3.55\times10^5$ A/cm^2. The sign of the spin current is positive which means +y directed spins move in +z direction and get absorbed by the ferromagnet, which is consistent with Fig. 6.2 and the polarity of the switching in Ta/CoFeB/MgO heterostructures reported by us (Section 3.3) and other groups. Our obtained expression for spin current (equation 1.5) also matches with that obtained by Liu *et al.* [25]. Plot of spin current (J_s) versus thickness of Ta layer (W_1) shows that the spin current increases as the thickness of the Ta layer increases but when the thickness is much larger than the spin diffusion length of Ta (2 nm) the spin current saturates (Fig. 6.3b).

Now let us consider a bilayer of two heavy metal layers (Fig. 6.4a): metal 1 (Ta) and metal 2 (Pt) with the layer of metal 2 below the layer of metal 2 (metal 2: $z = -W_2$ to $z = 0$; metal 1: $z = 0$ to $z = W_1$). Thickness of metal 1 is W_1, as before, and thickness of

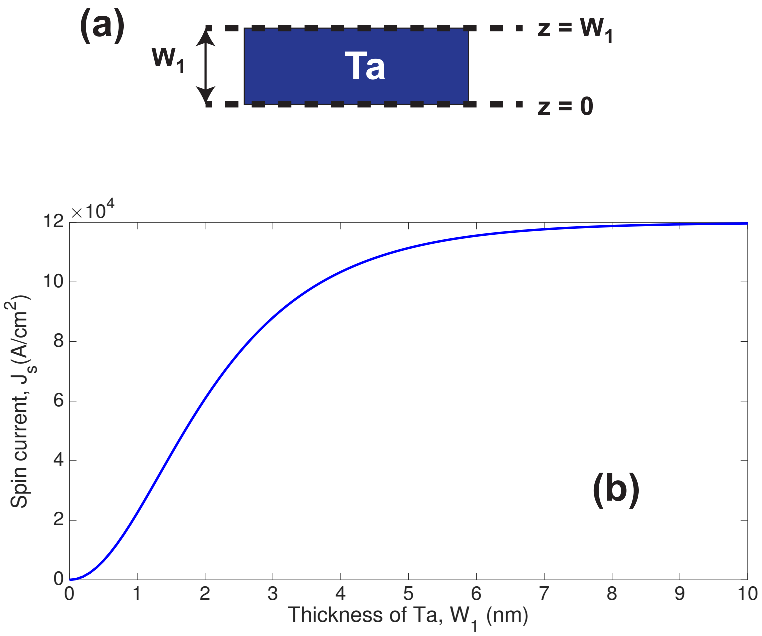

Figure 6.3: (a) Spin diffusion theory is used to simulate spin transport in a single layer of heavy metal (Ta here) of thickness W_1 in the presence of spin Hall effect. The figure shows the Ta layer which ranges from $z = 0$ to $z = W_1$. At the lower boundary ($z = 0$) spin current is 0 and at the upper boundary ($z = 0$ all the spins are absorbed by the ferromagnet above, and so the spin potential (difference between potential of +y and -y directed spins) is 0. (b) Spin current calculated at the upper boundary ($z = 0$) plotted against the thickness of the Ta layer ($W1$) shows saturation for a thickness which is much larger than the spin diffusion length (1.5 nm).

metal 2 is W_2. Other parameters of metal 1 are same as before. For metal 2, conductivity= C_2, spin Hall conductivity $=C_{h,2}$, spin Hall angle= $\theta_{SHE,2}$ and spin diffusion length= D_2. Equations for spin potential and spin current of metal 1 are same as before (Equation 1.1 and equation 1.3). Similarly, spin dependent chemical potential in metal 2 is:given by:

$$\mu_2^{\uparrow}(z) = \frac{1}{2}(A_2 e^{\frac{z}{D_2}} + B_2 e^{-\frac{z}{D_2}}); \mu_2^{\downarrow}(z) = -\frac{1}{2}(A_2 e^{\frac{z}{D_2}} + B_2 e^{\frac{z}{D_2}}) \tag{6.6}$$

and spin current in metal 2 is given by:

$$\begin{aligned} J_2^{\uparrow}(z) &= -(\frac{C_2}{2})\frac{d\mu^{\uparrow}(z)}{dz} - (\frac{C_{h2}}{2})E_x = -(\frac{C}{4})(\frac{A_2}{D_2}e^{\frac{z}{D_2}} - \frac{B_2}{D_2}e^{-\frac{z}{D_2}}) - (\frac{C_{h1}}{2})E_x; \\ J_2^{\downarrow}(z) &= -(\frac{C_2}{2})\frac{d\mu^{\downarrow}(z)}{dz} + (\frac{C_{h2}}{2})E_x = (\frac{C_2}{4})(\frac{A_2}{D_2}e^{\frac{z}{D_2}} - \frac{B_2}{D_2}e^{-\frac{z}{D_2}}) + (\frac{C_{h2}}{2})E_x \end{aligned} \tag{6.7}$$

The boundary conditions at the upper surface ($z = W_1$) and lower surface ($z = -W_2$) now are the following:

$$J_2^{\uparrow}(z = -W_2) - J_2^{\downarrow}(z = -W_2) = 0; \mu_1^{\uparrow}(z = W_1) - \mu_1^{\downarrow}(z = W_1) = 0 \tag{6.8}$$

and at the interface ($z = 0$) owing to the continuity of the spin current and spin potential, the boundary conditions are:

$$J_1^{\uparrow}(z = 0) - J_1^{\downarrow}(z = 0) = J_2^{\uparrow}(z = 0) - J_2^{\downarrow}(z = 0); \mu_1^{\uparrow}(z = 0) - \mu_1^{\downarrow}(z = 0) = \mu_2^{\uparrow}(z = 0) - \mu_2^{\downarrow}(z = 0) \tag{6.9}$$

Solving equations 1.2,1.3, 1.7 and 1.8 under the boundary conditions 1.8 and 1.9 results in the following final expression of spin current density (J_s) at the top surface of metal 1, which gets absorbed by the ferromagnet:

$$J_s = -\frac{C_1}{D} \frac{e^{\frac{W1}{D}}(-C_{h2}E_x - \frac{(C_{h1}-C_{h2})E_x}{2}(e^{\frac{W_2}{D}} + e^{-\frac{W2}{D}})}{(\frac{C_1+C_2}{4D})e^{-\frac{W_2}{D}} - (\frac{C_2-C_1}{4D})e^{\frac{W_2}{D}} - (\frac{C_2-C_1}{4D})e^{\frac{2W_1-W_2}{D}} + (\frac{C_1+C_2}{4D})e^{\frac{2W_1+W_2}{D}}} - C_{h1}E_x \tag{6.10}$$

where the spin diffusion lengths of the two metals are assumed to be equal, which is almost the case with Ta and Pt: $D_1 = D_2 = D$.

For conductivity of Ta $C_1 = 5.26 \times 10^5 \Omega^{-1} m^{-1}$ [10], spin Hall angle of Ta $\theta_{SHE,1} = -0.12$ [10], conductivity of Pt $C_1 = 6.4 \times 10^6 \Omega^{-1} m^{-1}$ [25,48], spin Hall angle of Pt $\theta_{SHE,2} = 0.07$ [25,48] and spin diffusion lengths $D_1 = D_2 = 1.5$ nm [80], the spin current density J_s is plotted as a function of the thickness of the top layer (Ta) (W_1) for current density through Ta $J_{x,1} = C_2E_x = 1 \times 10^6$ A/cm^2 keeping the summation of the thickness values of the two layers constant ($W_1 + W_2 = 10nm$). We see that as the thickness of Ta layer increases and thickness of Pt layer goes down, spin current goes up (Fig. 6.4b). We next plot spin current density J_s as a function of current density through Ta $J_c = C_2E_x$ (Fig. 6.4c), for three different bilayers (7 nm Ta, 3 nm Pt; 5 nm Ta, 5 nm Pt; 3 nm Ta, 7 nm Pt). We observe that to generate the same amount of spin current density, higher current density needs to flow through the Ta layer if the thickness of the Ta layer is lower and thickness of the Pt layer is higher in the bilayer. This result is consistent with the intuitive picture presented before (Fig. 6.2). Spin Hall angle of Pt is of opposite polarity as that of Ta. So oppositely directed spins diffuse from the Pt layer to the Ta layer thereby reducing the spin current that the Ta layer injects into the CoFeB layer. So to inject the same amount of spin current density into the ferromagnet that can switch the ferromagnet, current density through Ta needs to be higher if the thickness of the Ta lower and the thickness of the Pt layer is higher. However, in experiments, we observe the reverse trend. If the thickness of the Ta layer is lower and thickness of the Pt layer is higher, lower current density is needed to switch the ferromagnet. This means that the physics of the system cannot be totally captured by the spin diffusion theory used here. Something interesting probably happens at the Ta-Pt interface, the theoretical understanding of which eludes us at this point.

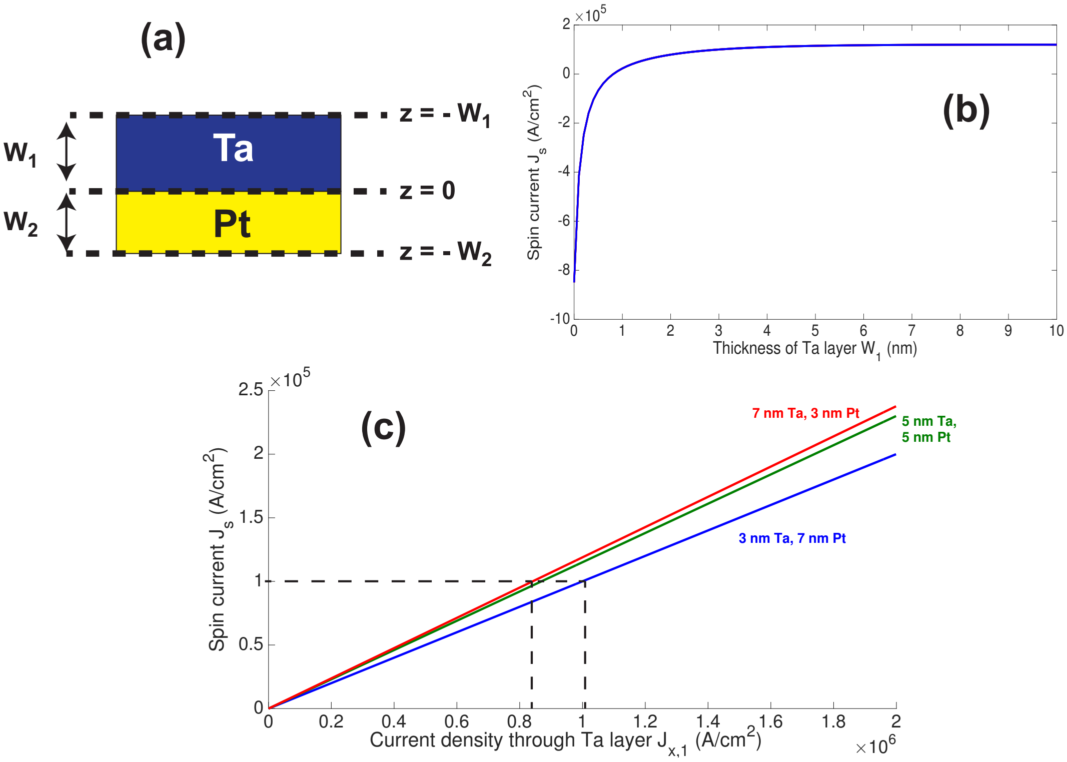

Figure 6.4: (a)A bilayer of Ta and Pt is shown for which the spin transport has been modeled. Ta ranges from $z = 0$ to $z = W_1$ while Pt ranges from $z = 0$ to $z = -W_1$. Thus thickness of Ta layer is W_1 and thickness of the Pt layer is W_2. (b) Current density through the Ta layer ($J_{x,1} = 10^6$ A/cm^2 is set equal to 1×10^6 A/cm^2 by keeping the electric field (E_x) that drives the current constant at 1.9×10^4 V/m ($J_{x,1} = C_1 E_x$). We see that as the thickness of the Ta layer goes down spin current also lowers and finally it reverses sign. This is because oppositely directed spins from Pt diffuse into Ta. (c) For three different combinations of Ta and Pt layers (7 nm Ta, 3 nm Pt; 5 nm Ta, 5 nm Pt; 3 nm Ta, 7 nm Pt) the current density is varied from 0 to 2×10^6 A/cm^2 by sweeping the electric field. As expected from the intuitive picture, when the thickness of Ta goes down and Pt goes up, larger current density through Ta needs to flow to generate the same amount of spin current density which will eventually switch the magnet. For example, in order to generate a spin current density of 10^5 A/cm^2 at the top surface of a bilayer of Ta and Pt, the current density that needs to flow through Ta is 8.2×10^5 A/cm^2 for a 7 nm thick Ta, 3 nm thick Pt bilayer (red plot) but it is equal to 1×10^6 A/cm^2 for a 3 nm thick Ta, 7 nm thick Pt bilayer (blue plot). Thus according to intuition and these calculations switching current density should go up for lower thickness of Ta but instead it goes down in the experiment (Fig. 6.1d)

Chapter 7

Conclusion and Future Work

In this chapter we summarize the key results presented in this work below:
1. We demonstrate spin orbit torque driven switching in micron sized Hall bars made from perpendicularly polarized Ta-CoFeB-MgO heterostructures in the presence of in-plane and out of plane external magnetic fields. We explain the result qualitatively with a single domain model and argued why such a simplistic model cannot provide a quantitative match between the current densities needed for switching in simulations and experiments. We then introduce a micromagnetic model which provides a microscopic understanding of the switching process. We then show longitudinal domain wall motion orthogonal to current flow in such devices and explained the result quantitatively with a micromagnetic model. These results are presented in Chapter 3 of the thesis and can also be found in the following references [81,82,83]:
2. We experimentally demonstrated spin orbit torque driven switching in perpendicularly polarized magnets (Ta-CoFeB-MgO) with the dimensions of hundreds of microns as opposed to mirons wide Hall bars. We then use spin orbit torque driven switching of nanomagnets to "clock" a realistic nanomagnetic logic circuit. We show that the current needed for clocking is two orders of magnitude lower compared to previous experimental demonstrations that used conventional Oersted field based clocking. This makes spin orbit torque driven switching useful for logic applications. This result is presented in Chapter 4 of the thesis and can also be found in the following reference [84]:
3. We explain through micromagnetic simulations how a wedge shape in a ferromagnet can tilt the anisotropy axis of the ferromagnet and how that tilt can be used to deterministically switch the magnet from up to down and down to up in the absence of an external magnetic field. This makes spin orbit torque driven switching useful for memory applications. This result is presented in Chapter 5 of the thesis and can also be found in reference [85].
4. We report our experimental observation of enhancement of spin orbit torque efficiency in a bilayer of Ta-Pt as opposed to a monolayer of Ta. We provide a spin diffusion theory based model which shows results that are consistent with our intuitive understanding of the system but contradicts the experimental results. This work is documented in Chapter 6 of the thesis as well as in reference [86] .

The discussion of experimental results of other groups in Chapter 2 of the thesis can also be found in reference 82. In terms of future work, the following projects can be pursued as a direct followup of the results mentioned above:

1. We have experimentally demonstrated longitudinal domain wall motion orthogonal to the current in Chapter 3 of the thesis. The current pulses applied are 1s in duration. Shorted current pulses of nanoseconds duration can be applied to measure the velocity of a longitudinal domain under under spin orbit torque.
2. We have experimentally shown information propagation along a chain of nanomagnets driven by spin orbit torque. This circuit can be thought of as a chain of NOT gates or inverters. More logic circuits like NAND and NOR gates can be fabricated with nanomagnets and spin orbit torque driven clocking can be demonstrated in them. The dimensions of the device can also be scaled to reduce the amount of current needed for the clocking. Thus it can be checked if spin orbit torque driven nanomagnetic logic can indeed commercially replace CMOS based logic or not.
3. We have shown through experiments and simulations that a wedge shape in a ferromagnet can tilt the anisotropy axis and make it possible to deterministically switch the magnet in the absence of external magnetic field. However creating such a wedge shape for very small magnets at an industrial scale for a MRAM cell can be very challenging. Hence new materials can be researched upon which already have a tilt in the anisotropy axis and hence a wedge shape does not need to be engineered. [Co/Pd]-NiFe exchange springs look promising in this regard.[87]
4. The spin diffusion theory based modeling of Ta-Pt bilayers that we reported in Chapter 6 does not explain the enhancement of spin orbit torque efficiency for Ta-Pt bilayers compared to a single Ta layer. This probably means that there is rich physics associated with the interface of Ta and Pt, which needs to be further explored both theoretically and experimentally.

Several other related ideas can be pursued to develop a better understanding of spin orbit torque. For example, this thesis mainly focusses on the mechanism of spin orbit torque driven switching in ferromagnets assuming that the heavy metal is a source of spin polarized electrons that apply a spin orbit torque on the ferromagnet. The phenomenon considered responsible for generation of spin polarized electrons in the heavy metal is spin Hall effect. This thesis does not describe many experiments that directly deal with spin Hall effect of the heavy metal. So we would like to explore the origin of spin Hall effect in our future work. The exact origin of spin Hall effect is still a subject of debate [88]. Several mechanisms may be responsible for the the origin of spin Hall effect like scattering with impurities, which is an extrinsic mechanism (side jump scattering and skew scattering) or intrinsic mechanism like the Berry phase originating from the band-structure of the material. Also, it is still not clear whether the ferromagnetic layer on the top of the heavy metal influences the spin Hall effect of the heavy metal or not. We plan to do systematic experiments and develop theoretical models that can throw light on this subject.

We have studied the motion of magnetic domain walls in this thesis. We want to investigate how spin orbit torque controls other interesting topological objects like magnetic skyrmions [35] formed in similar heavy metal- ferromagnet heterostructures. Apart from the rich physics associated with skyrmions, they also have potential use in high density memory just like domain walls, thereby increasing the importance of such an investigation.

Bibliography

[1] Borkar, S. and Chien, A. The future of microprocessors. *Communications of the ACM* 54 (5) , 67-77 (2011).

[2] Danowitz, A. *et al.* CPU DB: Recording microprocessor history. *Communications of the ACM* 10(4), 1-18 (2012).

[3] Salahuddin, S. and Datta, S. Use of Negative Capacitance to Provide Voltage Amplification for Low Power Nanoscale Devices. *Nanoletters* 8(2), 405-410 (2008).

[4] Theis, T. N. and Solomon, P. M. It's time to reinvent the transistor! *Science* 327 (5973), 1600-1601 (2010).

[5] Nikokov, D. E. and Young, I. A. Overview of beyond CMOS devices and a uniform methodology for their benchmarking. *Proceedings of the IEEE* 101 (12), 2498-2533 (2013)

[6] Ralph, D. C. and Stiles, M. D. Spin transfer torques. *J. of Magn. Magn. Mater.* 321 (16), 1190- 1216 (2008).

[7] Wong, P. H. S. and Salahuddin, S. Memory leads the way to better computing. *Nature Nano.* 10 (2015).

[8] Ikegami, K. *et al.* Low power and high density STT-MRAM for embedded cache memory using advanced perpendicular MTJ integrations and asymmetric compensation techniques. *Proceedings of the IEDM* 28.1.1-28.1.4(2014).

[9] Miron, I. M. *et al.*. Current-driven spin torque induced by the Rashba effect in a ferromagnetic metal layer. *Nature Mater.* 9, 230-234 (2010).

[10] Liu, L. *et al.* Spin-torque switching with the giant spin Hall effect of tantalum. *Science* 336, 555-558 (2012).

[11] Parkin, S. S. P. *et al.* Magnetic domain-wall racetrack memory. *Science* 320, 190-194 (2008).

[12] Hirsch, J. E. Spin Hall effect. *Phys. Rev. Lett.* 83, 1834 (1999).

[13] Manchon, A. and Zhang, S. Theory of spin torque due to spin-orbit coupling. *Phys. Rev. B* 79, 094422 (2009).

[14] Jackson, J.D. Classical Electrodynamics, John Wiley and Sons (1998).

[15] Thomas, L.H. The motion of the spinning electron. Nature 117, 514 (1926)

[16] Zhang, S., Spin torques due to large Rashba fields, Spin current, Oxford University Press (2011).

[17] Maekawa, S. *et al.* Spin Hall effect, Spin current, Oxford University Press (2011).

[18] Morota, M. *et al.* Indication of intrinsic spin Hall effect in 4d and 5d transition metals. *Phys. Rev. B.* 83, 174405 (2011).

[19] Tanaka, T. *et al.* Intrinsic spin Hall effect and orbital Hall effect in 4d and 5d transition metals. *Phys. Rev. B.* 77, 165117 (2008).

[20] Kontani, H. *et al.* Giant orbital Hall Effect in Transition Metals: Origin of Large Spin and Anomalous Hall Effects. *Phys. Rev. Lett.* 102, 016601 (2009).

[21] Zhang, S. Spin Hall Effect in the presence of spin diffusion. *Phys. Rev. Lett.* 85, 393 (2000).

[22] Manchon, A. Spin Hall effect versus Rashba torque. arxiv: 1204.4869. (2012).

[23] Gambardella, P. *et al.* Current induced spin orbit torques. *Phil. Trans. R. Soc. A* 369, 3175-3197(2011).

[24] Miron, I. M. *et al.* Perpendicular switching of a single ferromagnetic layer induced by in-plane current injection. *Nature* 476, 189-193 (2011).

[25] Liu, L. *et al.* Current-Induced Switching of Perpendicularly Magnetized Magnetic Layers Using Spin Torque from the Spin Hall Effect. *Phys. Rev. Lett.* 109, 096602 (2012).

[26] Hayashi, M. *et al.* Quantitative characterization of the spin-orbit torque using harmonic Hall voltage measurements. *Phys. Rev. B.* 89, 144425 (2014).

[27] Kim, J. *et al.*, Layer thickness dependence of the current-induced effective field vector in Ta/CoFeB/MgO. *Nature Mater.* 12, 240-245 (2013).

[28] Emori, S. *et al.* Current driven dynamics of chiral ferromagnetic domain walls. *Nature Mater.* 12, 611-616 (2013).

[29] Haney, P. M. *et al.* Current induced torques and interfacial spin orbit coupling: Semiclassical modeling. *Phys. Rev. B.* 87, 174411 (2013).

[30] Garello, K. *et al.* Symmetry and magnitude of spin-orbit torques in ferromagnetic heterostructures. *Nature Nanotech.* 8, 587-593 (2013).

[31] Fan, X. *et al.* Observation of the non-local spin-orbital effective field. *Nature Communications* 4, 1799 (2013).

[32] Khvalkovskiy, A. V. *et al.* Matching domain-wall configuration and spin-orbit torques for efficient domain-wall motion. *Phys. Rev. B.* 87, 020402 (2013).

[33] Zhang, C. *et al.* Magnetotransport measurements of current induced effective fields in Ta/CoFeB/MgO. *Appl. Phys. Lett.* 103, 262407 (2013).

[34] Ryu, K. S. *et al.* Chiral spin torque at magnetic domain walls. *Nature Nanotech.* 8, 527-533 (2013).

[35] Fert, A. *et al.* Skyrmions on the track. *Nature Nanotech.* 8, 152-156 (2013).

[36] Thiaville, A. *et al.* Dynamics of Dzyalonshinskii domain walls in ultrathin magnetic films. *Europhys. Lett.* 100, 57002 (2012).

[37] Chen, G. *et al.* Tailoring the chirality of magnetic domain walls by interface engineering. *Nature Communications* 4, 2671 (2013).

[38] Ikeda, S. *et al.* A perpendicular-anisotropy CoFeB-MgO magnetic tunnel junction. *Nature Mater.* 9, 721-724 (2010).

[39] Yang,H. X. *et al.* First principles investigation of very large perpendicular magnetic anisotropy at Fe/MgO and Co/MgO interfaces. *Phys. Rev. B* 84, 054401 (2011).

[40] Chikazumi, S.C. *et al.* Physics of ferromagnetism. Oxford Science Publications (1997).

[41] Aharoni, A. Introduction to the theory of Ferromagnetism (Oxford University Press, 2009).

[42] Coey, J. M. D. Magnetism and Magnetic Materials (Cambridge University Press, 2010).

[43] Zhang, S. and Li, Z. Roles of non-equilibrium conduction electrons on the magnetization dynamics of ferromagnets. *Phys. Rev. Lett.* 93, 127204 (2004).

[44] Tatara, G. and Kohno, H. Theory of current driven domain wall motion: Spin transfer versus momentum transfer. *Phys. Rev. Lett.* 92, 086601 (2004).

[45] Donahue, M. J. and Porter, D. G. OOMMF User?s Guide, Version 1.0, Interagency Report NISTIR 6376 (1999).

[46] OOMMF extension module for current induced domain wall motion- IBM Research-Zurich.

[47] Delalande, M *et al.*. Measurement of the nucleation and domain depinning field in a single Co/Pt multilayer dot by Anomalous Hall effect. *J. Magn. Magn. Mater.* 324, 1277-1280 (2012).

[48] Lee, O. J. *et al.* Central role of domain wall depinning for perpendicular magnetic switching driven by spin torque from the spin Hall effect. *Phys. Rev. B.* 89, 024418 (2014).

[49] You, C. Micromagnetic simulations for spin transfer torque in magnetic multilayers. *J. of Magnetics.* 17, 73 (2012).

[50] Emori, S. *et al.* Spin Hall torque magnetometry of Dzyaloshinskii domain walls. *Phys. Rev. B.* 90, 184427 (2013).

[51] Haazen, P. P. J. *et al.* Domain wall depinning governed by the spin Hall effect. *Nature Mater.* 12, 299-303 (2013).

[52] Franken, J. H. *et al.* Tunable chiral texture in magnetic domain walls. *Scientific Reports* 4, 5248 (2014).

[53] Koyama, T. *et al.* Observation of the intrinsic pinning of a magnetic domain wall in a ferromagnetic nanowire. *Nature Mater.* 10, 194-197 (2011).

[54] Torrejon, J. *et al.* Interface control of the magnetic chirality in CoFeB/MgO heterostructures with heavy-metal underlayers. *Nature Communications* 5, 4655 (2014).

[55] Malozemoff, A. P. and Slonczewski, J. C. Magnetic Domain Walls in Bubble Material (Academic, 1979).

[56] Yu, G. *et al.* Magnetization switching through spin-Hall-effect-induced chiral domain wall propagation. *Phys. Rev. B.* 89, 104421 (2014).

[57] Schwartz, N. *et al.* Temperature coefficient of resistance of beta-Tantalum films and mixtures with b.c.c. Tantalum. *Thin Solid Films.* 14 (2), 333-346 (1972).

[58] Salahuddin, S. and Datta, S. Interacting systems for self-correcting low power switching. *Appl. Phys. Lett.* 89, 093503 (2007).

[59] Behin-Aein, B. *et al.* Proposal for an all-spin logic device with built-in memory. *Nature Nano.* 5, 266-270 (2010).

[60] Nikonov, D. E. *et al.* Proposal of a spin torque majority gate logic. *IEEE Electron Device Lett.* 32(8), 1128-1130 (2011).

[61] Ikeda, S. *et al.* Magnetic tunnel junctions for spintronic memories and beyond. *IEEE Trans. Electron Devices* 54 (5), 991-1002 (2007).

[62] Ohno, H. *et al.* Magnetic tunnel junction for nonvolatile CMOS logic. *IEEE IEDM* Tech. Digest 2010, 218-221 (2010).

[63] Cowburn, R. P. and Welland, M. E. *Science* 287, 1466 (2000).

[64] Imre, A. *et al.* Majority logic gate for magnetic quantum-dot cellular automata. *Science* 311, 205-208 (2006).

[65] Atulasimha, J. and Bandyopadhyay, S. Bennett clocking of nanomagnetic logic using multiferroic single-domain nanomagnets. *Appl. Phys. Lett.* 97, 173105 (2010).

[66] Carlton, D. B. *et al.* Simulation studies of nanomagnet-based logic architecture. *Nano Lett.* 8 (12), 4173-4178 (2008).

[67] Alam, M. T. *et al.* On-chip clocking of nanomagnetic logic lines and gates. *IEEE Trans. Nanotechnol.* 11 (2), 273-286 (2012).

[68] Ju, X. *et al.* Nanomagnetic logic from partially irradiated Co/Pt nanomagnets. *IEEE Trans. Nanotechnol.* 11 (1), 97-104 (2012).

[69] Breitkreutz, S. *et al.* Majority gate for nanomagnetic logic with perpendicular magnetic anisotropy. *IEEE Trans. Magn.* 48 (11), 4336-4339 (2012).

[70] Lambson, B. *et al.* Exploring the thermodynamic limits of computation in intergrated systems: magnetic memory, nanomagnetic logic, and the Landauer limit. *Phys. Rev. Lett.* 107, 010604 (2011).

[71] Lambson, B. *et al.* Exploring the thermodynamic limits of computation in intergrated systems: magnetic memory, nanomagnetic logic, and the Landauer limit. *Phys. Rev. Lett.* 107, 010604 (2011).

[72] Alexandrou, M. *et al.* Spatial sensitivity mapping of Hall crosses using patterned magnetic nanostructures. *J. Appl. Phys.* 108, 043920 (2010).

[73] Ju, X. *et al.* Error analysis of Co/Pt multilayer based nanomagnetic logic. *Nanotechnology (IEEE-NANO), 2011 11th IEEE Conference on*, 1034-1037 (2011).

[74] Carlton, D. B. *et al.* Investigation of defects and errors in nanomagnetic logic circuits. *IEEE Trans. Nanotechnol.* 11(4), 760-762 (2012).

[75] Niemier, M. T. *et al.* Clocking structures and power analysis for nanomagnet-based logic devices. *ACM/IEEE International Symposium on Low Power Electronics and Design (ISLPED)*, vol., no., pp.26,31, (2007).

[76] You, L. *et al.* Switching of perpendicularly polarized nanomagnets with spin orbit torque without an external field by engineering a tilted anisotropy. *Proc. Natl. Acad. Sci.* 112 (33), 10310-10315 (2015).

[77] Sato, H. *et al.* CoFeB thickness dependence of thermal stability factor in CoFeB/MgO perpendicular magnetic tunnel junctions. *IEEE Magn. Lett.* 3, 300204 (2012)

[78] Moriyama, T. *et al.* Tunnel magnetoresistance and spin torque switching in MgO-based magnetic tunnel junctions with a Co/Ni multilayer electrode. *Appl. Phys. Lett* 97, 072513 (2010)

[79] Yu, G. *et al.* Switching of perpendicular magnetization by spin-orbit torques in the absence of external magnetic fields. *Nature Nanotech.* 9, 59-63 (2014).

[80] Qu, D. *et al.* Self-consistent determination of spin Hall angles in selected 5d metals by thermal spin injection. *Phys. Rev. B* 89,140407 (2014).

[81] Bhowmik, D., You, L. and Salahuddin, S. Possible Route to Low Current, High Speed, Dynamic Switching in a Perpendicular Anisotropy CoFeB-MgO Junction Using Spin Hall Effect Of Ta. 29.7.1- 29.7.4 *IEEE IEDM Tech. Digest 2012* (2012).

[82] Bhowmik, D. *et al.* Magnetization switching and domain wall motion due to spin orbit torque. Chapter 6 of Nanomagnetic and Sprintronic devices for energy efficient memory and computing. Edited by Bandyopadhyay, S. and Atulasimha, J. Wiley and Sons (under press).

[83] Bhowmik, D. *et al.* Deterministic Domain Wall Motion Orthogonal To Current Flow Due To Spin Orbit Torque. *Scientific Reports* 5, 11823 (2015).

[84] Bhowmik, D., You, L., Salahuddin, S. Spin Hall effect clocking of nanomagnetic logic without a magnetic field. *Nature Nano.* 9(1), 59-63 (2014).

[85] Bhowmik, D. and Salahuddin, S. Deterministic spin orbit torque switching of a perpendicularly polarized magnet using wedge shape of the magnet (under preparation).

[86] Abdel-Raziq, H., Bhowmik, D. and Salahuddin, S. Enhancement of spin orbit torque efficiency in bilayers of two metals with opposite polarities of spin Hall angle (under preparation).

[87] Nguyen, T. N. A. *et al.* [Co/Pd]-NiFe exchange springs with tunable magnetization angle. *Appl. Phys. Lett.* 98, 172502 (2011).

[88] Hoffman, A. Spin Hall effects in metals. *IEEE Transactions on Magnetics* 49(10), 5172-5193 (2013).